Study Of Dielectric And Magnetic Properties Of (1-x) PVDF – x FeOOH Nanocomposite Thin Films (x= 0 to15 wt%)

A write-up thesis submitted in partial fulfillment of the requirements
For award of the degree of

Masters of technology in Nanoscience and Technology

Under the guidance of
Dr. Chandan Kumar Ghosh
Jadavpur University

By
DEBADRITA BHADURI

Registration number: 163815 of 2022-23
Class Roll No. – 002230701014
Examination Roll No. - M4NST24012
ACADEMIC YEAR: 2023-2024

DEPARTMENT : School of Materials Science and Nanotechnology
Jadavpur University

Duration: 01.09.2023-31.05.2024

School of Materials Science and Nano Technology

Jadavpur University,

Kolkata- 700032, INDIA.

CERTIFICATE OF RECOMMENDATION

We hereby recommend that the thesis entitled as Study Of Dielectric and Magnetic Properties of (1-x) PVDF – xFeOOH nanocomposite thin films (x= 0 to15 wt%) prepared by Ms. Debadrita Bhaduri (Class Roll No 002230701014, Registration No. 163815 of 2022-23, Examination Roll No. M4NST24012 under our guidance, be accepted in partial fulfilment of the requirement for the award of the Degree of Master of Technology in Nano Science and Technology from the School of Materials Science and Nano Technology of Jadavpur University.

Thesis Supervisor

Dr. Chandan Kumar Ghosh (Assistant Professor),

School of Materials Science and Nanotechnology

Jadavpur University

Director

Dr. Mahua Ghosh Chowdhuri (Director),

School of Materials Science & Nanotechnology

Jadavpur University

Dean-FISLM,

Jadavpur University,

Kolkata – 700 032

School of Materials Science and Nano Technology

Jadavpur University,

Kolkata- 700032, INDIA

CERTIFICATE OF APPROVAL

The foregoing thesis "Study Of Magnetic And Dielectric Properties Of (1-X)$PVDF_2$ – Feooh(X_2-0to15 Wt%)."was hereby approved by the committee of the final examination for evaluation of the thesis as a credited study of an engineering subject carried out and presented by Ms. Debadrita Bhaduri (Class Roll No: 002230701014, Registration No. 163815 of 2022-23, Examination Roll No. M4NST24012) in a manner satisfactory to warrant its acceptance as a prerequisite to the degree of Masterof Technology in Nano Science and Technology. It was understood by this approval, the undersigned do not necessarily endorse or approve any statementmade, opinion expressed or conclusion drawn therein but approve the thesis only for the purpose for which it was submitted. Committee of final examinationfor evaluation of thesis.

_____ _____

_____ _____

_____ _____

_____ _____

Signature **Date**

School of Materials Science and Nano TechnologyJadavpurUniversity, Kolkata-700032, INDIA.

Declaration of Originality and Compliance of Academic Ethics

I hereby declare that this thesis titled "Study Of Magnetic And Dielectric Properties Of (1-X)$PVDF_2$ – Feooh(X_2-0to15 Wt%)."contains literature survey and original research workby the undersigned candidate, as part of my Degree of Master of Technology inNanoscience and Technology. All Information in this document has been obtained and presented in accordance with academic rules and ethical conduct.

I also declare that, as required by these rules and conduct, I have fully cited and referenced all material results that were not original to this work.

Name (Block Letters): DEBADRITA BHADURI

Class Roll No: 002230701014

Registration No: 163815 of 2022-23

Examination Roll No: M4NST24012

Signature with date

ACKNOWLEDGEMENT

I extend my heartfelt gratitude to everyone who helped elevate these ideas frombasic concepts to something substantial. I am deeply thankful to my thesis supervisor, Dr. Dr.Chandan Kumar Ghosh, for his strong support, patience, and constant availability for technical discussions. Special thanks to my advisor, Dr.Sudipta Goswami, for her continuous support, guidance, andencouragement during my thesis work. I am also grateful to Ph.D. scholars Raushan Kabir and Roshni Begum, whose valuable suggestions, support, and knowledge guided me throughout my research. I would like to thank all the members of the School ofMaterials Science & Nanotechnology at Jadavpur University, Kolkata, for providing me the opportunity to carry out my M.Tech thesis work in a resourceful and supportive research environment. My appreciation also goes tomy fellow lab mates at the Nano Lan, School of Materials Science and Nanotechnology, Jadavpur University, Kolkata, and the Faculty of Engineering and Technology, Jadavpur University, Kolkata, for their moral support throughout my thesis work. Above all, my deepest appreciation goes to my parents for their unwavering faith, unconditional love, support, encouragement, and quiet patience.

Debadrita Bhaduri

School of Materials Science &

Nanotechnology,Jadavpur University,

Kolkata

INDEX

Chapter no.	Subject	Pages
	Abstract	
1.	Introduction	12-13
	1.1 Nanocomposites	13-16
	1.1.1. Types Of Fillers	16-18
	1.1.2. Types Of Nanocomposite	18-21
	1.1.3. Advantages Of Polymer Matrix Nanocomposite	21-22
	1.2 Fundamentals of dielectric properties	22-28
	1.3 Iron Oxides and Geothite	28
	1.3.1 Types	29
	1.3.2 Introduction to Geothite (α-FeOOH)	29-30
	1.3.3 structure	30-31
	1.4 PVDF based nanocomposite thin films	31
	1.4.1 Introduction to PVDF	31-32
	1.4.2. structure	32-33
	1.4.3 Properties	33-34
2.	Objective of the work	36
3.	Literature review	37-39
4.	Spin coating	41
	4.1 Spin coating technique	41-41
	4.2 parts of a spin coater	42
	4.3 Process of Spin coating	42-45
5.	Synthesis of composite	47
	5.1 Synthesis of the Geothite	48-51
	5.1.1. preparation of nano composite	51-52
	5..1.2. Preparation if the ITO substrate	53
	5..1.3. spin coating procedure	53-54

6.	Characterization tools	56
	6.1 XRD	56-57
	6.2 FTIR	57-58
	6.3 UV-VIS	58-60
	6.4 FESEM	60-62
7.	Results and Discussions	64
	7.1 Sample charecterisation	64
	7.1.1 XRD analysis	64-66
	7.1.2 FESEM analysis	66-69
	7.1.3 FTIR analysis	69-71
	7..1.4 UV-VIS analysis	71-72
	7.2 Study of dielectric and analysis	73
	7.2.1 sample preparation	
	7.2.2 Dielectric measurement	
	7.2.3 Magnetic measurement	
8.	Conclusion	80
9.	Future study	81
10.	References	82-86

Sl no.	List of figures	Page no.
1.	Various Dielectric materials used everyday	11
2.	Figure 2 : classification of Nanocomposite	13
3.	Figure: 3 a&b, (3a) Basic structure of nanocomposite & (3B) Interactionzones of nanocomposite	13
4.	Figure 4 : Flowchart for application of nanocomposite	15
5.	Figure 5 : Types of Nanofiller	16
6.	Figure 6 : Types of nanocomposites	17
7.	Figure 7: Schematics of Polymer matrix nanocomposite	19
8.	Figure 8: Applications of Polymer nanocomposite	19
9.	Figure 9 : Polarization of Dielectric Field Figure 9a. (a) Polarization of a paraelectric material is linear with the applied electric field. (b) Schematic of the hysteresis loop associated with ferroelectric behavior. (c) The temperature dependence of the permittivitynear the ferroelectric/paraelectric transition at the Curie temperature.	21
10.	Figure 10 : Frequency response of dielectric mechanisms	23
11.	Figure 11 : Parallel plate capacitor, DC case	24
12	Figure 12 : Availability of Iron Oxides	25
13	Figure 13 : Application of Iron Oxides	25
14	Figure 14 : Types of Iron Oxides	26
15	Figure 15 : Crystal structure of Geothite (Vesta Image)	28
16	Figure 16 : Molecular structure of PVDF	30
17	Figure 17: Flow chart of spin coating	37
18	Figure 18 : Spin coater device	38
19	Figure 19 : Parts of a Spin coater	39
20	Figure 20 : Stages of spin coating	40
21	Figure 21 : Schematics of spin coating	42
22	Figure 22 : a. Ferric chloride , b. NaOH pellets , C. N,N-Dimethyl Formide (DMF), d. PVDF	44
23	Figure 23 : Ferric chloride solution	46
24	Figure 24 : NaoH solution	46
25	Figure 25 : Freshly synthesized Geothite powder	47
26	Figure 26 : Schematic Representation of the synthesis process	47
27	Figure 27 : Schematic Representation of the synthesis process	48
28	Figure 28 : a. DMF, B. PVDF, C. Geothite	49
29	Figure 29: Teflon wrapped ITO Substrate	50
30	Figure 30 : Schematic representation of Spin coating	51
31	Figure 31 : Working of XRD	54
32	Figure 32: Working of FTIR	55
33	Figure 33 : Working of UV-VIS	57
34	Figure 34 : Working of FESEM	59
35	Figure 35 : XRD graph plotted for pure Geothite (α-FeOOH)	61
36	Figure 36 : FESEM images	63
37	Figure 37 : EDX of α-FeOOH	63

38	Figure 38 : EDX of α-FeOOH	64
39	Figure 39: Length and Diameter frequency distribution curves	65
40	Figure 40 : FTIR graph plotted for goethite.	66
41	Figure 41: UV-VIS graph plotted for goethite	67
42	Figure 42 : Direct band gap calculation using Tauc's plot	68
43	Figure 43: Electroded spin coated Ito substrate	70
44	Figure 44 : Impedence Analyzer Kit	71
45	Figure 45 : Graph for Frequency vs Capacitence	72
46	Figure 46 : Cp'vs Frequency	73
47	Figure 47 : Cp"vs Frequency	73
48	Figure 48 : Cp'vs Wt%FeOOH	74
49	Figure 49: VSM Apparatus for Magnetic measurement	75
50	Figure 50: Magnetic Moment Vs Field	77
51	Figure 51: stack plot for all wt%	78

ABSTRACT

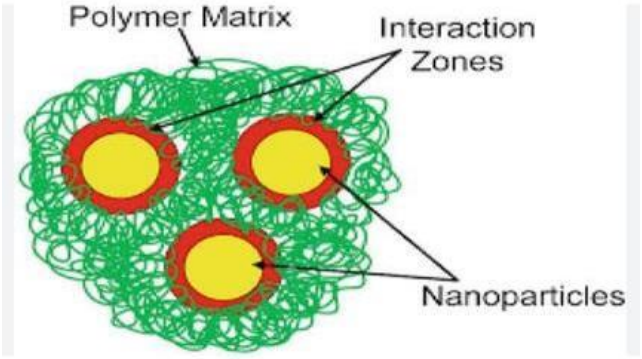
In this study, we have set out with two primary objectives, each targeting specific properties and capabilities of the materials involved. Firstly, our focus rests on the utilization of polyvinylidene fluoride (PVDF) as a pivotal component in device fabrication. PVDF is chosen for its dual advantages: flexibility and ferroelectric properties. Its flexible nature allows for ease of processing and adaptation to various device architectures, while its inherent ferroelectricity adds an extra dimension of functionality, enabling the manipulation of electrical polarization within the material.

Conversely, we turn our attention to goethite, a material renowned for its high surface-to-volume ratio. This characteristic suggests the potential for goethite to possess enhanced capacitance or charge storage capacity. By incorporating goethite into PVDF matrix, we aim to exploit its unique surface properties to augment the charge storage capabilities of the overall device. On the other hand, the magnetic properties of FeOOH nano particles, emerges due to the inherent strain, plays a crucial role on the dielectric behavior of the devices. This integration of a dielectric material, having finite magnetic moment, into a ferroelectric matrix, like PVDF, holds promise for the development of a composite material that not only retains the ferroelectric properties of PVDF but also exhibits improved charge storage performance, thanks to the contribution of goethite.

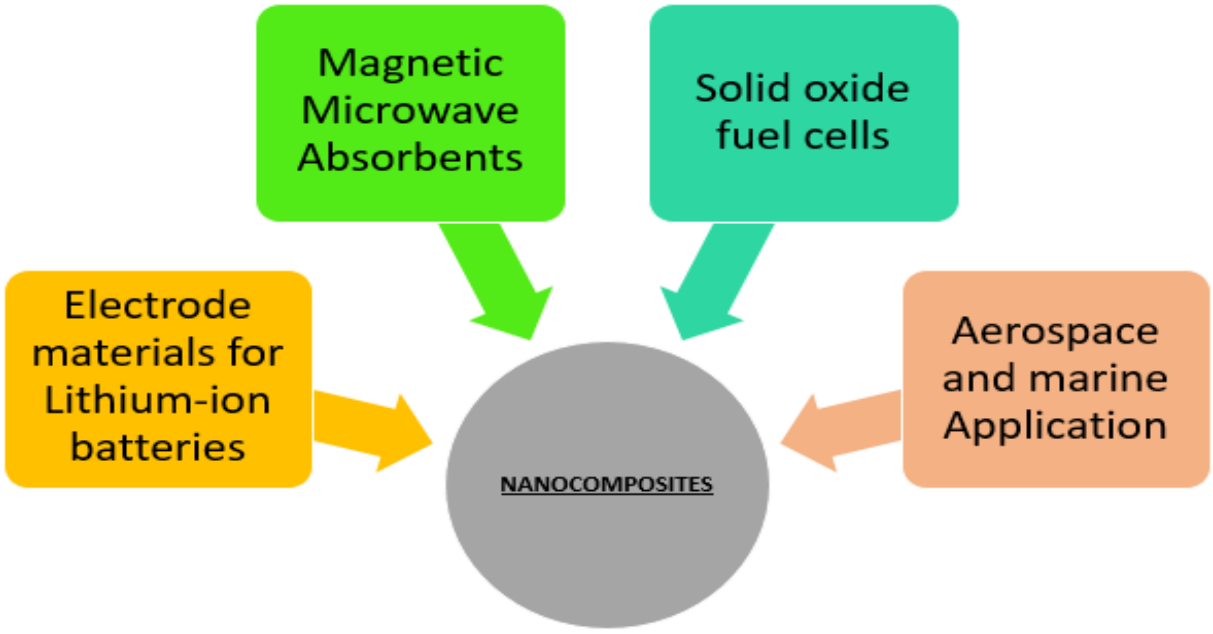
Our investigation goes beyond simply combining materials; we're exploring the potential correlation between magnetic and dielectric properties of PVDF – FeOOH nanocomposite. This correlation could open up new possibilities for device fabrication having magneto dielectric response.

CHAPTER 1

"This chapter discusses the fundamental concepts of Nano composites, including their varieties and applications, as well as an introduction to Dielectric properties, Goethite, and PVDF".



- Nanocomposites
- Fundamentals of Dielectrics
- Iron oxides and Geothite
- PVDF nanocomposite thin films



1. INTRODUCTION

Dielectric materials are essential elements in electrical power equipment and systems, with solid dielectrics serving various functions, including electrical insulation, mechanical reinforcement, and the creation of dielectric barriers. Solid dielectrics typically offer superior insulating capabilities compared to liquids and gases. Nonetheless, their effectiveness is constrained by drawbacks such as low thermal conductivity and the absence of self-repairing characteristics in the material.

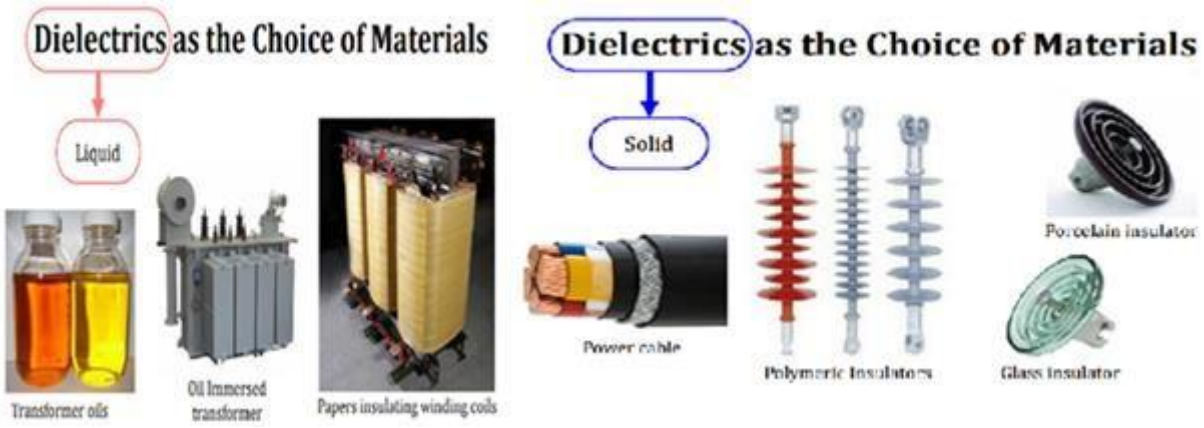


Figure 1 : Various Dielectric materials used everyday

Despite possessing numerous desirable material characteristics, the electrical power industry has faced challenges in fully harnessing the immense potential of polymer insulation (Figure 1). Issues such as the accumulation of space charge at high direct current (DC) fields, a limited operational temperature range, inadequate stiffness, and susceptibility to degradation under various electrical discharges have hindered the widespread adoption of polymer insulation.

In contrast, inorganic oxide materials exhibit superior thermo-mechanical properties compared to polymers, while polymers demonstrate superiority in electrical properties. Over the years, composite structures have emerged as a popular approach for combining the advantageous attributes of host materials and additives. The incorporation of inorganic oxide fillers into polymer matrices is anticipated to enhance the performance of electrical insulation under a range of stresses, including electrical, thermal, mechanical, and environmental conditions.

Determining the dielectric strength of an electrically insulating material stands as a pivotal task in evaluating its electrical properties. Polymer nanocomposites (PNCs) have demonstrated significant potential across a spectrum of scientific and engineering applications. Hence, it is imperative to examine the breakdown characteristics of PNCs to assess their viability as electrical insulators.

PVDF-based homopolymers, renowned as dielectric materials and alternatively referred to as dielectric macromolecules, comprise elongated molecular structures composed of monomers known as vinylidene fluoride (VDF).

Recent advancements in technology suggest that goethite, a mineral primarily composed of iron oxide, may exhibit favorable dielectric properties. These advancements have sparked renewed interest in exploring the electrical characteristics of goethite and its potential applications in various technological domains. Studies indicate that goethite's unique crystal structure and chemical composition contribute to its dielectric behavior, paving the way for innovative uses in fields such as electronics, telecommunications, and energy storage. As researchers delve deeper into understanding the electrical properties of goethite and develop methods to harness its inherent capabilities, the mineral holds promise as a versatile material with exciting possibilities in the realm of modern technology.

1.1. NANOCOMPOSITES

Nanocomposites represent a class of solid materials characterized by the presence of multiple phases, wherein at least one phase possesses one, two, or three dimensions that fall within the nanometer scale range (Figure 2).[1-4] These nanoscale dimensions confer unique properties and functionalities to the material, distinguishing nanocomposites as a versatile and highly promising class of materials for various applications across diverse industries.

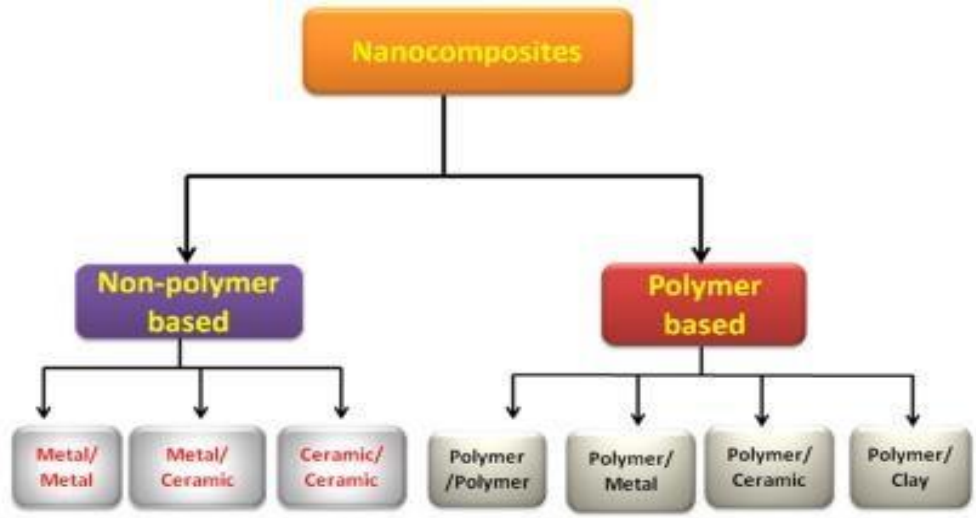


Figure 2 : classification of Nanocomposite

Within the realm of nanocomposites, a wide array of nanomaterials finds application, including nanoparticles, nanofibers, and nanoclays. These nanoscale constituents contribute to the enhanced mechanical, electrical, thermal, and optical properties exhibited by nanocomposite materials.

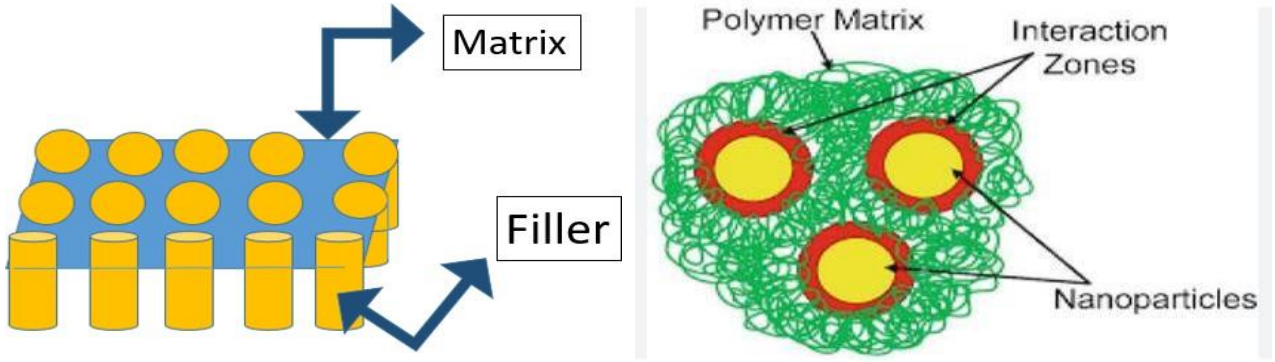


Figure: 3 a&b, (3a) Basic structure of nanocomposite & (3B) Interaction zones of nanocomposite

Nanoparticles, typically ranging from 1 to 100 nanometers in size, are discrete units with high surface area-to-volume ratios, enabling tailored surface functionalities and interactions within the composite matrix (Figure 3). Nanofibers, elongated structures with diameters in the nanometer range, offer exceptional mechanical strength, flexibility, and aspect ratios, thereby reinforcing the structural integrity of nanocomposite materials. Nanoclays, consisting of nanometer-sized layers stacked together, provide barrier properties, flame retardancy, and improved mechanical performance due to their high aspect ratio and surface chemistry.

The incorporation of these nanomaterials into composite matrices allows for precise control over material properties and performance characteristics, facilitating the development of advanced materials with tailored functionalities and enhanced performance metrics. Additionally, the synergistic interactions between the nanoscale constituents and the matrix material further amplify the beneficial properties of nanocomposites, unlocking novel applications in fields such as aerospace, automotive, electronics, biomedical engineering, and environmental remediation.

Moreover, the scalable synthesis and processing techniques available for nanocomposite fabrication enable the production of materials with tailored compositions, morphologies, and architectures to meet specific application requirements. As research in nanocomposite materials continues to advance, the integration of nanotechnology into diverse industrial sectors holds immense potential for revolutionizing material design, manufacturing processes, and technological innovation.

Properties of material changes when the material constituent size is under a particular level, known as 'critical size'. A Nanocomposite is composed of two main components – Matrix and Filler.

The factors responsible for the application of nanocomposite in various fields are –

a. MULTIFUNCTIONALITY-
   One of the most useful property of nanocomposite is its multifunctionality and the ability to retain the properties of boyh the matric and the filler.

b. SMALL FILLER SIZE – The small size of the filler aims to high surface to volume ratio and small distance between the fillers.

c. MECHANICAL PROPERTIES- often increases the ductility with out increasing the strength (eg, - scratch resistance)

d. OPTICAL PROPERTIES - light transmission charecteristics are particle size dependent.

- **APPLICATION OF NANOCOMPOSITE**

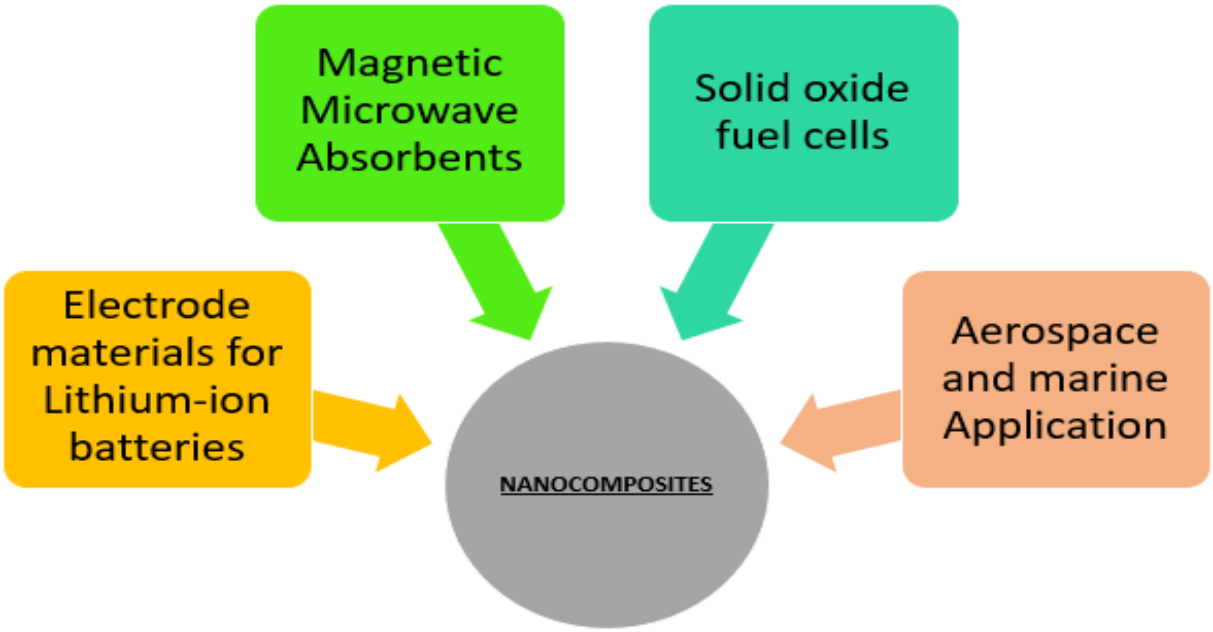


Figure 4 : Flowchart for application of nanocomposite

1.1.1. TYPES OF NANOSCALE FILLERS

Nanoscale fillers, marvels of modern materials science, come in diverse forms and sizes, each with unique properties. When integrated into polymer matrices, they create ultra-large interfacial regions, profoundly altering material properties. This synergy enhances mechanical strength, stiffness, and thermal conductivity. Nanofillers enable a range of innovations, from lightweight structural components to flexible electronics and advanced biomaterials [5-8]. Challenges include achieving optimal dispersion and ensuring compatibility. Despite these hurdles, the transformative potential of nanoscale fillers is undeniable, promising revolutionary advancements in technology and manufacturing. as shown in figure 5.

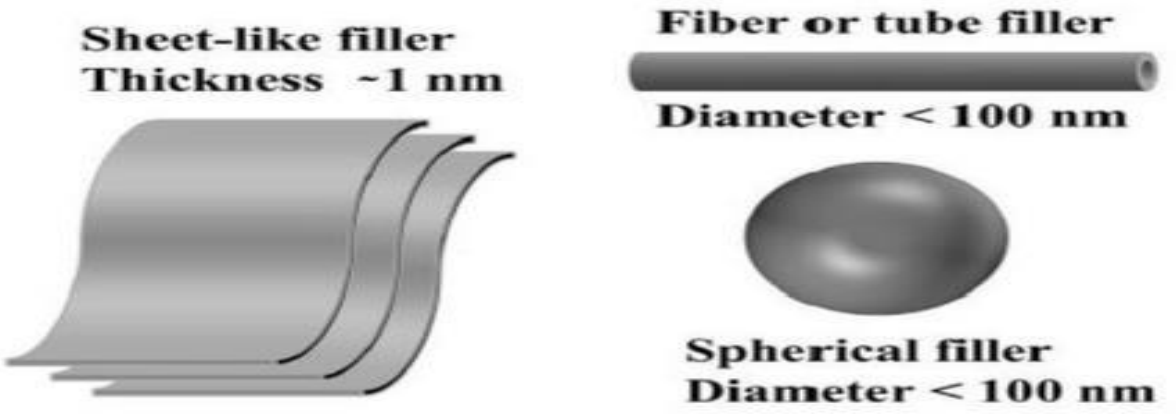


Figure 5 : Types of Nanofiller

- **Sheet-like nanoscale fillers**
  Sheet-like nanoscale fillers, like graphene and layered clays, are gaining attention in nanotechnology and materials science for their unique properties. Graphene, composed of a single layer of carbon atoms, offers exceptional strength and conductivity, making it useful in various fields such as aerospace engineering and energy storage. Layered clays, like montmorillonite, can enhance mechanical and barrier properties in composite materials. Additionally, other two-dimensional materials like transition metal dichalcogenides show promise in electronics and catalysis. Research focuses on synthesizing and modifying these fillers to optimize their performance in diverse applications, promising advancements in fields like energy, electronics, and healthcare.

- **Nanotubes and nanofibers and nano rods**
  Nanotubes, nanofibers, and nano rods are captivating nanomaterials with elongated structures that hold immense potential across diverse fields. Carbon nanotubes, including single-walled and multi-walled varieties, offer exceptional strength and conductivity, promising advancements in electronics and composite materials. Meanwhile, nanofibers, produced through techniques like electrospinning, offer high surface area for applications in filtration and tissue engineering. Nano rods, such as metal and semiconductor variants, exhibit unique properties useful in sensing, photovoltaics, and more. Research focuses on optimizing their properties and compatibility with matrices, paving the way for innovative solutions in various industries.

- **Nanoscale spherical fillers**

Nanoscale spherical fillers, with their tiny size and spherical shape, are incredibly versatile materials that have attracted considerable attention in nanotechnology and materials science. These engineered nanoparticles, spanning various materials like metals, semiconductors, and polymers, offer unique properties and find applications in diverse fields. They include metallic nanoparticles with fascinating optical and catalytic properties, semiconductor nanoparticles with tunable electronic properties, and polymeric nanoparticles used in drug delivery and imaging. Additionally, naturally occurring and synthetic microspheres, such as silica and polymer microspheres, serve in drug delivery, cosmetics, and diagnostics. Research focuses on refining their properties through surface modification and precise synthesis techniques to optimize their performance in various applications. Overall, nanoscale spherical fillers represent a dynamic class of materials with broad utility, driving innovation in electronics, healthcare, and consumer products.

1.1.2. TYPES OF NANOCOMPOSITES

Nanocomposite materials can be divided into three groups, similar to micro composites, based on their matrix materials : Metal, Polymer and Ceramic Matrix Nanocomposites (MMNC, PMNC and CMNC) [10-12].

By categorizing nanocomposites based on their matrix materials, researchers and engineers can tailor the properties of these materials to suit specific application requirements. Moreover, understanding the nuances of each nanocomposite category facilitates the development of innovative manufacturing techniques and processing methods aimed at harnessing the full potential of these remarkable materials.

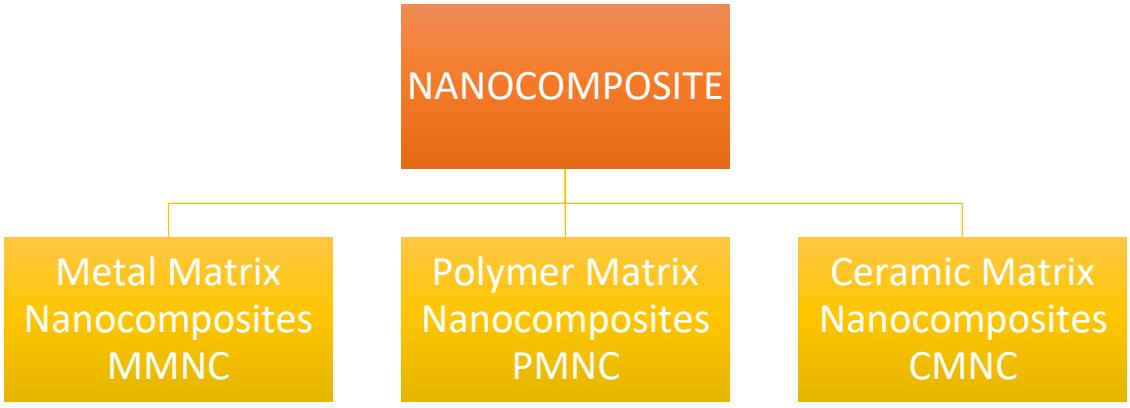


Figure 6 : Types of nanocomposites

a. Metal Matrix Nanocomposites MMNC

Metal matrix composites (MMCs) [13-15], akin to other composite materials, consist of a minimum of two phases with distinct physical and chemical properties dispersed in such a manner that they confer properties unattainable by either phase alone. Typically, these composites feature two phases within a metallic matrix: a fibrous or particulate phase. For instance, in applications like power transmission lines, MMCs are fabricated using an aluminum matrix reinforced with continuous $A1_2O_3$ fibers. Similarly, cutting tools and oil drilling inserts often comprise cobalt (Co) particulates and tungsten carbide (WC). Additionally, composites employing aluminum matrix reinforced with SiC particles find use in automotive, thermal management, and aerospace sectors.

Nano composite MMNCs represent a subtype of these materials, featuring a ductile alloy or metal matrix integrated with nanoscale reinforcing agents. Combining ceramic and metallic attributes such as toughness, ductility, high modulus, and strength, these materials are particularly adept at withstanding elevated service temperatures and shear/compression forces. Consequently, they hold immense promise across various fields, including automotive and aerospace industries, as well as in the manufacturing of structural materials.

b. Ceramic Matrix Nanocomposites CMNC

Ceramic matrix nanocomposites (CMNCs) [16-19], particularly those based on the aluminum oxide (Al2O3)/silicon carbide (SiC) system, hold significant promise. Extensive research has demonstrated that the addition of a low volume fraction (approximately 10%) of SiC, with specific sizing for the Al2O3 matrix, yields notable enhancements in matrix properties. Certain studies have attributed this improvement to the crack-bridging function of nanoscale reinforcements, elucidating a toughening mechanism.

By incorporating high-strength nanofibers into ceramic matrices, novel nanocomposites exhibiting superior failure resistance and heightened toughness have been developed, contrasting with the rapid failure observed in conventional ceramic materials. Various methodologies have been employed in the preparation of ceramic matrix nanocomposites. These include conventional powder methods, vapor techniques (such as CVD and PVD), spray pyrolysis, polymer precursor routes, and chemical methods encompassing colloidal and precipitation procedures, c template synthesis, and the sol-gel process, which are widely utilized for micro composites.

The sol-gel process, in particular, offers considerable versatility, with numerous factors influencing its outcome, including solvent type, duration, pH, water-to-metal ratio, precursor material, and more. This comprehensive control permits fine-tuning of the structure and chemical properties of the resulting material.

c. Polymer Matrix Nanocomposites PMNC

The most prevalent variety of nanocomposite is PMNC [20-25], comprising nano-scale particles dispersed evenly within a polymer in an ideal scenario (Figure 7). However, in practical applications, the polymer matrix is utilized to disperse agglomerated nanoparticles. Functional nanocomposites, endowed with superior physical properties, unlock novel opportunities in micro-optics, electronics, energy conversion, and storage (Figure 8). Typically, the extent of filler loading correlates with the alteration in the desired characteristic. Nonetheless, the flow characteristics of composites impose limitations on the incorporation of high solid loads due to shape or molding constraints, thereby influencing property modifications.

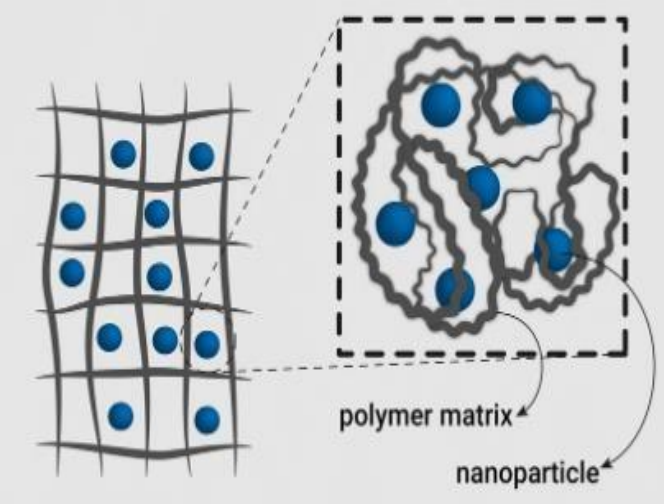


Figure 7: Schematics of Polymer matrix nanocomposite

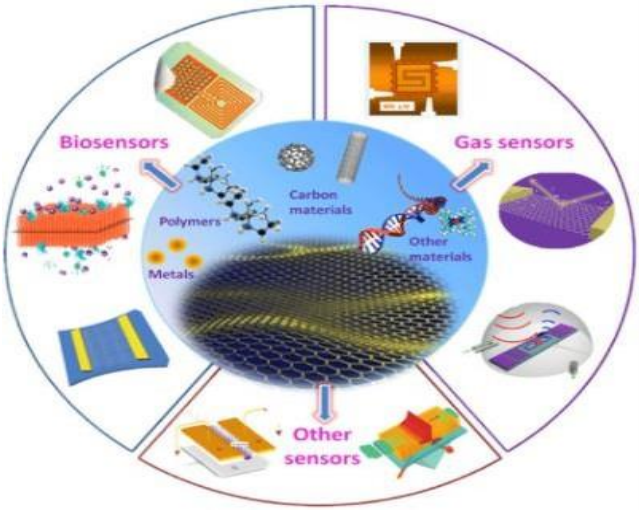


Figure 8: Applications of Polymer nanocomposite

Prior to the composite forming process, it is imperative to assess rheological properties (flow properties) through various tests to determine the appropriate shear rate and temperature. The rheological behavior is influenced by factors such as surface area and the resultant extensive polymer-filler interfacial layer. Polymer nanocomposites have heralded a new frontier in hybrid materials by integrating particle nanofillers into polymer matrices to enhance the properties of pristine polymers. Over the past decade, polymer nanocomposites have garnered considerable attention worldwide, with the sol-

gel process emerging as the most promising fabrication method. This technique ensures the dispersion of nanoparticles at the molecular or near-molecular level before integration with the polymer gel.

1.1.3. ADVANTAGES OF POLYMER MATRIX NANOCOMPOSITE

Polymer matrix nanocomposites offer a plethora of advantages that make them highly desirable materials across various industrial and technological domains [23]. Among these advantages are:

1. Mechanical and electrical conductivity: Polymer nanocomposites exhibit enhanced mechanical properties, such as stiffness, strength, and toughness, owing to the addition of nanofillers. Furthermore, certain nanofillers can impart electrical conductivity to the composite, expanding its utility in applications requiring electrical conduction.

2. Structural and thermal stability: The incorporation of nanofillers enhances the structural integrity and thermal stability of polymer matrices, making nanocomposites suitable for use in high-temperature environments and structural applications that demand robustness and durability.

3. Low density and permeability: Polymer nanocomposites typically possess lower densities compared to traditional materials, rendering them lightweight and ideal for applications where weight reduction is critical. Additionally, nanofillers can reduce the permeability of polymers, making nanocomposites suitable for barrier applications in packaging and gas storage.

4. Corrosion resistance: Nanocomposites often exhibit superior resistance to corrosion and degradation compared to pure polymers, making them suitable for use in harsh environments where exposure to corrosive agents is a concern.

5. Noise damping: Certain nanofillers incorporated into polymer matrices have the ability to dampen vibrations and reduce noise, making nanocomposites valuable in applications where noise reduction is essential, such as automotive and aerospace industries.

6. Low filler content: Polymer nanocomposites can achieve significant enhancements in properties with relatively low filler content compared to traditional composite materials, resulting in cost savings and improved processability.

7. Ease of manufacturing: The fabrication of polymer nanocomposites is often compatible with conventional polymer processing techniques, such as extrusion, injection molding, and solution casting, facilitating seamless integration into existing manufacturing processes.

By leveraging these advantageous properties, polymer matrix nanocomposites offer innovative solutions to address a wide range of technological challenges and enable the development of advanced materials for diverse applications.

1.2. FUNDAMENTALS OF DILELECTRIC PROPERTIES

A dielectric material is characterized by its non-metallic nature, exhibiting high specific resistance, a negative temperature coefficient of resistance, and a significant insulating resistance. Alternatively, it can be defined as a non-conductive substance capable of retaining electrical charges. When subjected to an electric field, a dielectric material does not conduct electric charges through its volume. Instead, the electric charges undergo a slight displacement from their average equilibrium positions, resulting in dielectric polarization [26].

Dielectric polarization induces the movement of positive charges towards the direction of the electric field, while negative charges shift in the opposite direction as shown in t figure 9 . This phenomenon generates an internal electric field, effectively mitigating the overall electric field strength within the dielectric material.The electric susceptibility of a dielectric material quantifies its susceptibility to polarization when exposed to an electric field, providing insight into how readily the material can be polarized.

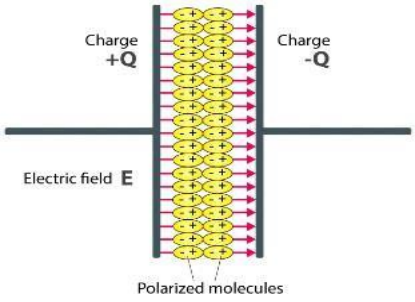


Figure 9 : Polarization of Dielectric Field

- **MATERIAL PROPERTIES OF DIELECTRICS**

All materials have an absolute measure of permittivity (ε), and also a relative permittivity (ε_r) which is measured relative to that of vacuum which is measured relative to that of vacuum (ε_0=8.854 x 10^{12} F/m):

$$\varepsilon_r = \frac{\varepsilon}{\varepsilon_0}$$

The values of ε_r vary across different materials, spanning from 1 to 10 for many plastics, 10 to 100 for polar solvents like water (crucial for magnetic resonance applications), and from 100 to several thousand for inorganic compounds such as perovskites. Certain specialized materials exhibit exceptionally high permittivity, exceeding 10,000, known as "giant permittivity." Permittivity is a complex property with both real (ε') and imaginary (ε") components, often dependent on temperature and frequency. A dielectric material has the ability to store energy under an external electric field. When subjected to such fields, small displacements or reorientations of atoms/ions occur within the material, resulting in polarization. The extent to which a material can be polarized is quantified by its permittivity or dielectric constant.

- **Paraelectric, Ferroelectric and Piezoelectric Properties of Dielectrics**

Dielectric materials can be categorized further as paraelectric, ferroelectric, and/or piezoelectric. In paraelectric materials, polarization occurs in response to an external electric field, but this polarization isn't retained once the field is removed (illustrated in Figure 4(a)). Any change in ionic displacement returns to its original state when the electric field is switched off. Conversely, in ferroelectric materials, polarization persists even after the electric field is removed, exhibiting a hysteresis effect in polarization (as depicted in Figure 4(b)). The applied electric field organizes the permanent electric dipoles into domains within the material and aligns these domains, resulting in significant polarization. When the electric field reaches a sufficient strength, the material becomes saturated, with all dipoles fully aligned.

Many dielectrics can exist in either paraelectric or ferroelectric states, depending on the temperature relative to the Curie temperature (Tc). Above Tc, a material behaves paraelectrically, while below Tc, it exhibits ferroelectric properties. The permittivity of the material changes rapidly in proximity to the

Curie temperature, as shown in Figure 4(c). Ferroelectric materials, such as barium titanate (discussed in the subsequent section), are typically crystalline and possess high permittivities (often exceeding 1,000), which are significantly influenced by temperature and frequency. It's important to note that the term "ferro-" is a historical misnomer, as most ferroelectric materials do not contain iron. Paraelectric materials have lower permittivities that remain relatively constant across temperature and frequency changes. Examples include tantalum oxide ($\varepsilon_r = 23$) and niobium oxide ($\varepsilon_r = 40$).

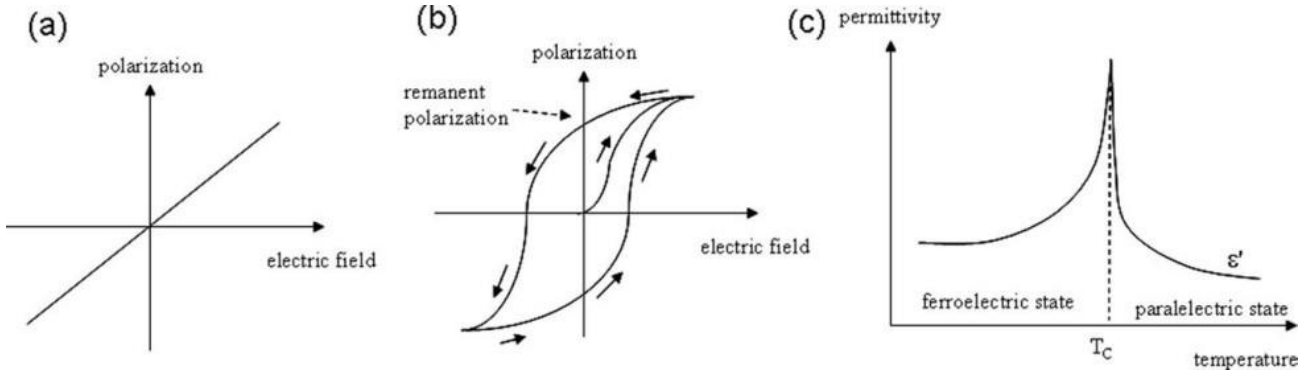


Figure 9a. (a) Polarization of a paraelectric material is linear with the applied electric field. (b) Schematic of the hysteresis loop associated with ferroelectric behavior. (c) The temperature dependence of the permittivity near the ferroelectric/paraelectric transition at the Curie temperature.

- **CURRENT IN CAPACITORS**

  Dielectric materials find widespread application in capacitors. Capacitors serve as a straightforward means to introduce the notion of complex permittivity. In the typical scenario where a capacitor is charged by a voltage source along with its accompanying charging current:

$$Q = CV = \frac{\varepsilon_r \varepsilon_0 A}{d} V$$

  In this context, Q represents the stored charge, A denotes the cross-sectional area of the parallel plates, d stands for the distance between the plates, and V represents the charging voltage. A material characterized by high permittivity results in a significant stored charge for a given driving voltage, as depicted in Figure 9.

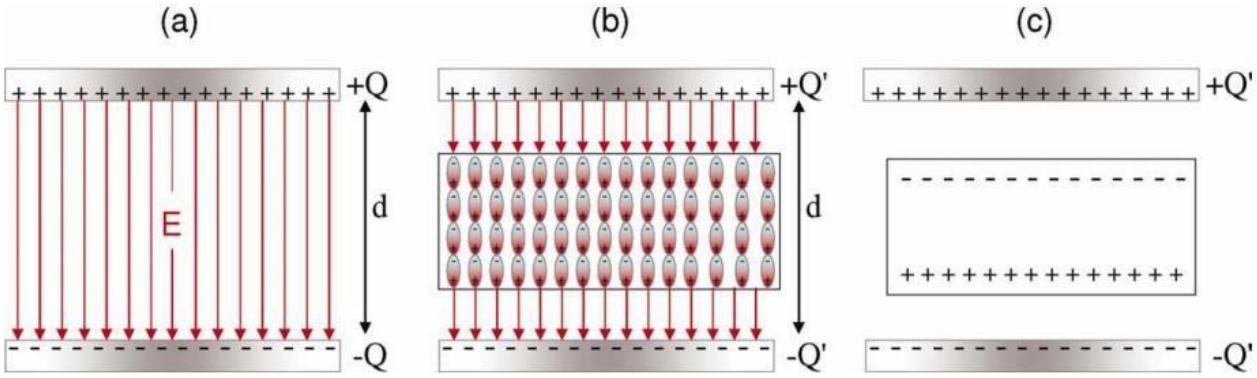


Figure 9 (a) A parallel plate capacitor with air between the two plates. There is a large electric field between the two plates. (b) The same capacitor with a high permittivity material sandwiched in between the plates. (c) The net effect of the dielectric material is to reduce the electric field by a factor ε_r.

- **Dielectric Mechanisms**

A material's overall permittivity is influenced by multiple dielectric mechanisms or polarization phenomena. Within a dielectric material, there exists an arrangement of electric charge carriers capable of being displaced under the influence of an electric field. [26-30] These charges undergo polarization to counteract the applied electric field, resulting in the movement of positive and negative charges in opposing directions.

At the microscopic level, various dielectric mechanisms contribute to the material's dielectric behavior. Notably, dipole orientation and ionic conduction play significant roles, particularly at microwave frequencies. For instance, water molecules exhibit permanent dipoles that align and rotate in response to alternating electric fields, a phenomenon responsible for the heating of food in microwave ovens.

These mechanisms, however, are inherently lossy, leading to energy dissipation. Atomic and electronic mechanisms, while comparatively weaker, remain relatively constant across the microwave frequency range. Each dielectric mechanism possesses a characteristic "cutoff frequency," beyond which its contribution diminishes as faster mechanisms become predominant.

As frequency increases, slower mechanisms gradually diminish in influence, allowing faster mechanisms to dominate and contribute to the material's permittivity (ε'). Correspondingly, the loss factor (ε'' or er'') exhibits peaks at critical frequencies associated with each dielectric mechanism. The magnitude and cutoff frequency of each mechanism vary among different materials.

For example, water exhibits a pronounced dipolar effect at lower frequencies, but its dielectric constant declines sharply around 22 GHz. In contrast, materials like PTFE lack

dipolar mechanisms, resulting in a remarkably consistent permittivity extending into the millimeter-wave region.

Resonant effects typically accompany electronic or atomic polarization, while relaxation effects are associated with orientation polarization. Understanding these dielectric mechanisms and their frequency-dependent behavior is crucial for tailoring material properties and optimizing performance across a range of applications.

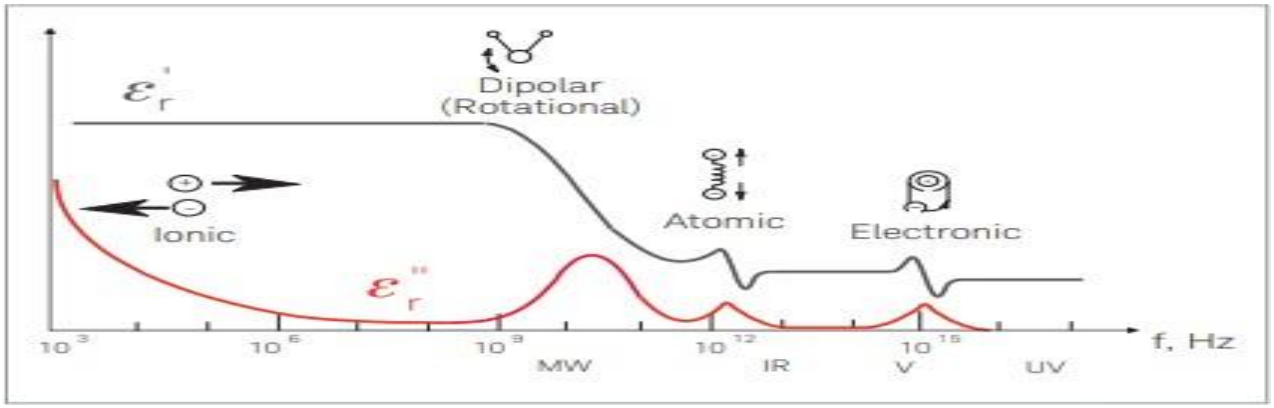


Figure 10 : Frequency response of dielectric mechanisms

- **Dielectric constant**

A substance earns the designation of "dielectric" when it possesses the capability to accumulate energy upon the application of an external electric field. In the scenario of a parallel plate capacitor subjected to a direct current (DC) voltage source, the presence of a dielectric material between the plates results in a greater accumulation of charge compared to an absence of material (i.e., a vacuum) between the plates. This is attributable to the dielectric material's capacity to enhance the capacitor's storage capability by counteracting charges at the electrodes that would typically contribute to the external field.

The dielectric constant depends on various factors such as:

- Frequency: The frequency of the applied voltage is one of the factors affecting dielectric constant. As the frequency of the applied voltage increases, the value of the dielectric constant becomes non-linear.
- Applied voltage: When a direct current voltage is applied, the value of the dielectric constant reduces while applying alternating current voltage would increase the value of the dielectric constant.

- Temperature: At low temperatures, aligning molecules in dielectric materials is challenging. As temperature rises, dipole moments become dominant, increasing the dielectric constant until reaching the transition temperature. Above this point, the dielectric constant gradually decreases.
- Humidity and moisture: The strength of the dielectric material decreases when either the humidity or the moisture is increased.
- Heating effect: Dielectric loss occurs when a dielectric material is heated, resulting in the dissipation of energy in the form of heat due to molecular movement induced by alternating current voltage. This phenomenon occurs as the material absorbs electrical energy.
- The structure and morphology of the material also influence the dielectric constant.
- Deterioration and weathering of the material also affect the dielectric constant.

Essentially, the dielectric material serves to augment the capacitance of the capacitor, a property directly influenced by its dielectric constant. When a DC voltage source, denoted as V, is applied across a parallel plate capacitor, the presence of a dielectric material between the plates leads to a heightened charge storage capacity in comparison to the scenario where the plates are separated solely by a vacuum, as illustrated in Figure bellow.

$$C_0 = \frac{A}{t}$$
$$C = C_0 \kappa'$$
$$\kappa' = \varepsilon_r' = \frac{C}{C_0}$$

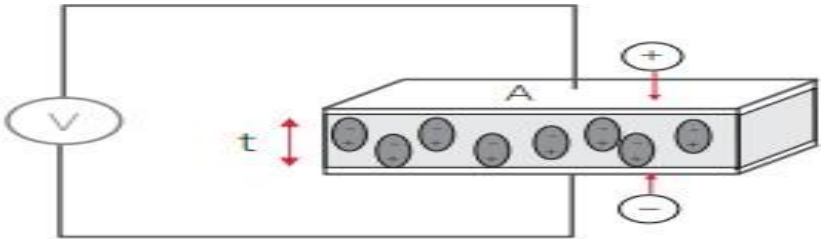


Figure 11 : Parallel plate capacitor, DC case

Where C and C0 are capacitance with and without dielectric, κ’ = ε’r is the real dielectric constant or permittivity, and A and t are the area of the capacitor plates and the distance between them. The dielectric material increases the storage capacity of the capacitor by neutralizing charges at the electrodes, which ordinarily would contribute to the external field. The capacitance of the dielectric material is related to the dielectric constant as indicated in the above equations.

Dielectric constant (k) is equivalent to relative permittivity (ε_r) or the absolute permittivity (ε) relative to the permittivity of free space (ε0). The real part of permittivity (εr ’) is a measure of how much energy from an external electric field is stored in a material. The imaginary part of permittivity (εr ’’) is called the loss factor and is a measure of how dissipative or lossy a material is to an external electric field. The imaginary part of permittivity (εr ”) is always greater than zero and is usually much smaller than (εr ’). The loss factor includes the effects of both dielectric loss and conductivity.

1.3. IRON OXIDES

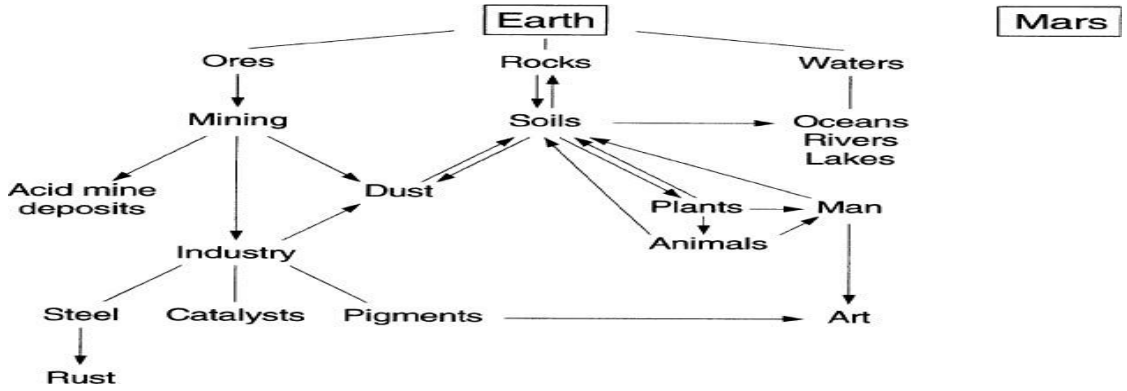


Figure 12 : Availability of Iron Oxides

Iron oxides, abundant in nature and labs, shape Earth systems. Present in air, soil, organisms, water, and rocks, they influence vital processes like aerosol formation, soil coloration, metabolism, and water quality. Their aerobic weathering from magmatic

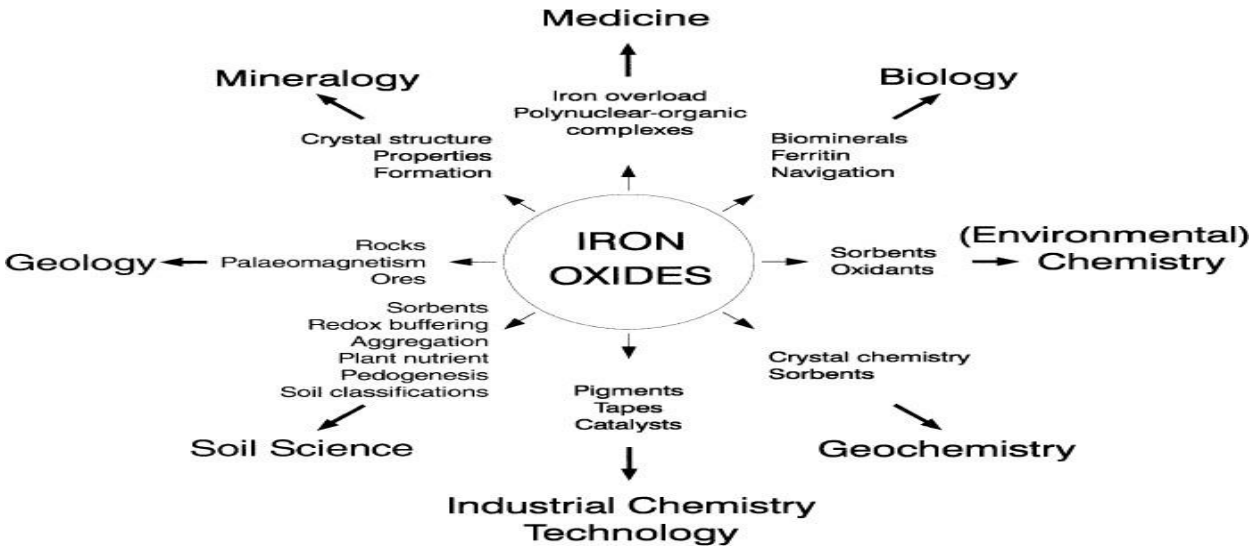


Figure 13 : Application of iron oxides

rocks forms stable, colorful iron(III) oxides, crucial for sustaining life and ecological balance. Understanding their behavior is key for broader ecological and geological understanding. Valuable in industry and environmental remediation, they act as efficient pollutant sorbents due to their catalytic activity and high energy of crystallization.

1.3.1. TYPES OF IRON OXIDES

Oxide–hydroxides and hydroxides	*Oxides*
Goethite α-FeOOH	Hematite α-Fe_2O_3
Lepidocrocite γ-FeOOH	Magnetite Fe_3O_4 ($Fe^{II}Fe^{III}_2O_4$)
Akaganéite β-FeOOH	Maghemite γ-Fe_2O_3
Schwertmannite $Fe_{16}O_{16}(OH)_y(SO_4)_z \cdot n\ H_2O$	β-Fe_2O_3
δ-FeOOH	ε-Fe_2O_3
Feroxyhyte δ′-FeOOH	Wüstite FeO
High pressure FeOOH	
Ferrihydrite $Fe_5HO_8 \cdot 4\ H_2O$	
Bernalite $Fe(OH)_3$	
$Fe(OH)_2$	
Green Rusts $Fe^{III}_x Fe^{II}_y(OH)_{3x+2y-z}(A^-)_z$; $A^- = Cl^-$; ½ SO_4^{2-}	

Figure 14 : Types of Iron Oxides

We will be working with Geothite in particular.

1.3.2. INTRODUCTION TO GEOTHITE (α-FeOOH)

Goethite, chemically known as α-FeOOH, stands as a ubiquitous presence in geological formations and diverse ecosystems worldwide [32]. Its structural configuration aligns with the diaspore structure, which is rooted in hexagonal close packing, defining its crystalline arrangement. Renowned for its stability, particularly at ambient temperatures, goethite frequently emerges as either the initial product or the ultimate endpoint in various geological transformations. When encountered in extensive crystal aggregates, its appearance tends toward dark brown or black hues, contrasting starkly with the yellowish tint it manifests when encountered in powdered form. This distinct coloration exerts a significant influence on the visual aesthetics of rocks, soils, and ochre deposits, shaping the landscapes in which it resides.

Beyond its geological significance, goethite assumes notable industrial importance as a valued pigment, contributing to a spectrum of applications across diverse sectors. Its pigmentation properties find extensive utilization in paints, coatings, and dyes,

where its inherent color characteristics impart vibrant hues and enhance visual appeal. Moreover, its chemical stability and compatibility with various substrates render it a preferred choice in the formulation of durable and long-lasting colorants for architectural, automotive, and artistic applications.

The nomenclature of goethite pays homage to the esteemed German polymath Johann Wolfgang von Goethe, who, in 1815, garnered recognition for his contributions to numerous fields, including literature, science, and philosophy. Through the designation of this mineral in his honor, the scientific community commemorates Goethe's enduring legacy and enduring impact on the realms of knowledge and inquiry.

In essence, goethite emerges as not merely a mineral of geological significance but also a substance of profound industrial utility and historical resonance, embodying a synthesis of natural beauty, scientific intrigue, and cultural heritage. Its enduring presence across geological formations and cultural contexts underscores its enduring relevance and multifaceted significance in the tapestry of human experience.

1.3.3. STRUCTURE OF GOETHITE

The structure of goethite is orthorhombic and each iron atom has six octahedrally distributed Oxygen and hydroxyl neighbors in an almost perfect hexagonal close packing with the 6-folded coordinated Fe atoms occupying the octahedral position (Figure 15). The Fe atoms are arranged in double rows to form what can be described as double chains of Octahedra running the length of the c-axis , while the bond between the double chains consists of relatively weak hydrogen bonding directed through the apical oxygen ions along the x-axis [32].

Geothite also has an interesting structure containing more than one type of hydroxyl group wthin its structure. According to Russel et al.,the Goethite structure contains condensed strips of Fe(O,OH) octahedral involving OH groups shared between three Fe(III) ions along its crystallographic [001] direction. These gives rise to triply coordinated hydroxyl groups ($\mu_3 - OH$) within the structure of Geothite and are referred to as ‘bulk’ hydroxyls. However on the surface there are two additional hydroxyl groups which are simply (-OH) and double (μ-OH) coordinated as well.

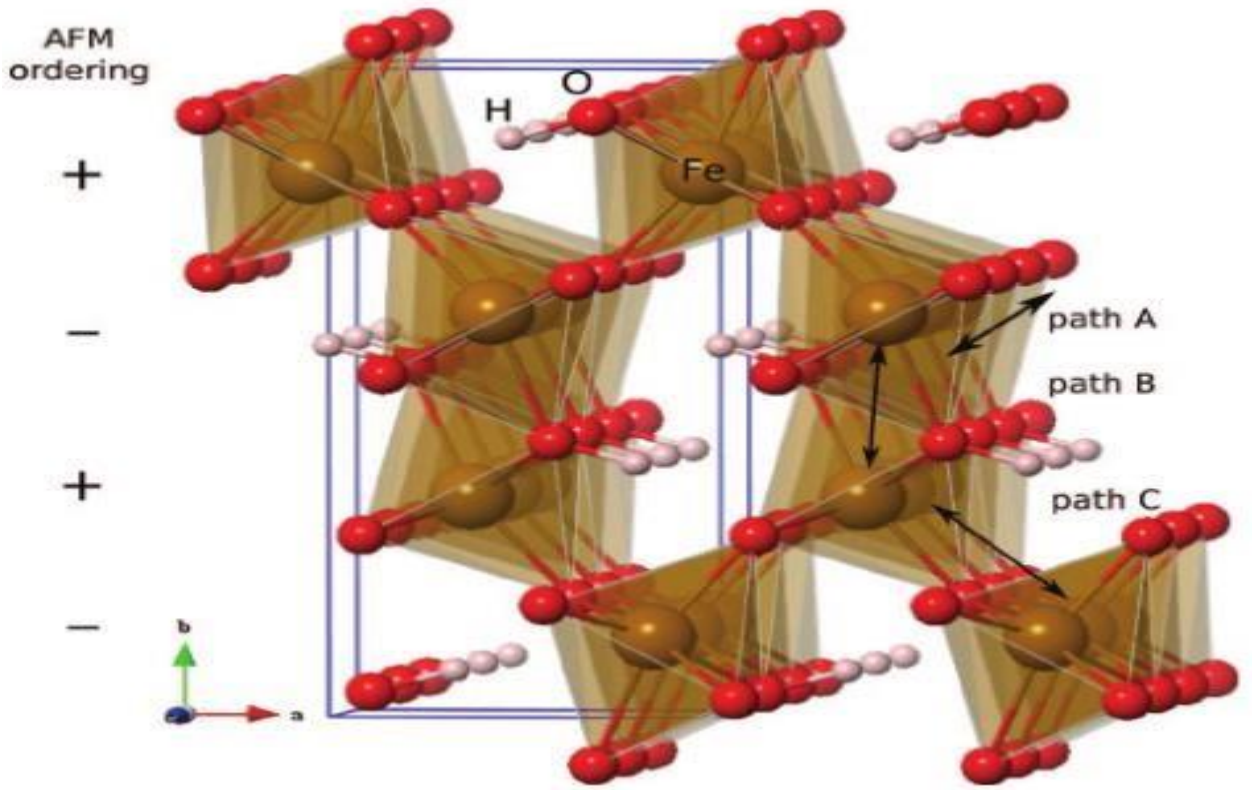


Figure 15 : Crystal structure of Geothite (Vesta Image)

1.4. PVDF BASED NANOCOMPOSITE THIM FLIMS

1.4.1. INTRODUCTION TO POLYVINYLIDENE FLUORIDE (PVDF)

Polyvinylidene fluoride, also known as PVDF, is a specialized thermoplastic fluoropolymer formed through the polymerization of vinylidene difluoride. Its chemical composition is represented by $(C_2H_2F_2)n$ [33-35].

This material is particularly valued for its exceptional purity and its ability to withstand solvents, acids, and hydrocarbons. With a relatively low density of 1.78 g/cm3 compared to other fluoropolymers like polytetrafluoroethylene, PVDF finds extensive use in various industries.

PVDF is found in a range of forms including piping products, sheets, tubing, films, plates, and insulation for premium wires. Its versatility extends to being injectable, moldable,

and weldable, making it a popular choice in industries such as chemicals, semiconductors, medicine, defense, and lithium-ion batteries.

Moreover, PVDF is available as a closed-cell foam, increasingly utilized in aviation and aerospace, and as a filament for 3D printing. Its FDA compliance and non-toxic properties below its degradation temperature make it suitable for repeated contact with food.

In addition to its industrial applications, PVDF serves as a key ingredient in high-end metal paints renowned for their excellent gloss and color retention. Notable structures worldwide, including the Petronas Towers and Taipei 101, feature coatings made with PVDF paints.

Furthermore, PVDF membranes play a crucial role in western blots for protein immobilization, owing to their non-specific affinity for amino acids.

Beyond these uses, PVDF serves as a binder component for carbon electrodes in supercapacitors and various other electrochemical applications.

1.4.2. STRUCTURE OF POLYVINYLIDENE FLUORIDE (PVDF)

PVDF stands as a renowned and highly inert fluoropolymer, characterized by its molecular formula $-(CH_2CF_2)_n-$. Illustrated in Figure 16, its chemical structure reveals a monomer unit composed of two carbon-hydrogen pairs and two fluorine atoms, $-CH_2CF_2-$, with its polymerization initially proposed in 1948 [36].

This straightforward chemical makeup contributes to PVDF's robustness and resilience, evident in its impressive tensile strength and impact resistance. Notably, PVDF exhibits exceptional resistance against both creep and fatigue. In applications involving thin sections like films, filaments, and tubing, PVDF displays flexible behavior and transparency.

Beyond these attributes, PVDF boasts a range of outstanding properties, including a high dielectric constant, remarkable strength, thermal stability, chemical inertness, UV resistance, resilience to nuclear radiation, and durability against weathering. Furthermore, PVDF can adopt various molecular crystal structures, influenced by the sample preparation method, thereby enabling the polymer to manifest diverse forms.

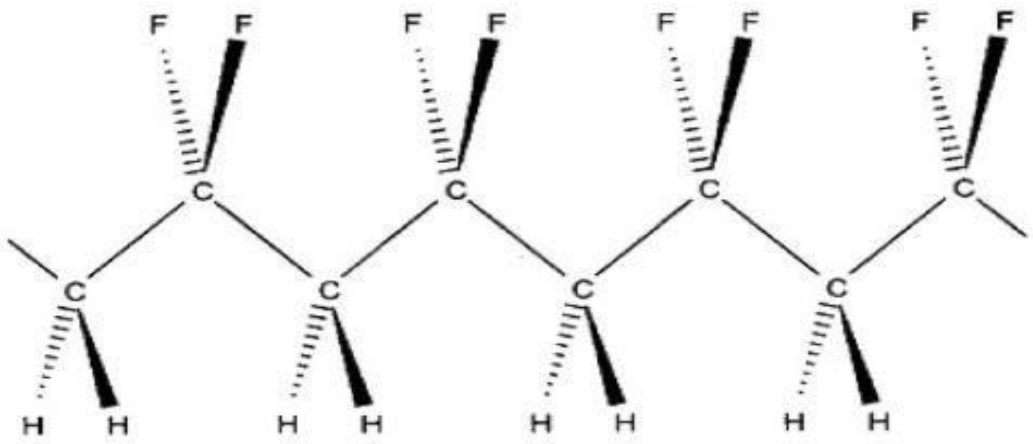


Figure 16 : Molecular structure of PVDF

1.4.3. PROPERTIES OF PVDF

In 1969, PVDF exhibited robust piezoelectricity, with poled thin films demonstrating a piezoelectric coefficient of approximately 6–7 pC/N. This measurement surpassed that of any other polymer by a factor of 10 [37].

PVDF possesses a glass transition temperature (Tg) of around −35 °C and typically exhibits 50–60% crystallinity. To impart its piezoelectric attributes, the material undergoes mechanical stretching to align molecular chains, followed by poling under tension. PVDF exists in various phases determined by chain conformations, such as trans (T) or gauche (G) linkages: α and δ phases adopt a TGTG' pattern, β phases feature TTTT arrangement, while γ and ε phases exhibit TTTGTTTG' conformation. The α and ε conformations lack piezoelectric properties due to antiparallel dipole alignment within the unit cell, whereas the β, γ, and δ phases display a polar crystal structure with a non-zero dipole moment, with the β phase being particularly notable for its significant remnant polarization and highest dipolar moment per unit cell, attracting more attention than other phases. When poled, PVDF becomes a ferroelectric polymer, showcasing efficient piezoelectric and pyroelectric characteristics. These qualities render it valuable in sensor and battery applications, with PVDF thin films utilized in some modern thermal camera sensors.

Dielectric properties of bare pvdf

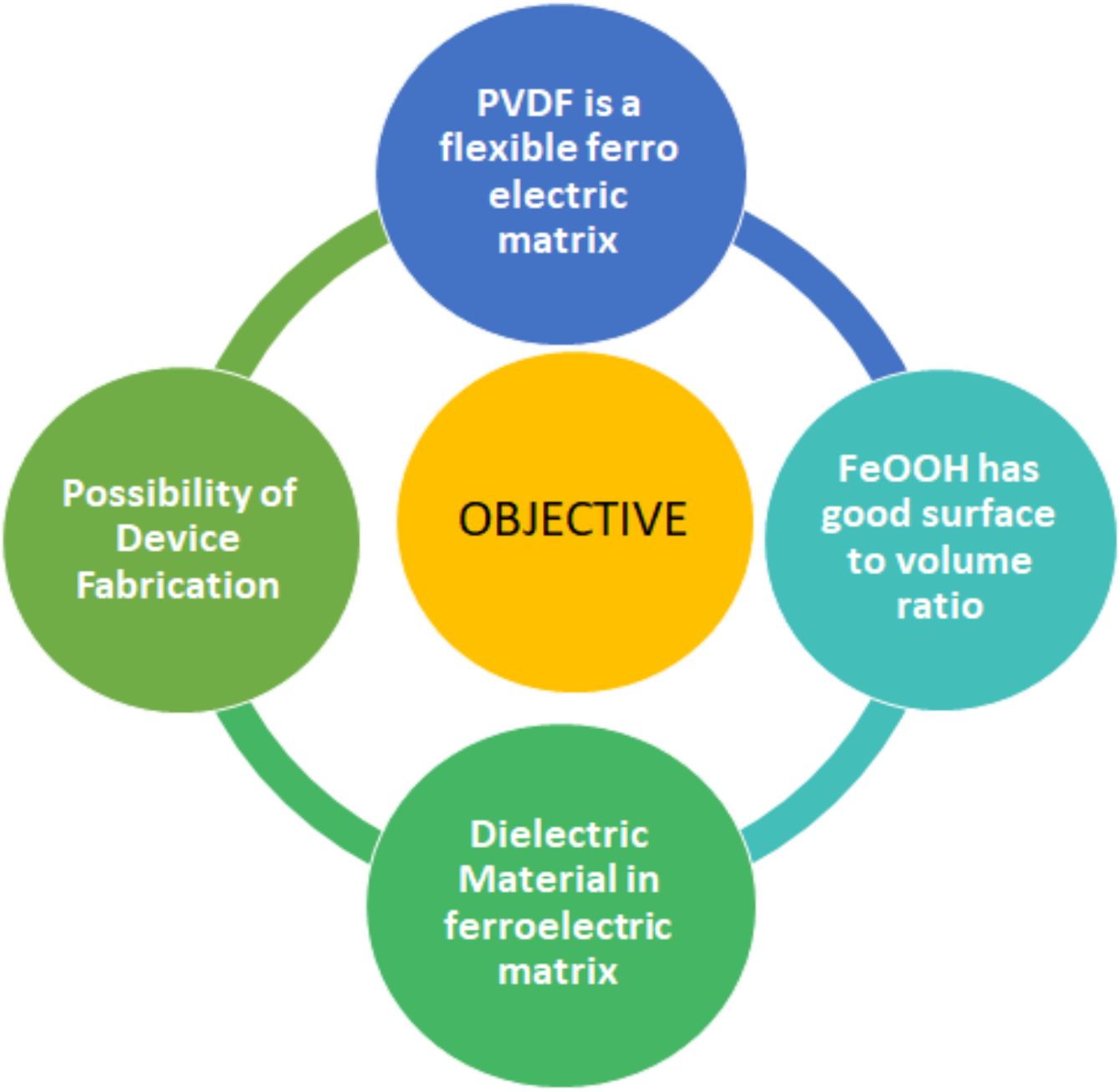
Poly(vinylidene fluoride) (PVDF) holds a prominent position in the realm of wire and cable insulation, owing to its exceptional dielectric properties [29], including a high dielectric constant and dissipation factor. However, while these properties are advantageous for insulation purposes, PVDF's inherent electrical characteristics also

enable the production of specialized films exhibiting piezoelectric and pyroelectric behaviors. These specialized films, fabricated from extruded PVDF films in the B-phase conformation, undergo a meticulous process to induce permanent polarization. This entails metallizing both surfaces of the film followed by subjecting it to high voltage, resulting in a permanently polarized state. The films thus produced demonstrate remarkable piezoelectric behavior, generating a voltage in response to mechanical deformation such as stretching or compression, as well as pyroelectric behavior, manifesting as a voltage output when subjected to changes in temperature near the melting point. Moreover, PVDF polymer films also exhibit intriguing ferroelectric properties, further enhancing their utility in various applications requiring precise control over electrical responses.

The significance of PVDF and its copolymers in the field of dielectrics cannot be overstated, as they boast a relatively elevated dielectric constant, typically around 10, coupled with minimal dielectric losses, with tan δ values ranging from 0.02 to 0.05. This combination of high dielectric constant and low losses positions PVDF as a material of choice for numerous technological applications demanding superior electrical performance and reliability.

CHAPTER 2

"This chapter focuses on the purpose of our work, our objectives, and our plans for the future."



2. OBJECTIVE

Our study endeavors are propelled by a comprehensive understanding of the intricate interplay between dielectric and magnetic properties within nano composites. By delving into these attributes, we seek to unravel the underlying mechanisms governing their behavior, thereby laying the foundation for pioneering advancements in the realm of energy storage technology.

To achieve this ambition, our approach entails a meticulously structured investigation, employing a combination of experimental methodologies and theoretical analyses. Through systematic experimentation, we aim to characterize the dielectric and magnetic behaviors of the nano composite materials under varying conditions and parameters. By meticulously scrutinizing the resulting data and discerning patterns and correlations, we strive to gain profound insights into the fundamental principles governing their functionality.

Furthermore, our research extends beyond mere observation to include active manipulation and optimization of these properties. By leveraging our understanding of the underlying mechanisms, we endeavor to engineer nano composites with tailored dielectric and magnetic characteristics optimized for enhanced energy storage performance. This iterative process of design, fabrication, and evaluation allows us to refine and enhance the performance of these materials iteratively.

Our focus is on creating sustainable energy storage solutions for the future. By maximizing the potential of nano composite materials and leveraging their synergies, we're driving advancements in renewable energy tech. Through collaboration and innovation, we're paving the way for a greener future where energy storage is key to powering our world.The main objective of this study is as follows:

- Preparation of phase pure α-FeOOH nanoparticle by simple solution chemistry route.
- Detail characterization of synthesized nanoparticles via FESEM, FTIR, and UV-Vis spectrophotometry.
- Preparation of (1-x)PVDF-xFeOOH (x= 0 to 15 wt%) nanocomposite thin film via spin coating technique.
- Measurement of dielectric and magnetic properties of the thin films

CHAPTER 3

"This chapter solely focuses on the literature survey done before conducting the work"

3. LITERATURE REWIEW

- Navinchandra et al prepared Goethite nanorods by combining (0.1 M) $FeCl_3 6H_2O$ and (0.5 g) CTAB in (40 ml) distilled water. After stirring the mixture for 30 minutes, NaOH was added drop by drop to maintain a pH of 11. The resulting mixture was then transferred to a Teflon-lined sealed stainless steel autoclave and heated to 120°C for 8 hours. The resulting yellow solid product (a-FeOOH nanorods) was purified by centrifugation and washed several times with distilled water to remove impurities. Finally, the purified product was dried in a vacuum oven at 100°C. Subsequently, they successfully investigated the phase band gap and photocatalytic activity of goethite. [38]
- John Godwin et al synthesized rod-like α-FeOOH nanoparticles hydrothermally using $Fe(NO_3)_2 \cdot 9H_2O$ (98.0%) and NaOH (97.0%). Initially, they prepared a 20.0 mL solution of ferric nitrate (0.2 M) by stirring at 600 rpm until it became clear. Simultaneously, a 10 mL solution of 2.5 M NaOH was prepared by stirring until the NaOH pellets completely dissolved. The alkaline solution was then gradually added to the nitrate solution in the beaker, maintaining continuous stirring at 600 rpm. After complete addition, stirring continued for 5 minutes before transferring the mixture to a Teflon autoclave. Water was added to fill approximately 70–80% of the autoclave's volume. The autoclave, along with its contents, was then placed in an oven preheated to 120°C and left for a hydrothermal reaction for 40 hours. This process enabled them to conduct successful thermodynamic and adsorption isotherm studies. [39]
- Gaorong et al synthesized α-FeOOH nanowires through a hydrothermal process. In their experimental procedure, they dissolved 4.85 g of $Fe(NO_3)_3 \bullet 9H_2O$ and 2.73 g of KOH in 10 ml of distilled water. This solution was then slowly added drop by drop into another solution under vigorous stirring. The resulting mixture was transferred into a 50 ml Teflon-lined autoclave, which was filled with distilled water up to 80% of its total volume. The autoclave was sealed and maintained at 100°C for 6 hours. Once the reaction was complete, the autoclave was naturally

cooled to room temperature, and the resulting solid products were filtered, washed multiple times with absolute ethanol and distilled water, and finally dried under vacuum at 60°C for 12 hours. He then studies the morphology of goethite. [40]

- Ali Reza Amani-Ghadim et al synthesized α-FeOOH nanostructures using the hydrothermal method. Initially, they dissolved 1.5 mmol of Fe(NO3)3•9H2O in 20 mL of deionized water (solution A), and separately prepared 10 mmol of sodium hydroxide in 20 mL of deionized water (solution B). Solution B was then added dropwise to the stirred solution A, adjusting the pH to approximately 10. The resulting aqueous solution was transferred into a 100 mL Teflon-lined autoclave for a hydrothermal reaction at 100°C for 3 hours. Subsequently, the system was naturally cooled to room temperature, and the obtained precipitates were washed multiple times with deionized water. The particles were then transferred into a desiccator and dried in ambient air. Amani-Ghadim proceeded to investigate the photocatalytic activity of goethite. [41]
- Weimin Xia et al conducted an extensive project to develop ferroelectric polymers based on polyvinylidene fluoride (PVDF). They focused on creating copolymers like P(VDF-TrFE) and thoroughly investigating their dielectric, ferroelectric, and magnetic properties. Through meticulous experimentation, they explored how these materials respond to electric fields, crucial for applications from electronics to energy storage. Additionally, they delved into the ferroelectric properties of the copolymers, aiming to utilize their spontaneous electric polarization for sensors and memory devices. The team also analyzed the magnetic properties, essential for fields like data storage and biomedical devices. Xia's research revealed promising insights into the multifaceted properties of PDVF-based ferroelectric polymers, laying the groundwork for future innovations in functional polymer materials. [42]
- Buscaglia et al conducted an extensive study on how microstructures influence the dielectric properties of PVDF-based nanocomposites with high-permittivity fillers, particularly for energy storage applications. They used BT@SiO2 to precisely control the arrangement of nanoparticles within the composite, aiming to enhance its ability to store and release electrical energy efficiently. Through experiments and modeling, they investigated how different microstructural configurations affect capacitance, breakdown strength, and overall energy storage capabilities. Their work highlights the importance of microstructural engineering in optimizing PVDF-based nanocomposites for energy storage, paving

the way for future advancements in high-performance energy storage devices. [43]

- Junjie Li et al meticulously fabricated PVDF films with α-phase crystal domains by casting PVDF solution onto a glass substrate and drying it at 100°C for 24 hours. They then extensively studied the films' dielectric relaxation, D-E hysteresis loops, breakdown strength, and energy storage characteristics. This investigation provided valuable insights into the films' behavior under varying electrical conditions, paving the way for their potential applications in diverse technological fields. [44]
- Emiliano et al conducted a thorough review exploring recent advancements in P(VDF-TrFE) composites, focusing on their enhanced properties and emerging applications in electronics. They investigated the roles of PVDF as the matrix material and TrFe as the filler material, particularly examining their dielectric and piezoelectric behaviors. The review aimed to uncover how the incorporation of TrFe affects the composite's properties and to identify potential applications in sensors, actuators, energy harvesting, and biomedical devices. By synthesizing existing knowledge, the review provides valuable insights for further research and development in this promising field. [46]
- Gregorio et al conducted a thorough investigation into enhancing the dielectric properties of poly(vinylidene fluoride) (PVDF) composites through surface functionalization of exfoliated graphene. They aimed to optimize the dispersion of graphene within the PVDF matrix and promote strong interfacial bonding between the filler and polymer. By employing experimental techniques and theoretical modeling, they systematically evaluated the impact of surface functionalization on the dielectric performance of the composites. This study holds promise for advancing high-performance dielectric materials for electronic and energy-related applications. [47]
- Sudipta et al explored the large room-temperature magnetodielectric effect in P(VDF-TrFE)/La0.7Sr0.3MnO3 composites, revealing the interplay between magnetism and dielectric properties. This research holds promise for applications in electronic devices, sensors, and energy conversion systems. By combining the unique properties of P(VDF-TrFE) and La0.7Sr0.3MnO3, the study aimed to engineer materials with enhanced magnetodielectric properties. Through comprehensive experiments, including synthesis and characterization techniques, the team shed light on the underlying mechanisms of this phenomenon, paving the way for future technological advancements.[45]

CHAPTER 4

"This chapter centres on the components of a spin coater, detailing their operational principles and stages."

- Principle of spin coating
- Parts of a Spin Coater
- Process of spin coating

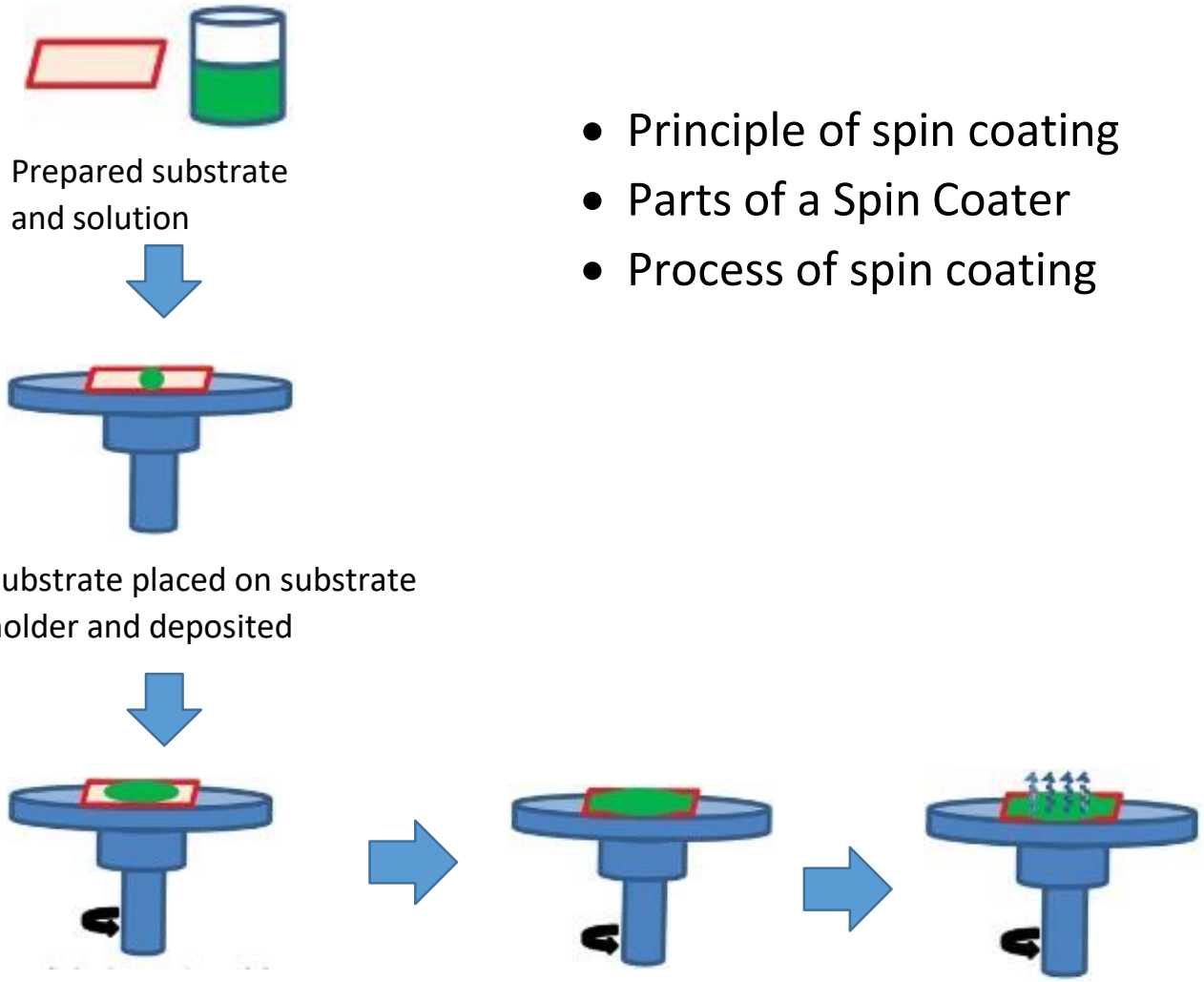


Figure 17: Flow chart of spin coating

4. SPIN COATING TECHNIQUE

Spin coating stands as a quintessential laboratory technique renowned for its rapid production of thin membranes [48].Typically employed to fabricate thin membranes, this technique involves the controlled application of a precursor solution onto a supportive surface, followed by its rapid spinning to induce spreading across the substrate's edge. The centrifugal force generated during spinning propels the solution, facilitating the formation of a uniform thin film as the solvent swiftly evaporates, as illustrated in Figure (Le Roux and Paul, 1992).



Figure 18 : Spin coater device

Traditionally, a small quantity of the coating material is introduced onto the central region of the substrate, which may either be stationary or spinning at low speeds, or occasionally, the material is delicately poured drop by drop onto the substrate surface. The thickness of the resultant membrane is intricately linked to three key experimental parameters: the rate of solvent evaporation, the velocity of the spinning substrate (spin rate), and the viscosity of the coating solution. Thus, meticulous control over parameters such as precursor volume, rotational speed, rotational duration, as well as the concentration of the solution or solids, is imperative for governing membrane formation. In this methodology, organic additives are frequently incorporated to fine-tune factors such as solid loading, viscosity, and volatility within the coating solution, ensuring precise control over the membrane's properties and characteristics.

The spin coating process commences with the substrate being set into motion, reaching rotational speeds of up to 10,000 revolutions per minute (rpm), facilitating the spreading

of the coating material through centrifugal force. A pivotal component in this process is the spin coater, also known as a spinner, which orchestrates the controlled rotation of the substrate. Furthermore, to expedite the drying of the coating, air is typically pumped outward along the surface of the disk, enhancing the evaporation process and contributing to the formation of a homogeneous coating layer. This integrated approach underscores the importance of both mechanical and environmental factors in achieving desired coating outcomes in spin coating applications.

4.1. PARTS OF A SPIN COATER

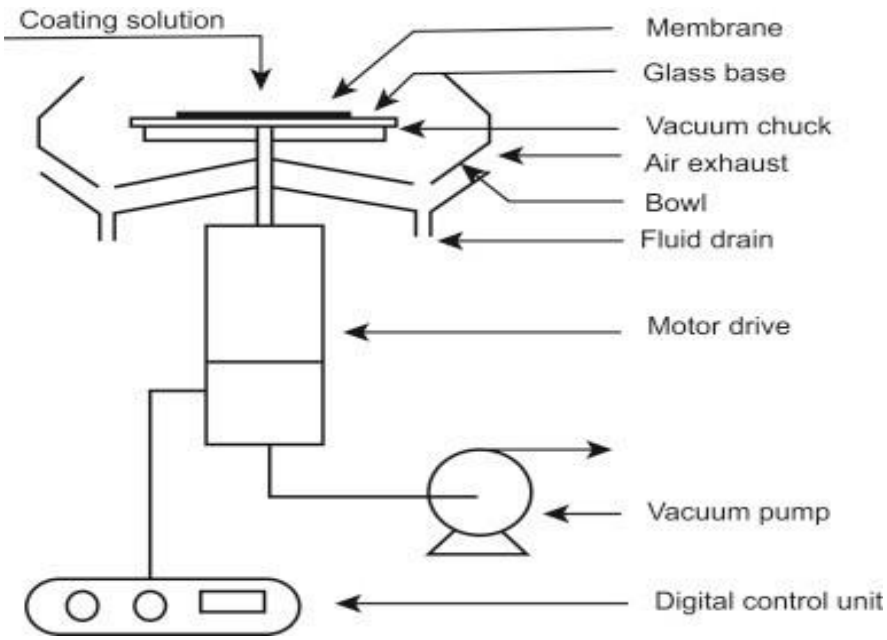


Figure 19 : Parts of a Spin coater

4.1.2. PROCESS OF SPIN COATING

Spin coating is the outcome of a solidified thin coating on a rigid flat disc, plate or a slightly curved bowl or lens. [48]

The process can be divided into four stages:

a. Deposition
b. Spin up
c. Spin off
d. Evaporation

The second may overlap the first but the first three stages are sequential , the fourth proceeds through out the process, precautions are taken to delay start the evaporation.

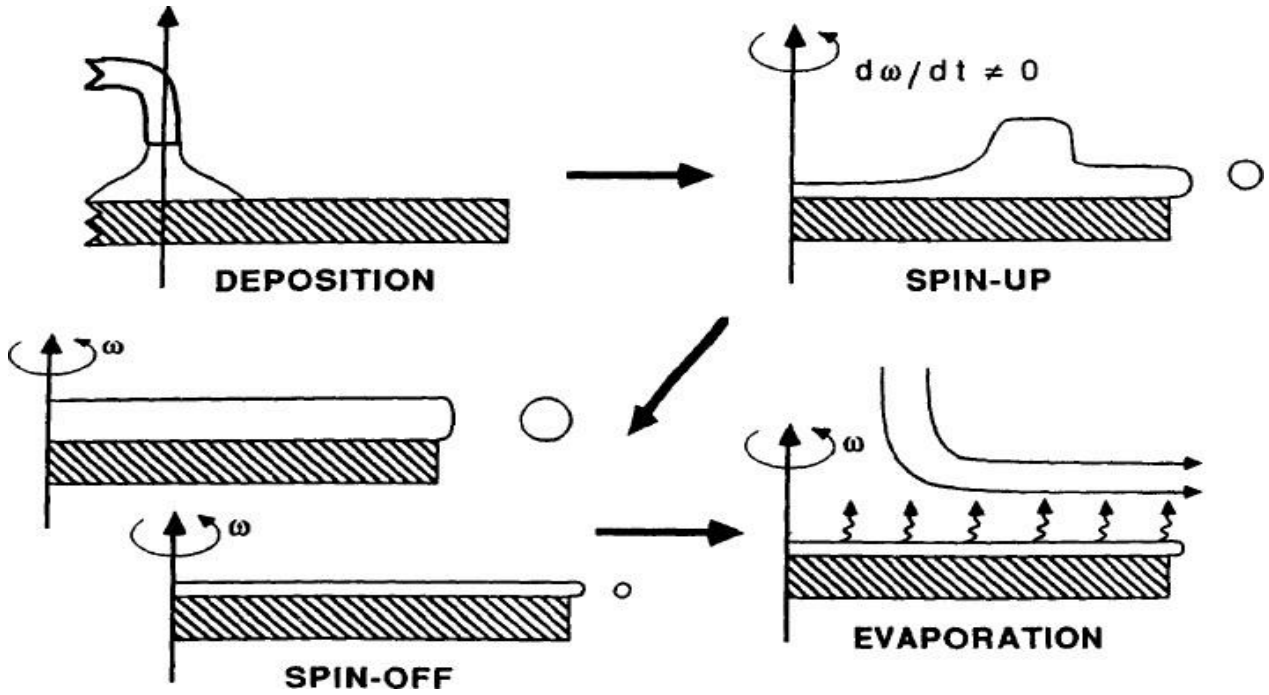


Figure 20 : Stages of spin coating

- **FIRST STAGE**

During the initial stage, a significant volume of the liquid is administered onto the substrate, which can either be stationary or in gentle rotation, exceeding the requisite amount for coating purposes. This surplus liquid is strategically distributed; it may be concentrated at the central point or distributed along the periphery of the hole if the substrate's center has been excised. Alternatively, an elevated mechanism can be employed to deliver the liquid in a controlled manner, ensuring even dispersion across the substrate's surface.

- **SECOND STAGE**

In the subsequent stage, the liquid exhibits a dynamic outward flow, propelled by the centrifugal force induced by the rotation of the substrate. This phase initiates promptly as the substrate begins to accelerate towards its maximum rotational speed, often reaching several thousand revolutions per minute. As this motion intensifies, the majority of the gas molecules initially in contact with the substrate surface are displaced, creating a pathway for the advancing liquid front, known as the dynamic melting line, to

extend radially outward. This outward movement marks the progression of the coating process, facilitating the formation of a uniform coating layer across the substrate's surface.

- **THIRD STAGE**

Following the coating process, the excess liquid within the film, which now envelops the substrate, undergoes a radial flow towards the perimeter. This movement results in a temporary accumulation, leading to the formation of unwanted swelling areas from which droplets may eventually detach and disperse. In instances where the substrate features a central aperture, this flow emanates from the edge of the hole, shaping the inner diameter of the resulting disc-like structure.

In the absence of such a central aperture, the spin-off flow operates differently, causing a more or less uniform thinning of the entire film, albeit with notable edge effects observable at the outer diameter. As the film continues to thin, the remaining liquid encounters increased resistance to its flow. It's important to note that the thinning of the film leads to a reduction in its overall viscosity, but concurrently enhances the concentration of non-volatile constituents essential for the coating process.

Furthermore, as the film becomes thinner, the evaporation rate intensifies, thereby augmenting the viscosity through the concentration of these non-volatile constituents. This intricate interplay between flow dynamics, evaporation, and viscosity modulation plays a crucial role in achieving the desired coating thickness and uniformity across the substrate's surface.

- **FOURTH STAGE**

In this subsequent stage, thinning of the coating film primarily occurs through evaporation. Even after the spin-off process has ceased entirely due to solidification induced by the concentration of non-volatile solutes and particulates, this thinning phenomenon persists. As the liquid film undergoes continuous evaporation, the concentration of the non-volatile components gradually increases, further augmenting the solidification process. This prolonged thinning phase is crucial for refining the coating's thickness and uniformity, as it allows for the gradual removal of excess solvent and volatile components from the film. The ongoing evaporation process facilitates the transformation of the liquid film into a more viscous and cohesive state, enhancing its adhesion properties and ensuring a more stable and durable coating.

Moreover, the gradual reduction in film thickness during this stage contributes to the achievement of precise coating thickness specifications, particularly in applications

requiring high levels of accuracy and consistency. Through careful control and optimization of the evaporation process, manufacturers can effectively tailor the coating's properties to meet specific performance requirements, such as durability, flexibility, and chemical resistance.

Overall, the thinning by evaporation stage represents a critical phase in the coating process, where meticulous attention to detail and precise control of operating parameters are essential for achieving optimal coating quality and performance.

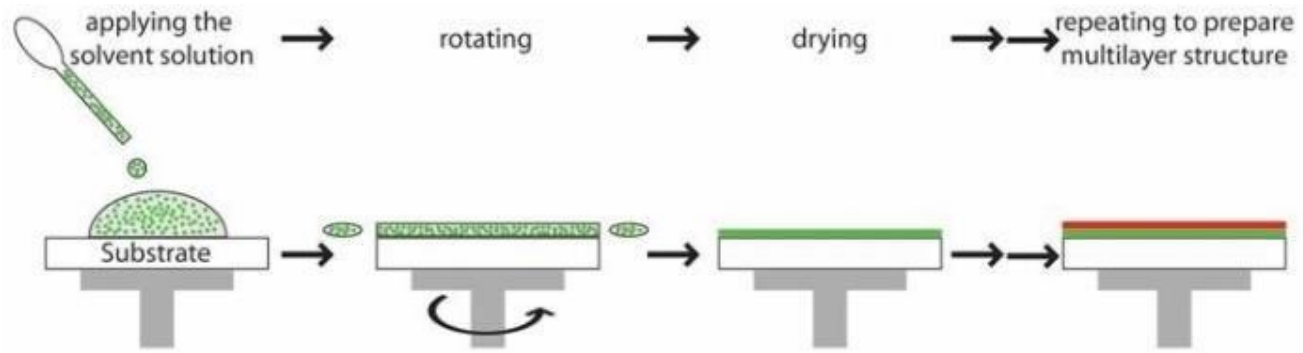
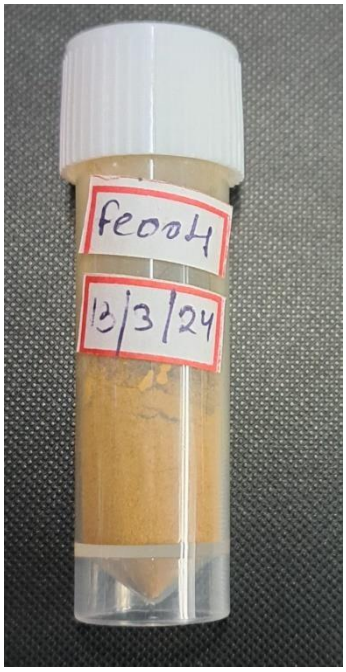


Figure 21 : Schematics of spin coating

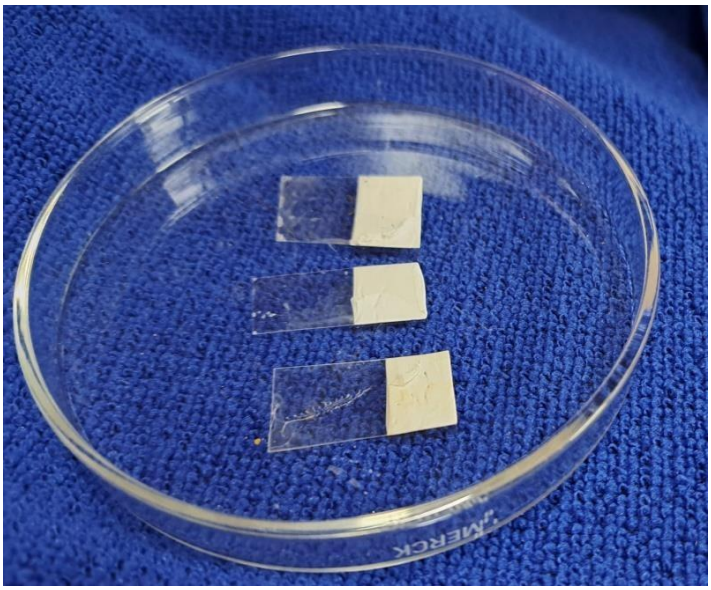
.

CHAPTER 5

" This chapter traces the study of PVDF-Geothite nanocomposite. Starting fro its synthesis from precursor, preparing the nanocomposite by spin coating and characterization of the



- Synthesis on goethite Nano rods
- Preperation of goethite PVDF composite solutions
- Spin coating the solutions on ITO substrate



5.1. SYNTHESIS OF THE COMPOSITE

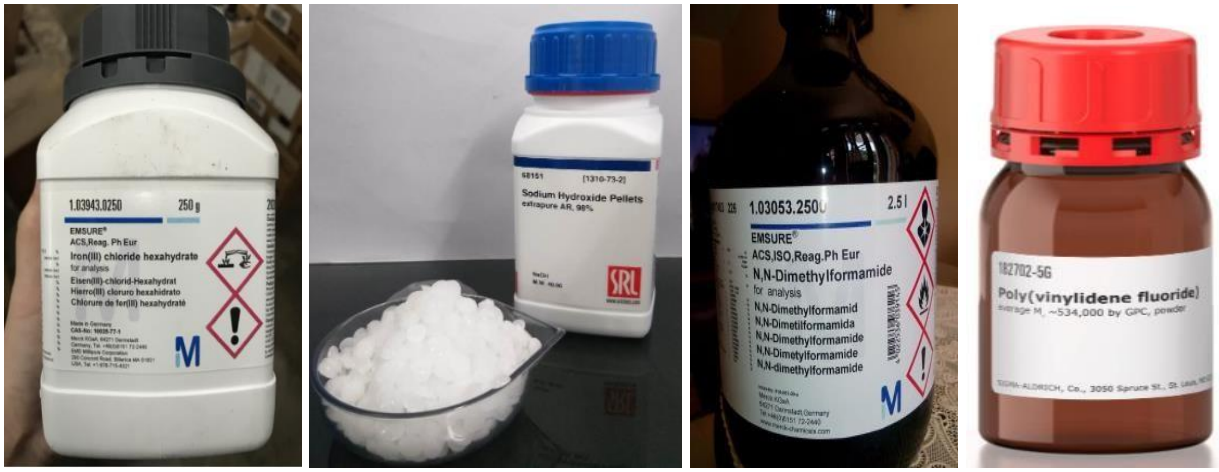
The synthesis process comprised three main phases. Initially, goethite filler was synthesized via the hydrothermal method. Subsequently, this filler goethite was blended uniformly with PVDF across seven distinct mixtures, each containing varying weight percentages of goethite. These mixtures were then spin-coated onto an ITO film, subjected to curing in a vacuum oven, quenched in cold, and ultimately dried.

Equipments used -

- Spin coater
- High accuracy weight balance
- Vaccum oven
- Stirrer
- Magnetic bid
- Borosil containers
- Scott bottle

Materials used -

- Ferric chloride
- NaOH pellets
- PVDF powder
- N, N-Dimethyl Formide
- Ethanol
- Ito (Indium – Tin –Oxide) coated substrate



a. b. c. d.

Figure 22 : a. Ferric chloride , b. NaOH pellets , C. N,N-Dimethyl Formide (DMF), d . PVDF

5.1.1. SYNTHESIS OF GEOTHITE

Geothite is synthesized by Hydrothermal process and heated for a period of 9 hrs.

HYDROTHERMAL PROCESS

Hydrothermal synthesis is a process for synthesizing single crystals, relying on the solubility of minerals in hot water under elevated pressure conditions. Crystal growth occurs within a specialized apparatus known as an autoclave, which is a steel pressure vessel. Within this vessel, a nutrient is supplied along with water. A temperature gradient is established along the length of the growth chamber. At the higher temperature region, the nutrient solute dissolves, while at the cooler end, it precipitates onto a seed crystal, facilitating the growth of the desired crystal.

The hydrothermal method offers several advantages over alternative crystal growth techniques. It enables the creation of crystalline phases that may not be stable at their melting points. Additionally, materials with high vapor pressures near their melting points can be grown using this method. Moreover, the hydrothermal technique is well-suited for producing large, high-quality crystals while maintaining control over their composition.

However, there are drawbacks associated with this method. It requires expensive autoclaves, and if a steel tube is used, observing the crystal growth process becomes impossible. Nevertheless, thick-walled glass autoclaves have been developed, capable of operating up to temperatures of 300 °C and pressures of 10 bar.

This process is usefull for the synthesis of Nano ,

a. Oxides of Tio_2 , VO_x , M_xMno_2
b. Layered oxides : nanowires and tubes
c. Carbon nanotubes
d. Some other elemental nanostructures

Importance of degree of filling of the autoclave :

a. The bomb (Autoclave) experiences an autogenous pressure in a closed vessel
b. At 32% filling , the water will expand to fill the autoclave at critical temp.
c. At higher filling degrees, the water will expand the water will expand to fill the autoclave at temperatures bellow the critical temperatures
d. This will result in a steep increase in the pressure inside the autoclave due to differences in compressibility of gas and liquid

e. At 80% filling the autoclave will eventually blast like a bomb due to extreme pressure

Here we have used scott bottles instead of Autoclave.

STEPS for the synthesis of Geothite (α- FeOOH)

Synthesizing α-FeOOH powders involved a hydrothermal method using pure chemical reagents. Initially, 0.81105 grams of $FeCl_3$ powder was dissolved in 50ml of DI water in Beaker 1, while 1 gram of NaOH pellets was dissolved in 50ml of DI water in Beaker 2. Both solutions were stirred for an hour until uniformly mixed. Beaker 1's solution turned slightly reddish, while Beaker 2's turned colorless. The colorless solution from Beaker 2 was then added dropwise to Beaker 1 until it turned dark reddish-brown, while monitoring pH until reaching 11. The addition of NaOH was stopped once pH 11 was achieved, indicating a dark green color on the pH paper. The entire NaOH solution was typically required to reach this pH.



Figure 23 : Ferric chloride solution

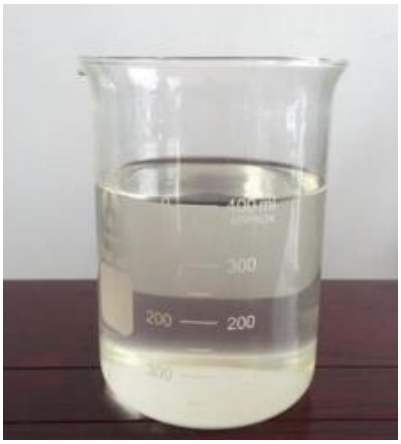


Figure 24 : NaoH solution

After dropwise addition, stirring of Beaker 1's new solution continued for another hour for uniform mixing. Once mixed, the solution was transferred to a Scott bottle (used instead of a conventional autoclave), previously cleaned with DI water and Ethanol. The Scott bottle was then placed in a 100˚C oven for 9 hours straight. After heating, the oven was turned off, and the Scott bottle was allowed to cool at room temperature overnight.

Once the Scott bottle solution had cooled entirely, it underwent thorough washing three times with DI water and once with Ethanol before being centrifuged at approximately

12000 rpm. During the final ethanol wash, the dense solution, containing pristine and finely sized goethite particles, was transferred to a petri dish and left to dry overnight in an oven set at 60˚C. Once fully dried, the yellowish powder was carefully removed from the petri dish and gathered into a pristine container, then stored within a desiccator for preservation.



Figure 25 : Freshly synthesized Geothite powder

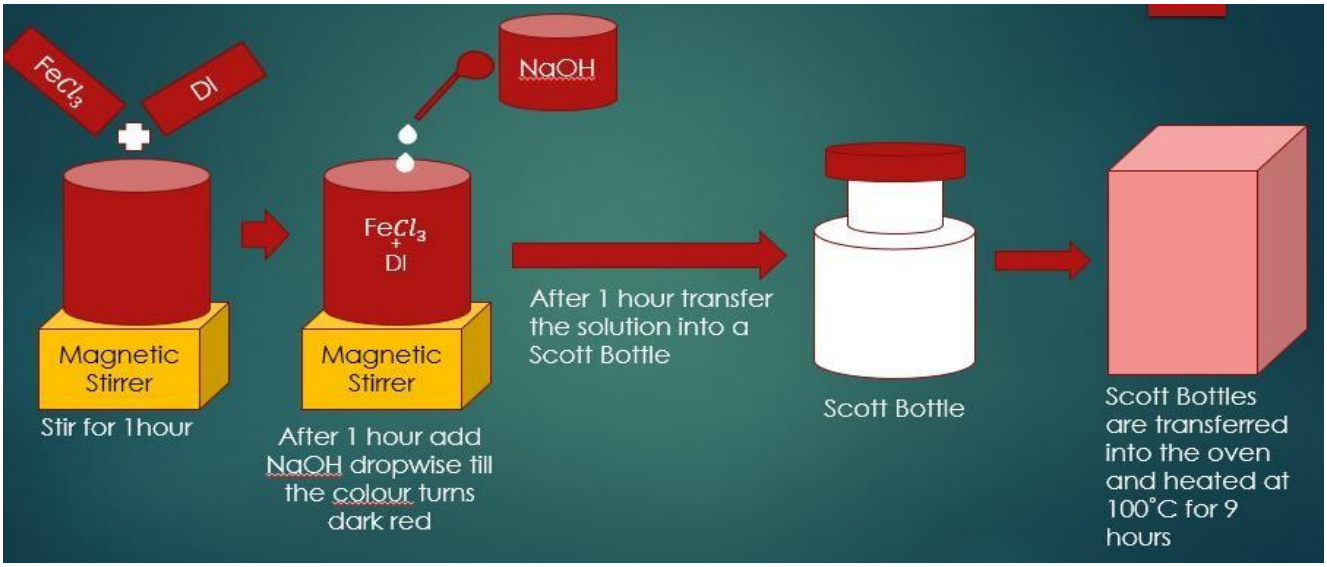


Figure 26 : Schematic Representation of the synthesis process

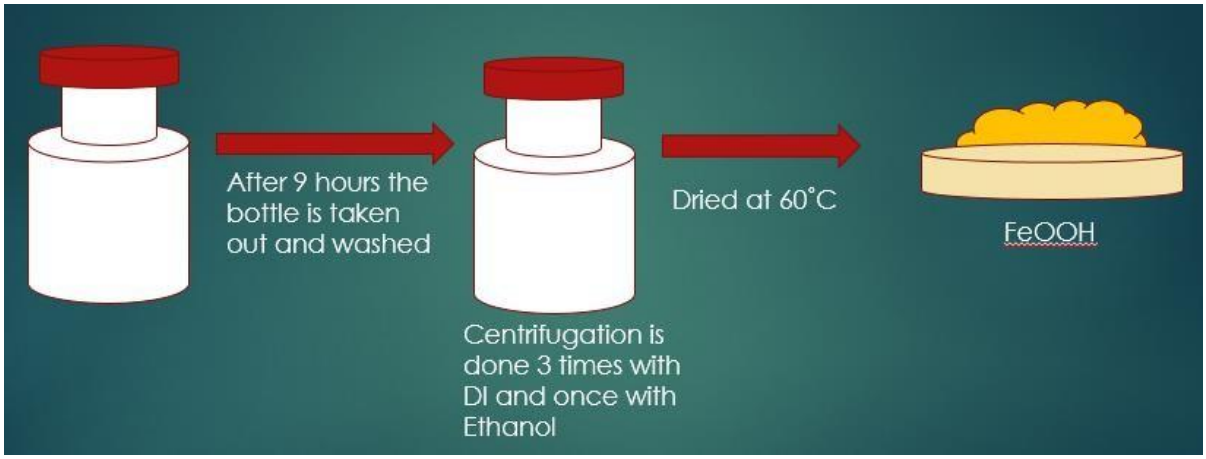


Figure 27 : Schematic Representation of the synthesis process

5.1.2. PREPARATION OF THE NANOCOMPOSITE

Sample preparation consisted of mixing PVDF and goethite at a constant volume fraction. PVDF, sourced from Sigma Aldrich, posed solubility challenges in DI water, necessitating its dissolution in N,N-Dimethyl Formamide (DMF). Specifically, 0.659 grams of PVDF were dissolved in 50ml of DMF and left to stir overnight. Subsequently, the newly synthesized goethite powder was partitioned into six portions, each representing various volume fractions based on the quantity of PVDF used. In total, seven sets of such solutions were prepared accordingly.

- Set 1

This set consisted of mixing 0.659 gm of PVDF in 50ml of DMF and was left to stir overnight.

- Set 2

This collection involved combining 0.659 grams of PVDF with 0.00659 grams of goethite powder, representing a 1% volume fraction of PVDF. Both components were dissolved in 50ml of DMF, and the solution was allowed to stir for 24 hours.

- Set 3

This ensemble involved combining 0.659 grams of PVDF with 0.01968 grams of goethite powder, representing a 3% volume fraction of PVDF. Both substances were dissolved in 50ml of DMF, and the solution was allowed to stir for 24 hours.

- Set 4

This grouping involved blending 0.659 grams of PVDF with 0.03295 grams of goethite powder, representing a 5% volume fraction of PVDF. Both components were dissolved in 50ml of DMF, and the solution was allowed to stir for 48 hours.

- Set 5

This particular collection involved combining 0.659 grams of PVDF with 0.049425 grams of goethite powder, representing a 7.5% volume fraction of PVDF. Both substances were dissolved in 50ml of DMF, and the solution was allowed to stir for 48 hours.

- Set 6

This specific grouping entailed combining 0.659 grams of PVDF with 0.0659 grams of goethite powder, representing a 10% volume fraction of PVDF. Both components were dissolved in 50ml of DMF, and the solution was allowed to stir for 48 hours.

- Set 7

This particular collection involved blending 0.659 grams of PVDF with 0.09887 grams of goethite powder, representing a 15% volume fraction of PVDF. Both substances were dissolved in 50ml of DMF, and the solution was allowed to stir for 48 hours.



a. **b.** **c.**

Figure 28 : a. DMF, B. PVDF, C. Geothite

5.1.3. PREPARATION OF ITO SUBSTRATE

The ITO films are first cut into rectangles of the desired size. These rectangles undergo a cleaning process by being sonicated in DI water for 10 minutes. Following this, any blue coating present on the films is removed using forceps. The clean ITO films are then treated with acetone and sonicated for another 10 minutes. After this, they are dried using an IR lamp. Subsequently, the conductivity of the films is examined using a multimeter, confirming the presence of the ITO coating. Once verified, one side of the ITO films is covered with Teflon tape, while the other side remains exposed for spin coating.

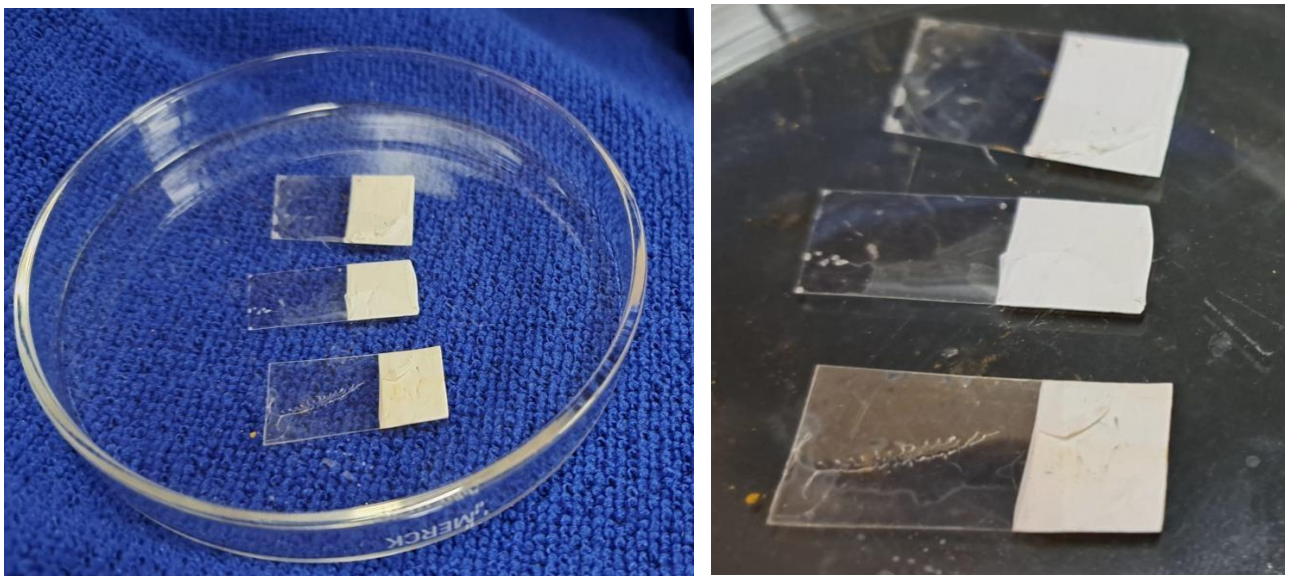


Figure 29: Teflon wrapped ITO Substrate

5.1.4. SPIN COATING PROCEDURE

The process of spin coating involves a series of carefully orchestrated steps to ensure optimal results. It commences with the preparation of the vacuum oven, where the temperature is set to 140˚C for preheating. Concurrently, the spin coater is activated and allowed to warm up. Once the vacuum oven reaches the desired temperature, the spin coating process begins, coinciding with the completion of the warm-up period.

To initiate spin coating, Teflon tape-wrapped ITO films are positioned on the chuck, with the conducting side facing upwards. The spin coater's rotational speed (RPM) is initially set to 2000 RPM at its maximum capacity. The RPM is then gradually increased from 0 to 500, 1000, and finally to 2000, followed by a subsequent decrease from 2000 to 1000,

500, 100, and finally to 0. After securing the substrate on the chuck, the vacuum pump is activated to prevent displacement of the substrate during the high-temperature spin coating process. Subsequently, the spin coater is turned on, and the RPM begins to rise steadily. When the RPM reaches 2000, 29 drops of the solution are carefully poured onto the substrate surface, ensuring even distribution across the substrate as the RPM gradually decreases to zero.

Once the spin coating process is complete, the substrate is cautiously removed and placed inside the preheated vacuum oven set at 140˚C for curing. The substrate is left to cure for a duration of 1 hour, allowing the coating to adhere and solidify effectively. Following the curing period, the substrate is retrieved from the oven and rapidly cooled by quenching in cold water. Finally, the substrate is dried under an infrared (IR) lamp to ensure complete removal of moisture and to facilitate the formation of a uniform and durable coating layer.The sample is then preserved in the desic measurement.

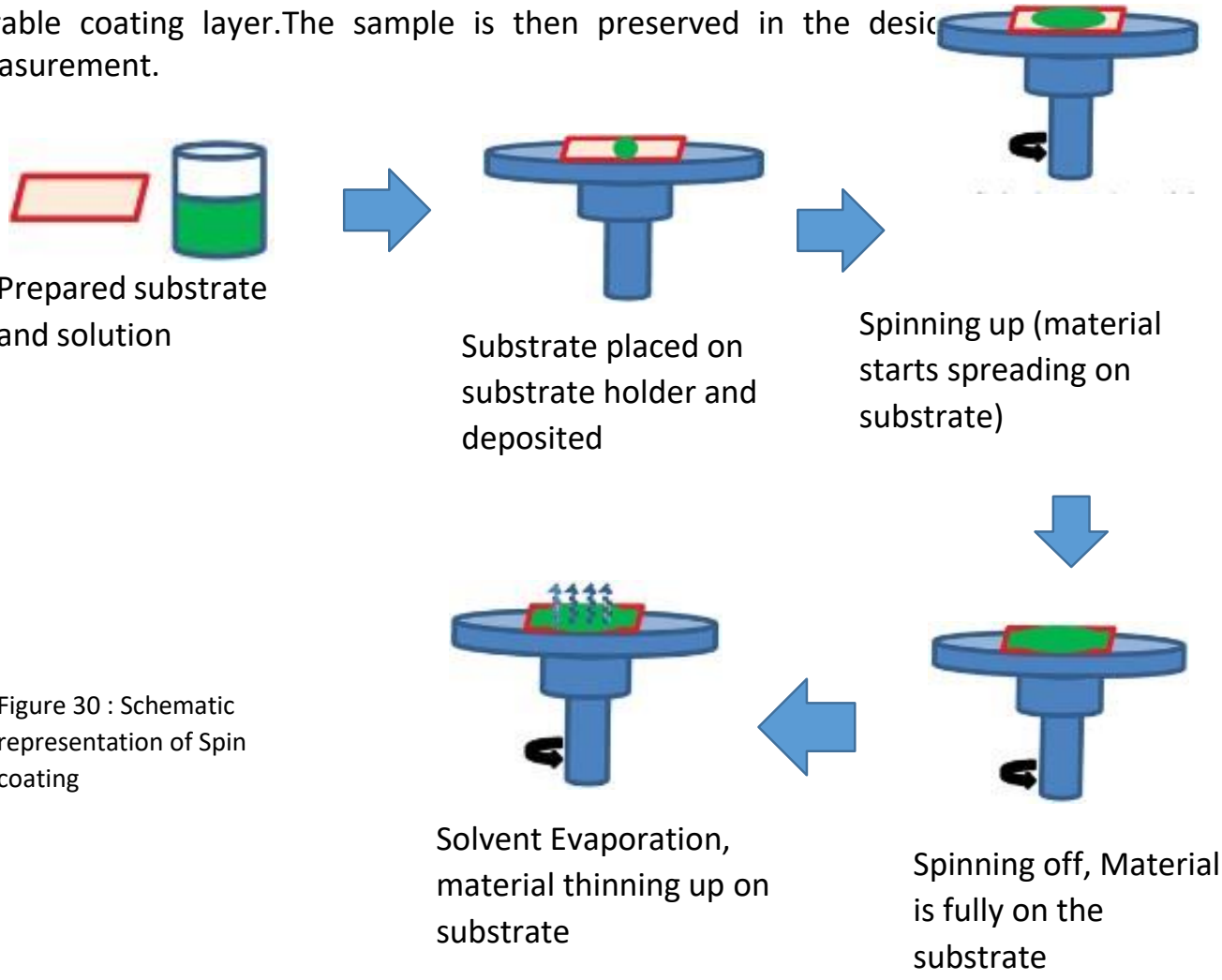


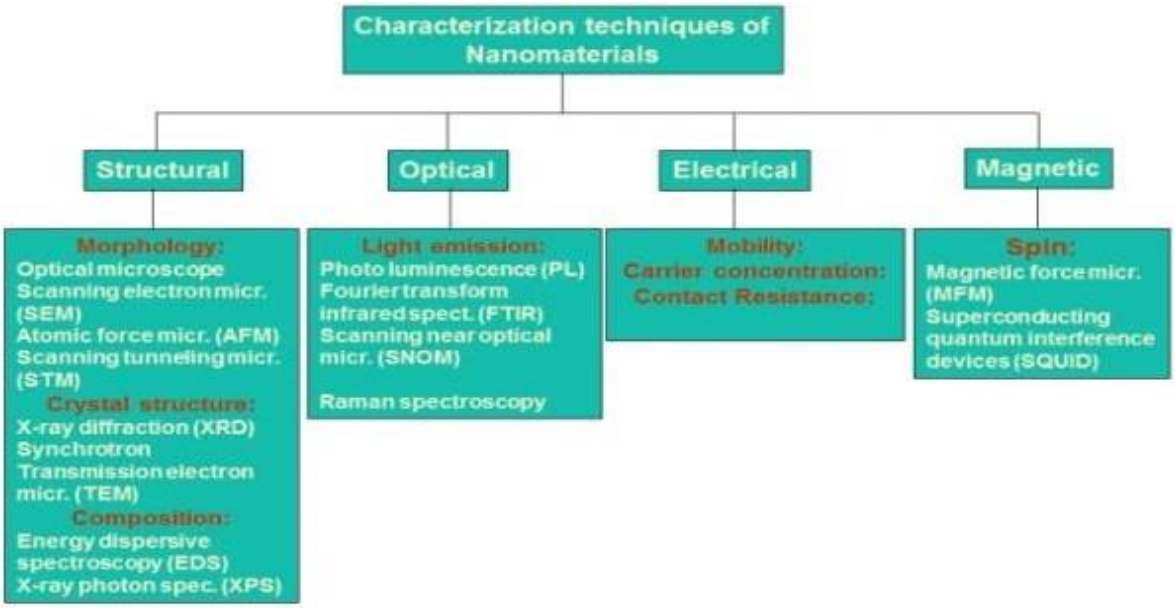
Figure 30 : Schematic representation of Spin coating

CHAPTER 6

"In this chapter, our attention will be directed towards the characterization tools, and we will analyse the results obtained from the characterization of our sample."



- Introduction to charecterization tools
- Charecterization and analysis of the prepared sample



6. CHARECTERIZATION TOOLS

6.1. X-RAY DIFFRACTION (XRD)

X-ray diffraction (XRD) stands as a cornerstone technique in the realm of material characterization, particularly in the analysis of nanoparticles (NPs). Its operational principle hinges upon the phenomenon of constructive interference, which occurs when monochromatic x-rays, meticulously generated by a cathode ray tube and refined for singular radiation, meet a crystalline sample. These x-rays, directed toward the sample with precision, interact with its crystalline structure, resulting in constructive interference as prescribed by Bragg's law. [50]

The utility of XRD in the characterization of nanoparticles lies in its capacity to unveil a plethora of vital information regarding the sample under scrutiny. Through XRD analysis, one can discern intricate details concerning the crystalline structure, the nature of its phases, lattice parameters governing its arrangement, and the crucial aspect of grain size. This latter parameter, vital in understanding the material's properties, is often estimated using the Scherrer equation. By scrutinizing the broadening of the most prominent peak in an XRD spectrum specific to the sample, researchers can derive insights into the grain size distribution within the material.

Practically, XRD analysis is commonly conducted on powdered samples, necessitating the drying of colloidal solutions to achieve optimal results (Figure 31). This methodological approach ensures that the data obtained is statistically representative, offering volume-averaged values that accurately depict the material's characteristics. To further elucidate the composition of the particles within the sample, analysts often resort to comparing the positions and intensities of XRD peaks with reference patterns meticulously curated within databases such as the International Centre for Diffraction Data (ICDD), formerly known as the Joint Committee on Powder Diffraction Standards (JCPDS).

Despite its myriad advantages, it's imperative to acknowledge the limitations of XRD. Notably, this technique proves inadequate when confronted with amorphous materials, rendering it unsuitable for such analyses. Additionally, the peaks discerned through XRD tend to broaden substantially when dealing with particles smaller than approximately 3 nanometers, thereby limiting its applicability in certain nanoscale investigations. Thus, while XRD remains an indispensable tool in the arsenal of material scientists and researchers, its judicious application must consider both its capabilities and limitations to derive meaningful insights from the analyses conducted.

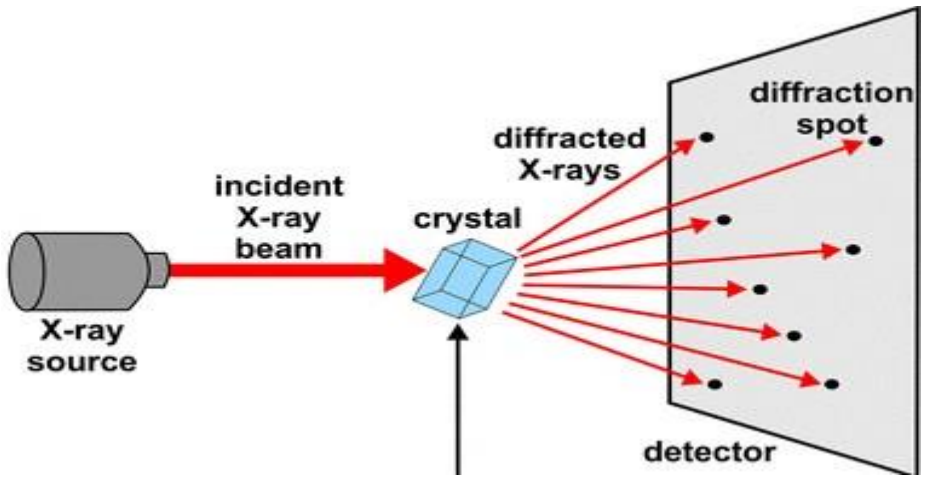


Figure 31 : Working of XRD

6.2. FOURIER TRANSFORM INFRARED SPECTROSCOPY (FTIR)

Fourier transform infrared spectroscopy (FTIR) operates on the principle of measuring the absorption of electromagnetic radiation specifically within the mid-infrared spectrum, which spans wavelengths ranging from 4000 to 400 cm−1. This technique capitalizes on the fundamental concept that when a molecule absorbs infrared radiation, it induces alterations in its dipole moment, thereby rendering the molecule infrared-active [51]. Consequently, the molecule exhibits characteristic absorption bands in the infrared spectrum. Interpreting the resultant FTIR spectrum provides a wealth of information regarding the molecular composition and structure of the analyzed sample. Each absorption band corresponds to specific vibrational modes within the molecule, which in turn are indicative of bond strengths, molecular configurations, and the presence of distinct functional groups. By analyzing the positions, intensities, and shapes of these absorption bands, researchers can glean valuable insights into the molecular architecture, chemical bonding, and intermolecular interactions within the sample.

Moreover, FTIR spectroscopy serves as a powerful tool in elucidating the composition and behavior of complex molecular systems across various scientific disciplines. In fields such as chemistry, biochemistry, pharmaceuticals, and materials science, FTIR analysis is routinely employed for structural elucidation, quality control, and characterization of diverse materials and compounds. Its non-destructive nature and high sensitivity make it particularly well-suited for studying samples in situ or in solution, enabling researchers to explore molecular interactions under physiologically relevant conditions (Figure 32).

Furthermore, advancements in FTIR instrumentation and data analysis techniques have expanded the scope and capabilities of this analytical method. Modern FTIR instruments

equipped with Fourier transform technology offer enhanced spectral resolution, signal-to-noise ratios, and spectral acquisition speeds, facilitating more precise and comprehensive analysis of complex molecular systems. Additionally, the integration of computational methods and spectral databases enables spectral interpretation, peak assignment, and spectral matching with unprecedented accuracy and efficiency.

In essence, Fourier transform infrared spectroscopy stands as a versatile and indispensable tool in the arsenal of analytical techniques, providing researchers with invaluable insights into molecular structures, chemical compositions, and intermolecular interactions essential for advancing scientific understanding and technological innovation.

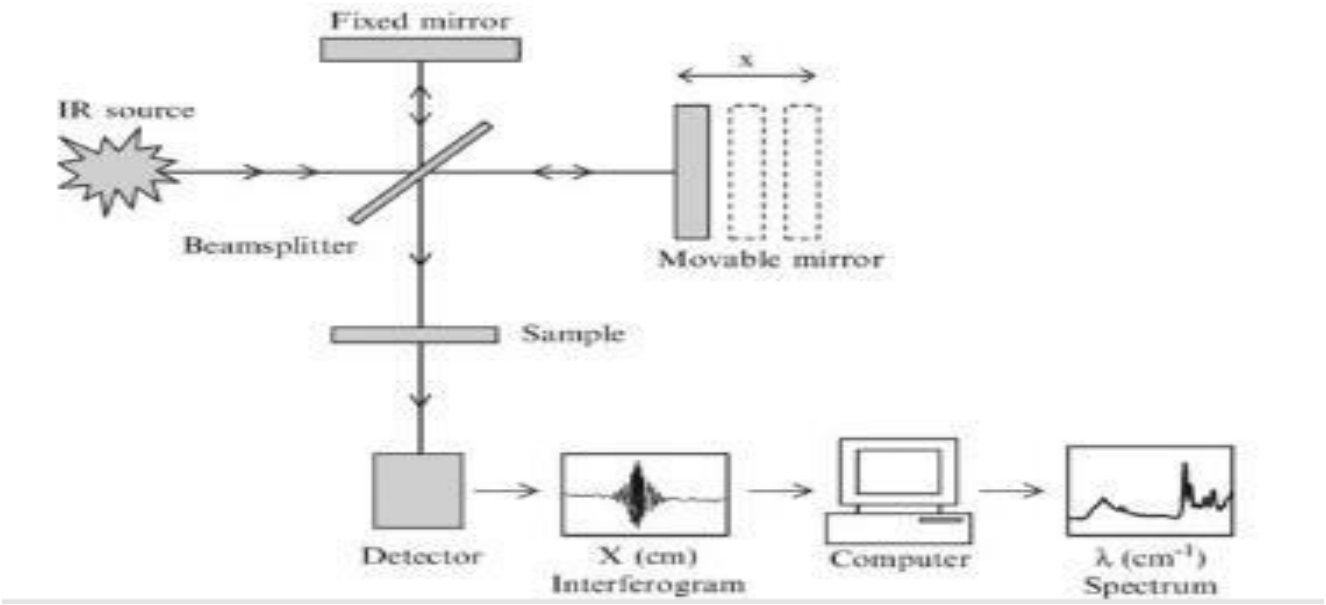


Figure 32: Working of FTIR

6.3. UV-VIS SPECTROSCOPY

UV-Vis spectroscopy, short for ultraviolet-visible spectroscopy (UV-Vis), stands out as a versatile and accessible analytical technique widely employed in the investigation and characterization of nanoscale materials. This method entails the measurement of the intensity of light absorbed or transmitted by a sample across the ultraviolet and visible regions of the electromagnetic spectrum. By comparing this measured intensity with that of a reference material, UV-Vis spectroscopy enables researchers to glean valuable insights into the optical properties and behavior of nanoparticles (NPs).[52]

Nanoparticles exhibit a plethora of optical phenomena and behaviors that are intricately linked to their size, shape, concentration, agglomeration state, and the refractive index in the vicinity of the nanoparticle surface. These characteristics render UV-Vis spectroscopy particularly well-suited for the identification, characterization, and investigation of nanomaterials. By analyzing the absorption or transmission spectra of NP-containing samples, researchers can discern distinct spectral features and absorption bands that provide information about the size distribution, morphology, and concentration of nanoparticles within the sample.

Moreover, UV-Vis spectroscopy serves as a valuable tool for evaluating the stability and colloidal behavior of nanoparticle dispersions and solutions. Changes in the optical properties observed in UV-Vis spectra can indicate alterations in the aggregation state, dispersity, or chemical composition of nanoparticles in solution, thereby providing valuable insights into the stability and shelf-life of colloidal suspensions.

In addition to its utility in fundamental research, UV-Vis spectroscopy finds widespread application in various scientific and technological domains. In fields such as materials science, nanotechnology, biotechnology, and environmental science, UV-Vis spectroscopy is employed for diverse purposes ranging from nanoparticle synthesis and characterization to the development of novel photonic and optoelectronic devices.

Furthermore, ongoing advancements in UV-Vis spectroscopy instrumentation and data analysis techniques continue to enhance the capabilities and versatility of this analytical method. Modern UV-Vis spectrophotometers offer improved spectral resolution, sensitivity, and data acquisition speeds, enabling more precise and comprehensive analysis of nanomaterials and complex molecular systems. Additionally, the integration of complementary techniques such as dynamic light scattering (DLS) and electron microscopy further augments the analytical power and accuracy of UV-Vis spectroscopy for nanomaterial characterization.

In summary, UV-Vis spectroscopy emerges as a valuable and indispensable tool for the characterization, analysis, and investigation of nanoscale materials, offering researchers a window into the optical properties and behavior of nanoparticles essential for advancing scientific understanding and technological innovation (Figure 33).

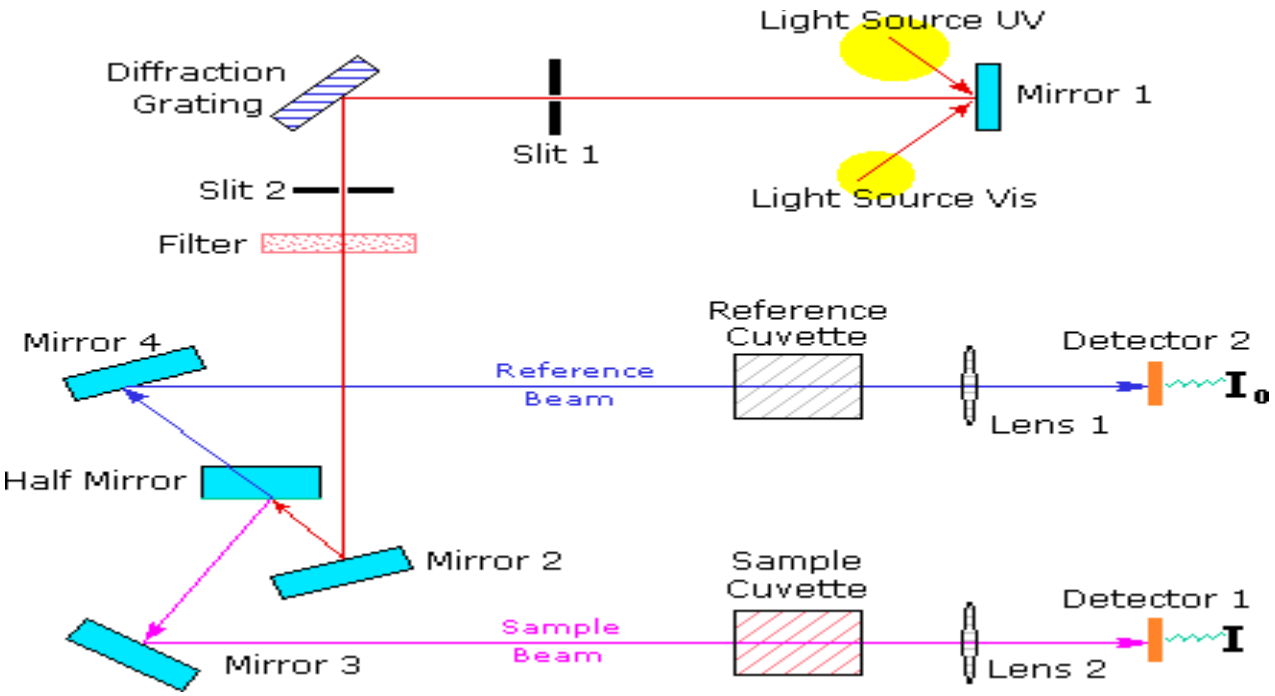


Figure 33 : Working of UV-VIS

6.4. FIELD EMISSION SCANNING ELECTRON MICROSCOPE (FESEM)

The Field Emission Scanning Electron Microscope (FESEM) stands as a pinnacle of technological advancement in microscopy, revolutionizing our ability to visualize and analyze nanostructures and materials with unprecedented clarity and precision (Figure 34). Unlike conventional optical microscopes that utilize light for imaging, FESEM harnesses the unique properties of electrons, the negatively charged particles, emitted from a field emission source nested within its intricate design. These emitted electrons are meticulously directed to traverse the surface of the specimen in a zig-zag pattern, facilitating comprehensive scanning and imaging at ultra-high resolutions.[53]

One of the most remarkable attributes of FESEM technology lies in its exceptional resolution capabilities, which surpass those achievable with traditional scanning electron microscopy (SEM). With image resolutions plummeting as low as 0.6nm at 15KV and 1.2nm at 1 kV, FESEM enables researchers to delve into the intricate details of nano powders, nanofilms, and nanofibers across a myriad of scientific domains. This unprecedented level of resolution opens avenues for in-depth exploration and analysis in fields ranging from mineralogy, ceramics, and polymer science to metallurgy, electronics, chemistry, physics, and life sciences.

Integral to the functionality of FESEM systems are the diverse array of detectors meticulously integrated within their architecture. These detectors, including secondary electrons (SE) detectors and back-scattered electrons (BSE) detectors, serve as invaluable tools for capturing and analyzing various signals emitted from the sample surface.

While SE detectors provide topographic information, BSE detectors offer insights into materials composition, collectively contributing to the generation of clear, minimally distorted images with spatial resolutions as fine as 1.5 nanometers.

A defining feature that sets FESEM apart from its predecessors is its innovative electron generation mechanism. Unlike traditional SEM instruments that rely on thermionic emission, FESEM utilizes a field emission gun to produce highly focused electron beams encompassing both high and low energy ranges.

This groundbreaking approach not only enhances spatial resolution but also facilitates operation at remarkably low potentials ranging from 0.02 to 5kV. Consequently, FESEM minimizes charging effects on non-conductive specimens while safeguarding electron beam-sensitive materials from damage, thereby expanding the scope and versatility of its applications.

Furthermore, FESEM systems incorporate state-of-the-art in-lens detectors optimized for high-resolution imaging at exceedingly low acceleration potentials. These specialized detectors play a pivotal role in optimizing the performance of the instrument, ensuring unparalleled imaging quality, and fidelity across a diverse array of scientific investigations. In essence, the Field Emission Scanning Electron Microscope epitomizes a cutting-edge tool in microscopy, offering unparalleled resolution and versatility for unraveling the complexities of nanostructures and materials across an expansive spectrum of scientific disciplines.

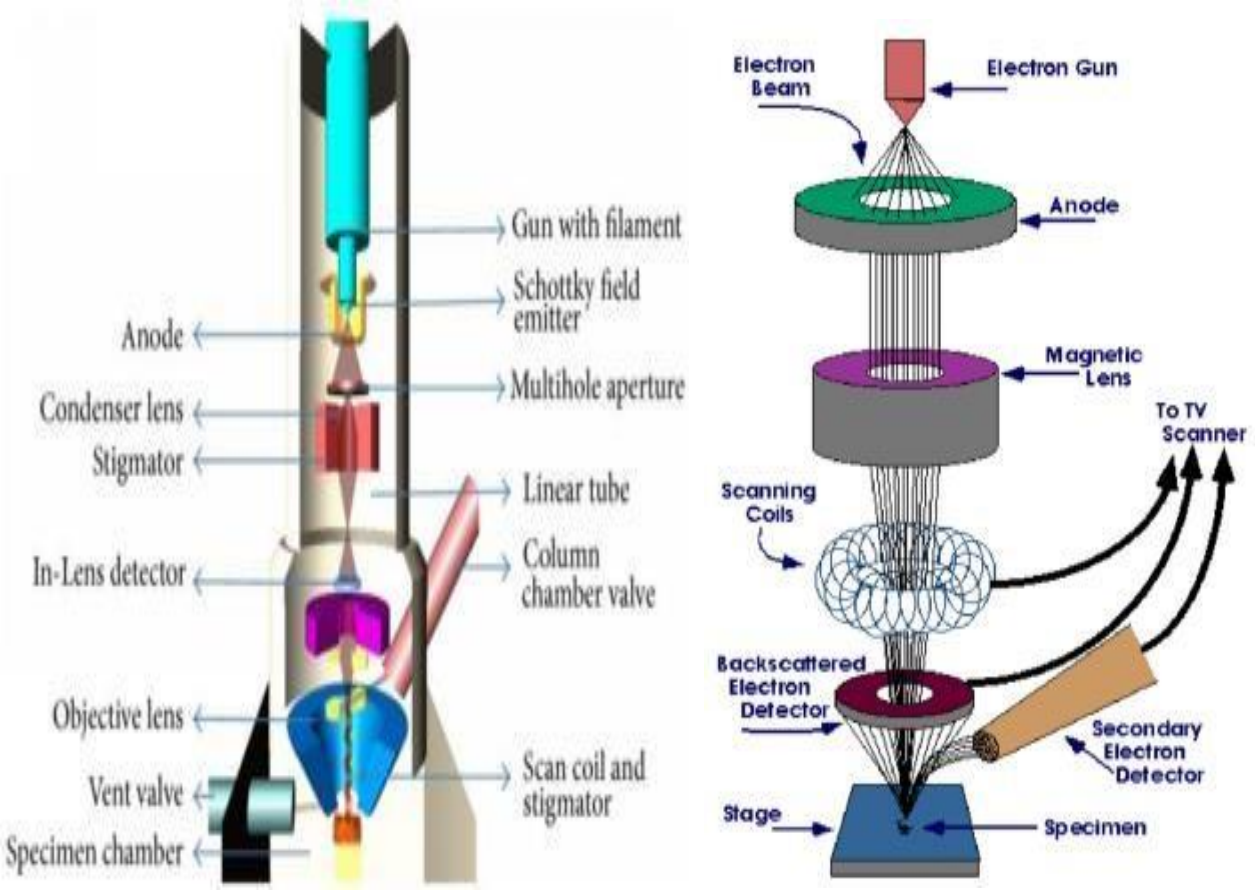
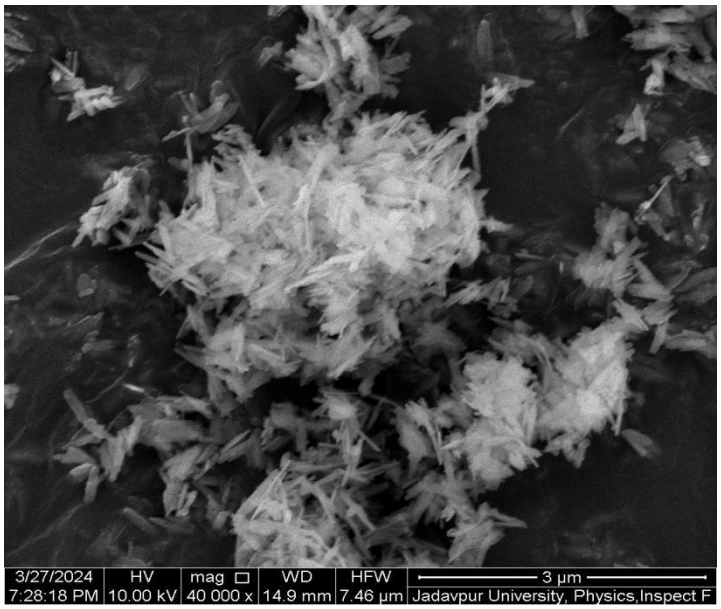


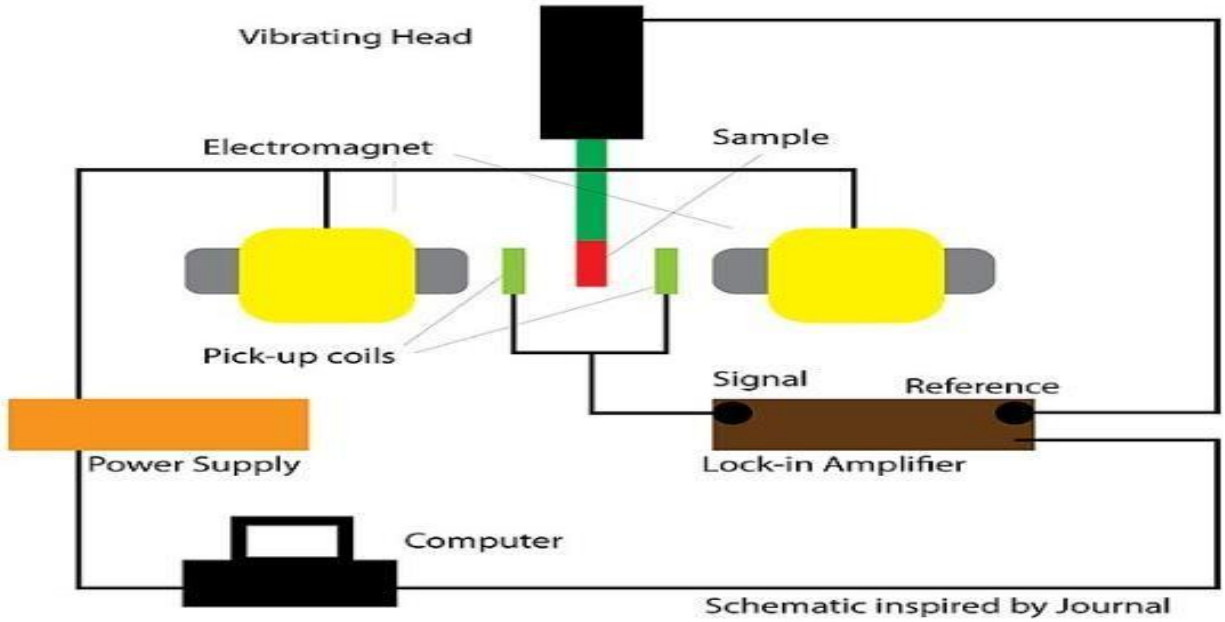
Figure 34 : Working of FESEM

CHAPTER 7

"This chapter highlights on the results and discussion afte the charecterization of the sample. Which includes structural and bond studies as well as electric and magnetic studies"



- XRD
- FTIR
- UV-Vis
- FESEM
- Dielectric properties
- Magnetic properties



7. REULTS AND DISCUSSION

7.1. CHARECTERIZATION OF THE SYNTHESIZED MATERIAL

7.1.1. XRD ANALYSIS

Powder X-ray diffraction (XRD) pattern for α-FeOOH samples were acquired using Bruker AXS (D8),Wisconsin, USA, equipped with Cu Kα radiation with a wavelength (λ) of 1.504 Å. This system boasts advanced capabilities and precision in material analysis. To ensure thorough examination of the α-FeOOH powder's phase purity, we employed a small step size of 0.02 during data collection. This meticulous approach allowed us to capture detailed information about the crystalline structure and composition of the synthesized powder.

The resulting XRD pattern, obtained from the powder synthesized via the hydrothermal method, is presented graphically in the accompanying figures. These figures provide a visual representation of the diffraction peaks observed during the analysis. To aid in interpretation, the standard diffraction peaks of α-FeOOH, as specified by JCPDF card no. 290713, have been highlighted in the figures. This serves as a reference point for comparison and verification of the synthesized material's structural characteristics.

It's worth noting that the synthesis methodology employed to produce the α-FeOOH powder is detailed extensively in the corresponding section dedicated to synthesis within this study. This section provides comprehensive insights into the experimental procedures, reaction conditions, and parameters involved in the synthesis process. By meticulously documenting the synthesis methodology, we aim to facilitate reproducibility and ensure transparency in our research findings.

Overall, the X-ray diffractograms and associated analysis presented in this study contribute valuable information about the structural properties of the synthesized α-FeOOH powder. Through careful examination and comparison with standard reference data, we gain deeper insights into the crystalline structure, phase purity, and potential applications of the synthesized material. Such detailed characterization is essential for advancing our understanding of materials science and guiding future research endeavors in this field.

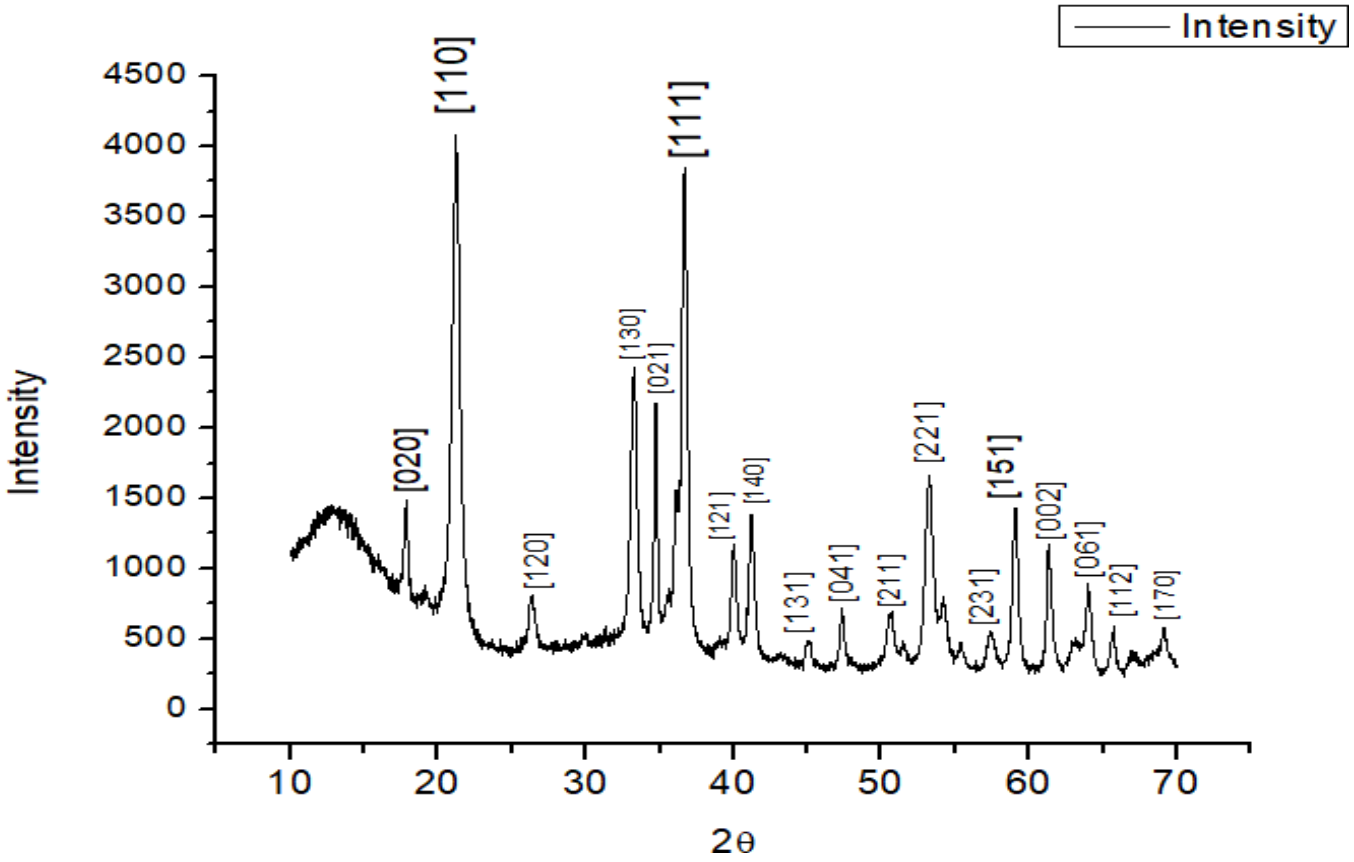


Figure 35 : XRD graph plotted for pure Geothite (α-FeOOH)

The presence of α-FeOOH in the synthesized powder has been unequivocally confirmed through analysis of the XRD graph. The distinct diffraction peaks observed align closely with the expected diffraction pattern of α-FeOOH, validating the successful formation of the desired phase. This characterization technique serves as a robust means of assessing the phase purity and crystalline structure of materials, providing valuable insights into their properties and potential applications.

The X-ray diffraction analysis yielded precise results, achieving a high score in expertise. By employing the Williamson-Hall plot, we determined the particle's dimensions and strain: a particle size of 55nm and a strain of 0.22%. Consequently, it's evident that the nano-sized particle bears a notable level of strain, which is inherent in the nanoscale realm. This strain fundamentally alters the electrical and magnetic characteristics of the sample, a topic delved into further in subsequent sections.

7.1.2. FIELD EFFECT SCANNING ELECTRON MICROSCOPY (FESEM)

- **Sample Mounting**

  A minute quantity of the sample is placed within a test tube, followed by the addition of acetone. Ultrasonic vibrations are then employed for a duration of 15 minutes to dissolve the particle and ensure its uniform dispersion. Subsequently, a sample holder resembling the letter 'T' is prepared, with double-sided tape securely attached to it. Two minuscule glass slides are carefully positioned onto the tape. Using a micro-pipette, a small droplet of the sample is deposited onto one of the glass slides. The glass slide is subsequently subjected to drying under an infrared (IR) lamp until a faint haze appears on its surface, indicating the completion of the drying process.

- **Morphology Analysis**

  Once the meticulous mounting process reached its completion, we proceeded to subject the sample to imaging through the sophisticated lens of a field emission scanning electron microscope (FESEM). This step allowed us to delve into the intricate microstructure and morphology inherent within the pristine α-FeOOH samples. Employing a cutting-edge FESEM instrument, specifically the Carl Zeiss Sigma 300 model sourced from Germany, operational parameters were set at 10KV to ensure optimal imaging quality. Enhancing the analytical capacity, the FESEM was equipped with an energy dispersive X-ray (EDX) module, facilitating comprehensive elemental analysis alongside morphological examination. Within the captured images, a distinctive rod-shaped structure emerged, shedding light on the unique characteristics of the samples under scrutiny. Furthermore, to augment our understanding, a meticulous qualitative analysis utilizing the EDX functionality was meticulously performed for both samples, enabling a comprehensive assessment of their elemental composition and distribution.

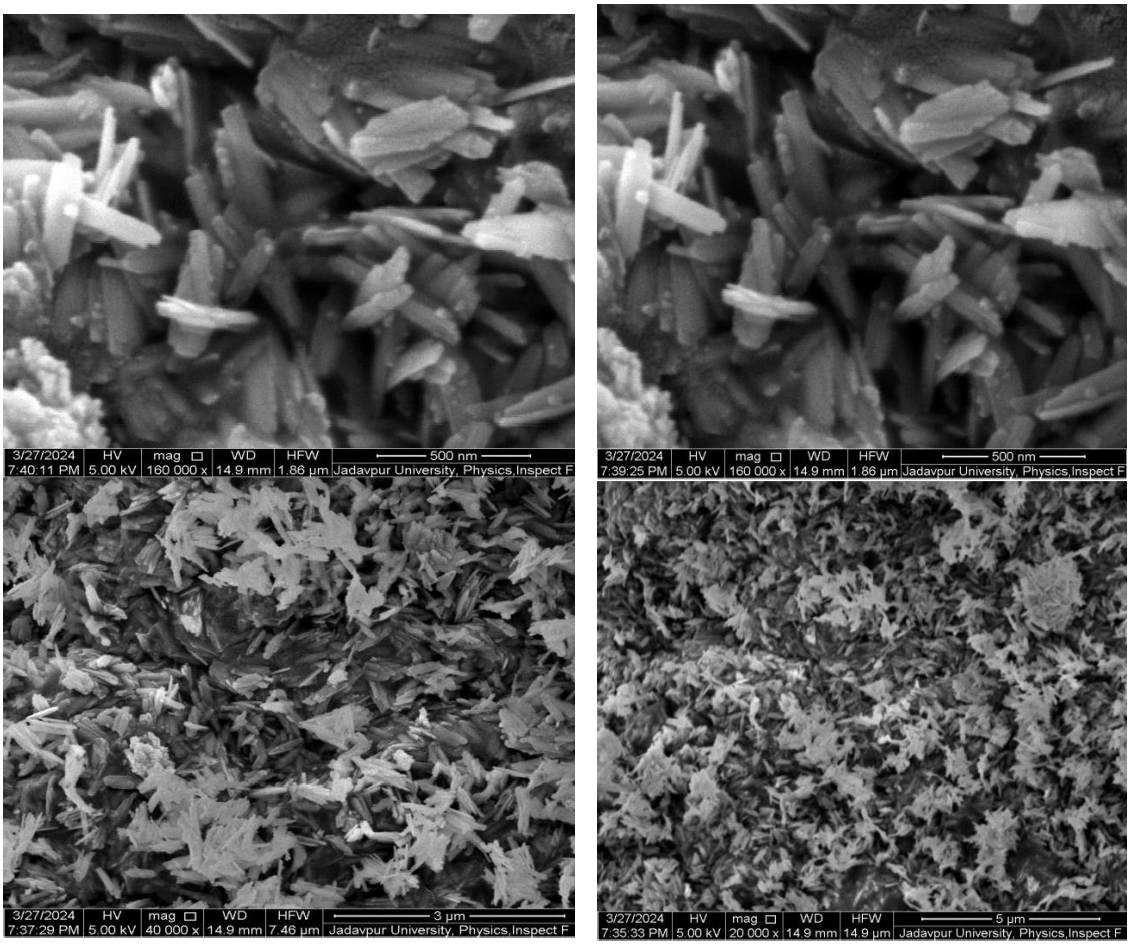


Figure 36 : FESEM images

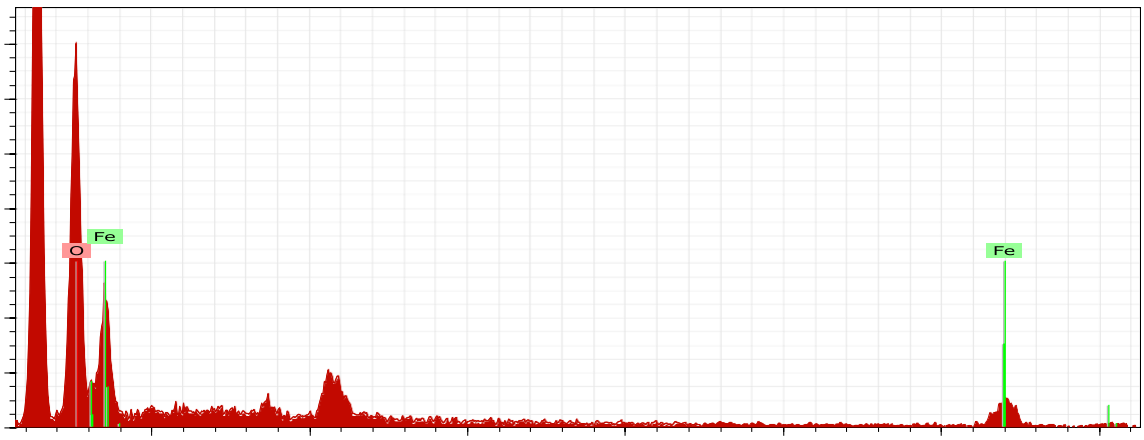


Figure 37 : EDX of α-FeOOH

In addition to visual analysis, we conducted quantitative assessments of the particle size and dimensions of the nano rods formed using field emission scanning electron microscopy (FESEM) images. Utilizing ImageJ software, we performed detailed measurements to determine both the average particle size and the average diameter of the nano rods.

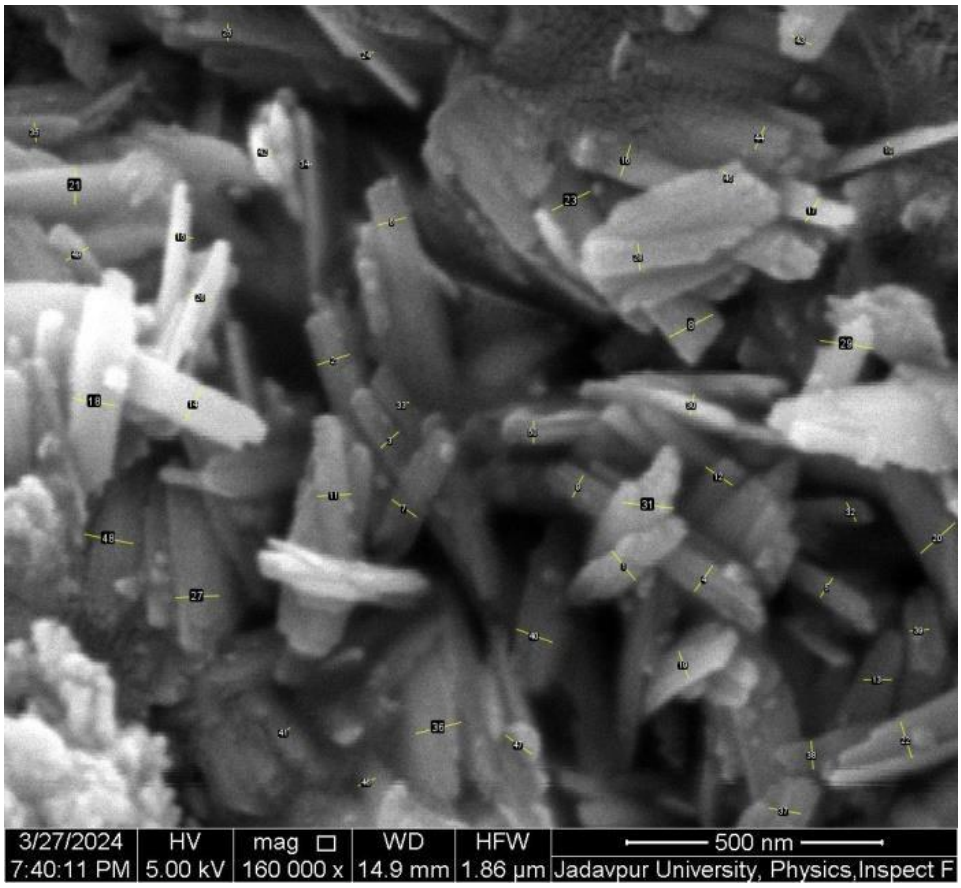


Figure 38 : Calculation of Average Diameter and length from ImageJ

Through our meticulous analysis, we uncovered significant data regarding the nano rods' dimensions. The examination yielded an average length of 250 nanometers and an

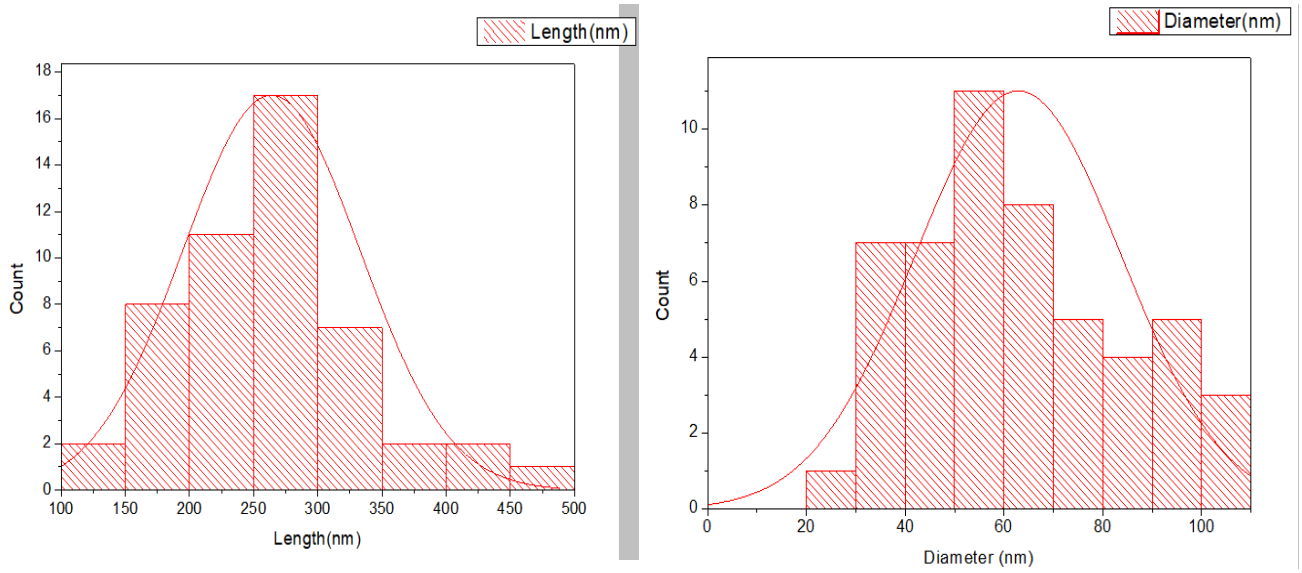


Figure 39 : Length and Diameter frequency distribution curves

Hence we concluded from our FESEM data that the synthesized goethite attained a nano rod morphology which enabled it to bind properly into the PVDF matrix.

7.1.3. FOURIER TRANSFORM INFRARED SPECTROSCOPY

The FTIR spectrum was carried out using a JASCO FTIR-6300 spectrometer from a wavenumber of 500 to 4000 cm^{-1}. From the below spectrum we can confirm the chemical composition and molecular structure of our sample.

The scrutiny of fingerprint regions within the graphical data serves as an indispensable tool for unraveling the intricate puzzle of functional groups encapsulated within our material. By meticulously analyzing these regions, we can unlock invaluable insights into the chemical composition and structural characteristics of our sample. Drawing upon established literature, we can discern

specific peaks that wield profound significance in delineating the molecular identity of our material.

For instance, our spectroscopic analysis has revealed the presence of two distinctand sharp peaks at 894 cm^{-1} and 796 cm^{-1}, attributed to Fe-O-OH bending

vibrations. These vibrational modes provide pivotal clues regarding the bonding configurations and chemical interactions within the material's framework. Furthermore, the absorption bands observed at 648 cm^{-1} are indicative of Fe-O stretching vibrations characteristic of α-FeOOH, shedding light on the specific chemical species present in our sample.

Moreover, our investigation has unveiled representative absorption bands at

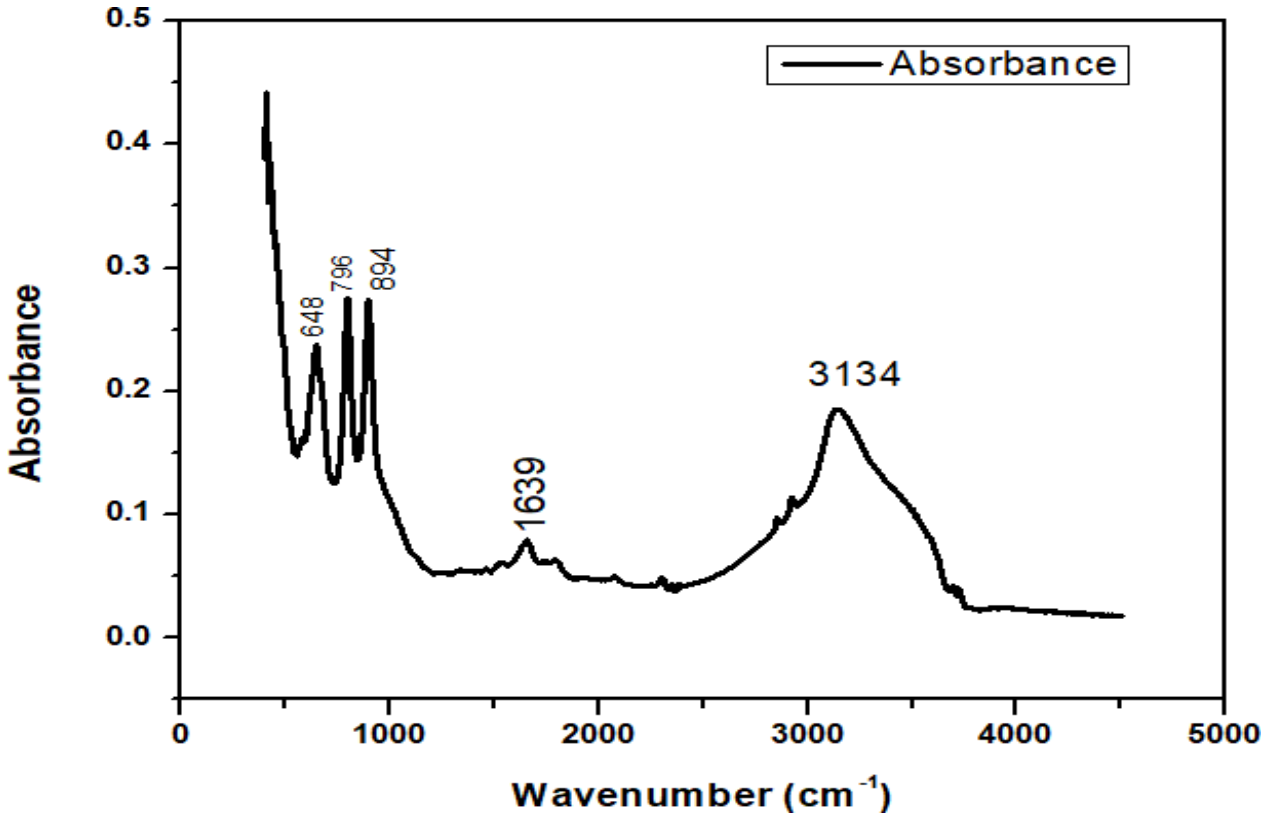


Figure 40 : FTIR graph plotted for goethite.

1639 cm^{-1} and 3134 cm^{-1}, corresponding to the δ(OeH) bending and ν(OeH) stretching vibrations, respectively. These vibrational signatures elucidate the dynamic interplay between oxygen and hydrogen atoms within the material's structure, offering deeper insights into its molecular architecture and functional properties.

By delving into the intricacies of these spectral features and aligning our findings with established literature, we can construct a comprehensive blueprint of the chemical landscape inhabiting our material. This synergistic approach not only enriches our understanding of its composition but also paves the way for leveraging its unique properties in diverse scientific and technological applications.

7.1.4. UV – VISIBLE SPECTROSCOPY

UV–Vis spectroscopy is a cost-effective, simple, versatile, non-destructive, and analytical technique, which is suitable for a large spectrum of organic compounds and some inorganic species. As a function of wavelength, UV–Vis spectrophotometers measure the absorption or transmission of light that passes through a medium. UV-Vis (V-630, JASCO) was used to obtain the absorption spectrum. (Figure 41)

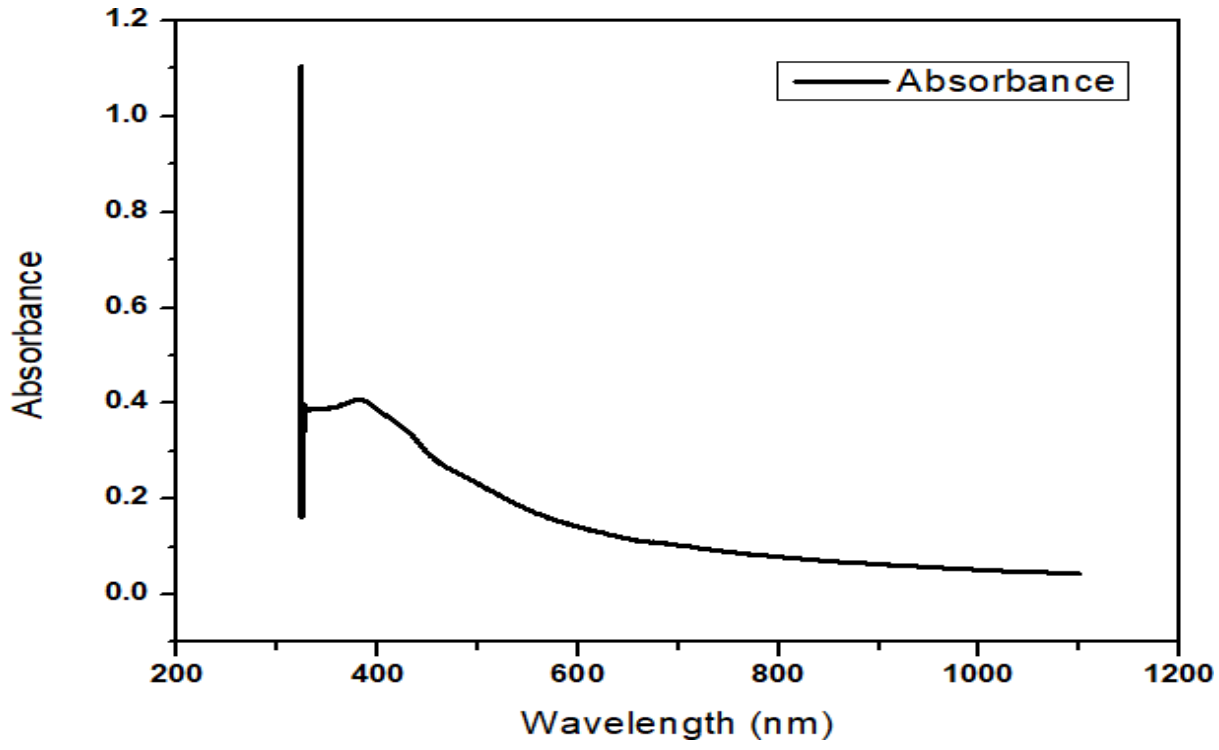


Figure 41: UV-VIS graph plotted for geothite

In addition to spectroscopic analysis, we utilized UV-visible spectroscopy to delve deeper into the electronic properties of our material, specifically to determine its band

gap. Employing Tauc's plot methodology, we conducted rigorous calculations to ascertain the band gap of α-FeOOH, a critical parameter that influences its optical and electronic behavior.

Our findings revealed that α-FeOOH exhibits a direct band gap of approximately 2.5 electron volts (eV) as shown in Figure 42, underscoring its semiconducting nature and offering valuable insights into its optical absorption characteristics. To validate the accuracy of our results, we meticulously cross-referenced our findings with existing literature, whereupon our calculated band gap closely aligned with previously reported values.

This alignment not only reaffirms the reliability and precision of our experimental techniques but also underscores the significance of α-FeOOH as a semiconductor (Direct Band gap) material with potential applications in optoelectronic devices, photovoltaics, and photocatalysis. By elucidating the fundamental electronic properties of α-FeOOH, our study contributes to a deeper understanding of its potential for advancing technological innovations and addressing contemporary challenges in materials science and engineering.

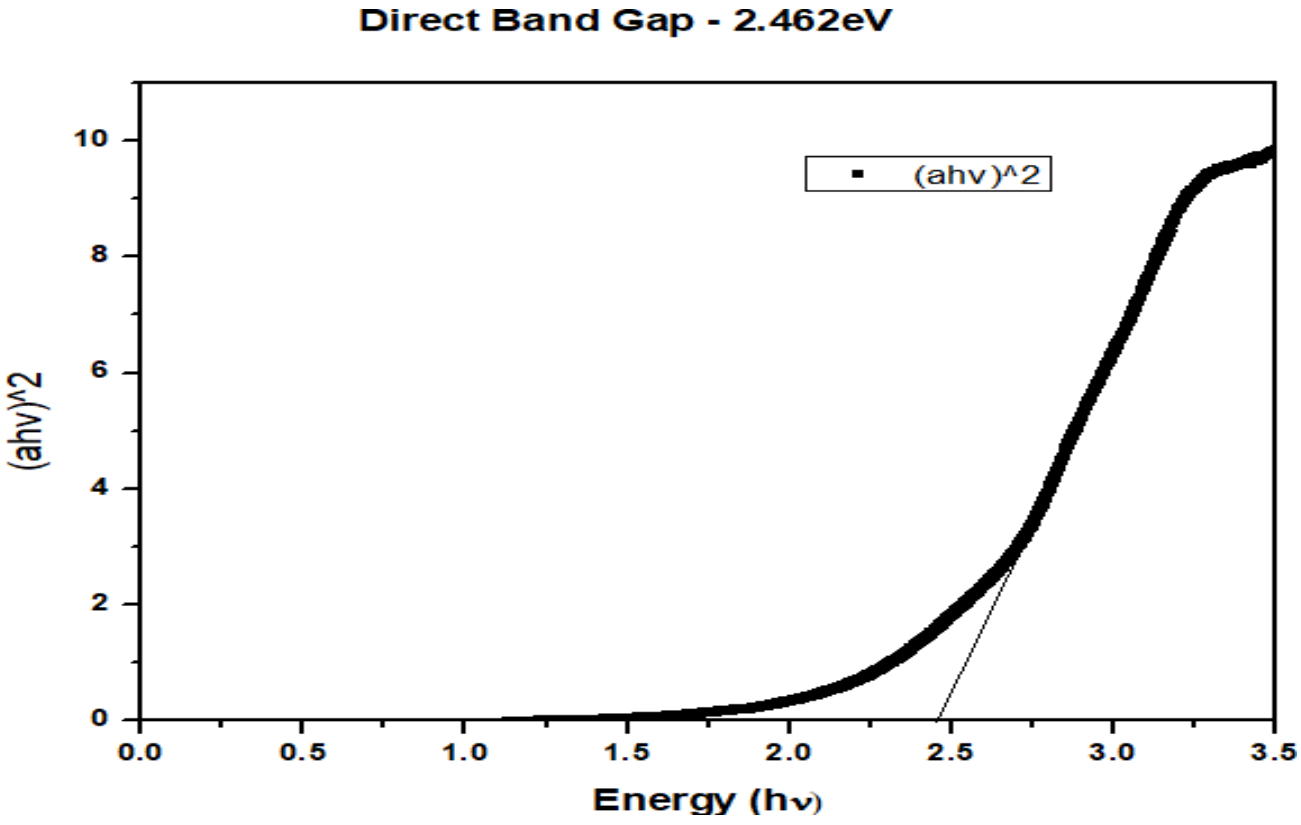


Figure 42 : Direct band gap calculation using Tauc's plot

7.2. DIELECTRIC AND MAGNETIC STUDY ANALYSIS

7.2.1. SAMPLE PREPARATION FOR DIELECTRIC STUDIES

After the spin coating process, the ITO-coated films underwent further experimentation for dielectric measurements. This involved a meticulous procedure to ensure the integrity of the coated films throughout the testing process.

Initially, great care was taken to delicately open the Teflon tape, mindful of preserving the films on the opposite side from any potential damage. Subsequently, electroding was carried out using silver paste on two distinct sides of the films: one on the surface coated with the composite material and the other on the bare ITO side, which had been shielded by the Teflon tape. This electroding process involved the application of silver paste onto the designated areas followed by the attachment of copper wires to each side through the silver paste.

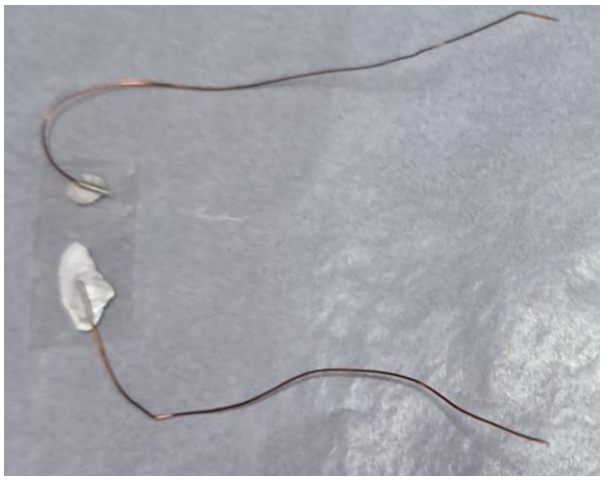


Figure 43: Electroded spin coated Ito substrate

To ensure the proper adhesion and functionality of the silver paste, it was subjected to drying under a UV lamp. This step facilitated the rapid curing of the paste, securing the electrical connections and minimizing the risk of displacement or detachment during subsequent measurements. This meticulous electroding process was crucial in preparing the films for accurate and reliable dielectric measurements, ensuring consistent and reproducible results in the evaluation of their electrical properties.

This process was repeated for all the seven sets.

7.2.2. Dielectric Measurement

Following the preparation of the composite-coated substrate, the next step involved the assessment of its dielectric properties. This crucial evaluation was conducted using a sophisticated impedance analyzer, which provided comprehensive data on various parameters including frequency, impedance, dispersion, capacitance, phase angle, and AC status.

To facilitate the measurement process, two crocodile clips were securely attached to the copper wires affixed to the substrate. This ensured a reliable electrical connection for accurate dielectric characterization. The impedance analyzer, equipped with advanced capabilities, enabled precise measurements over a wide frequency range spanning from 4Hz to 5GHz.



Figure 44 : Impedence Analyzer Kit

During the analysis, particular attention was given to the capacitance values exhibited by the composite samples at different doping concentrations. Interestingly, the observed trends in capacitance did not adhere to a monotonic pattern across the varying concentrations, with one notable exception observed in set 4, which contained 5% of α-FeOOH. This unexpected deviation from the anticipated trend underscored the complex interplay of factors influencing the dielectric behavior of the composite material and highlighted the need for detailed investigation and analysis to elucidate the underlying mechanisms governing its electrical properties.

The intriguing non-monotonic behavior observed in the capacitance versus frequency curves provides compelling evidence of the nuanced electrical characteristics exhibited

by our nanocomposite material. This distinctive feature serves as a pivotal indicator of the material's performance as a dielectric, offering valuable insights into its insulating properties across varying doping volume fractions.

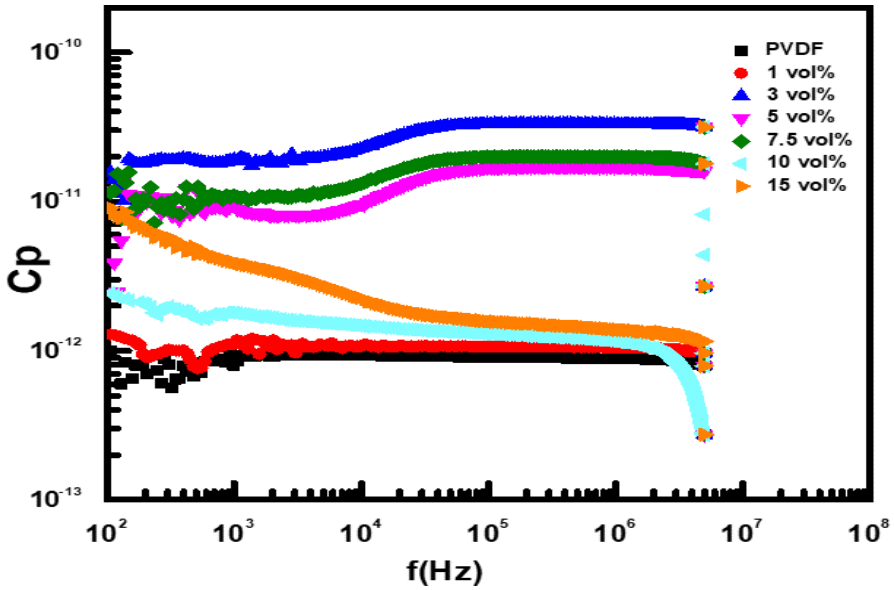


Figure 45 : Graph for Frequency vs Capacitence

Remarkably, the data reveals a discernible transition point at approximately 3 wt % doping volume fraction, beyond which the material undergoes a gradual transformation from exhibiting insulating behavior to displaying conductivity. This transition underscores the delicate balance between the dielectric and conductive properties inherent within the nanocomposite, highlighting its versatility and potential for diverse applications.

Furthermore, the anomalous behavior observed at the 5 wt % doping volume fraction, where the capacitance follows a monotonic trend, adds a layer of complexity to the material's electrical response. This anomaly warrants further investigation to elucidate the underlying mechanisms driving this deviation from the expected behavior.

In light of these findings, it can be confidently asserted that our goethite-PVDF nanocomposite has unequivocally demonstrated its efficacy as a dielectric material. Its ability to exhibit both insulating and conductive properties, depending on the doping volume fraction, underscores its versatility and suitability for a wide range of applications spanning from electrical insulation to advanced electronic devices. This comprehensive understanding of the material's electrical behavior paves the way for its strategic integration into innovative technologies, offering transformative solutions to contemporary challenges in various fields.

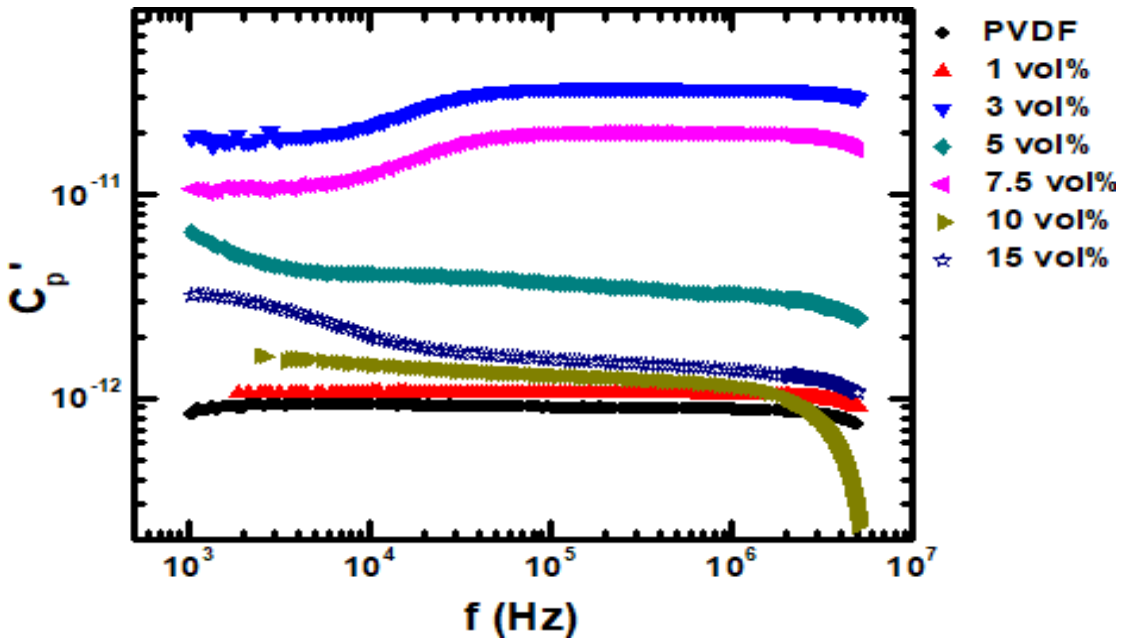


Figure 46 : Cp'vs Frequency

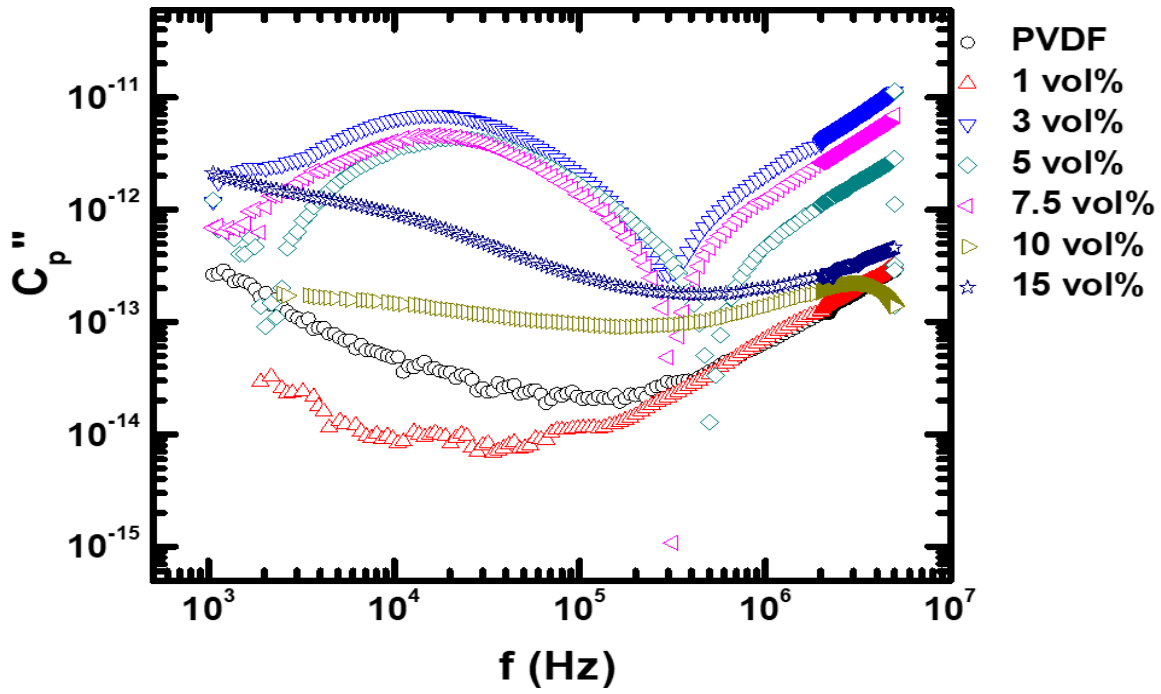


Figure 47 : Cp"vs Frequency

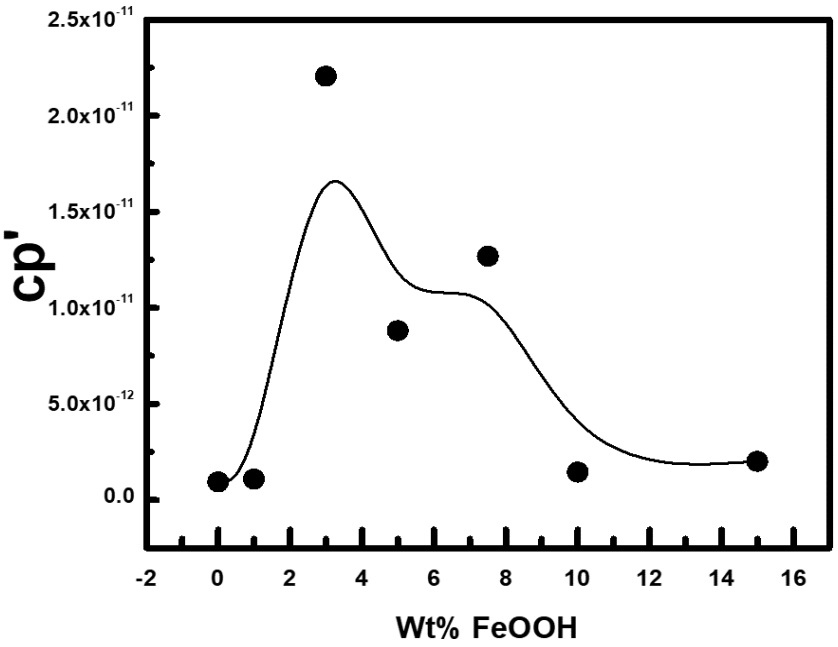


Figure 48: Cp'vs Wt%FeOOH

7.3. WEAK FERROMAGNETIC COMPONENT IN GOETHITE (α-FeOOH) AND ITS RELATION WITH MICROSTRUCTURAL CHARACTERISTICS

FeOOH, goethite exhibits antiferromagnetic ordering at room temperature with Neel temperature around 400K. (U. Schwertmann, R.M. Cornell, Wiley InterScience (Online Service), Iron Oxides in the Laboratory: Preparation and Characterization, second ed., Wiley-VCH, 2003) But weak ferromagnetism emerges as a consequence of finite size effect, defects, non-stoichiometry etc (Materials Chemistry and Physics 246 (2020) 122851). Imperfections and defects such as oxygen vacancies and/or low angel grain boundaries play a crucial role in determining the magnetic behaviour of goethite.

Room temperature magnetic measurements were carried out on samples by VSM (Lakeshore cryotronics, Model No. 7407); (Figure 49).

Figure 50, displays the room temperature magnetic hysteresis loop of FeOOH nanoparticles. The figure illustrates the emergence of weak ferromagnetism in the nanoparticles, characterized by a coercive field (H_c ~ 46 Oe) and exchange bias (H_{ex} ~ 46 Oe) both around 46 Oe. The central region of the ferromagnetic loop is magnified in Figure 50 for clarity. Despite FeOOH typically exhibiting antiferromagnetic behavior

at room temperature, a noticeable ferromagnetism arises in the nanoparticles due to strain. This phenomenon has been observed by others as well. The ferromagnetism exhibited by FeOOH nanoparticles is significant in the context of device fabrication, particularly when considering the magneto-dielectric properties of PVDF-FeOOH nanocomposites. The strain in the nanoparticles, determined to be 0.22% from the Williamson-Hall plot, contributes to this ferromagnetism, along with uncompensated spins at the nanoparticle surface. Similar types of ferromagnetism have been observed in other systems due to strain.

The strain in the nano particle (0.22%) as obtained from Williamson hall plot has been already discussed . the uncompensated spin at the surface of the nano particles and strain gives this type of ferromagnetism in other systems also .

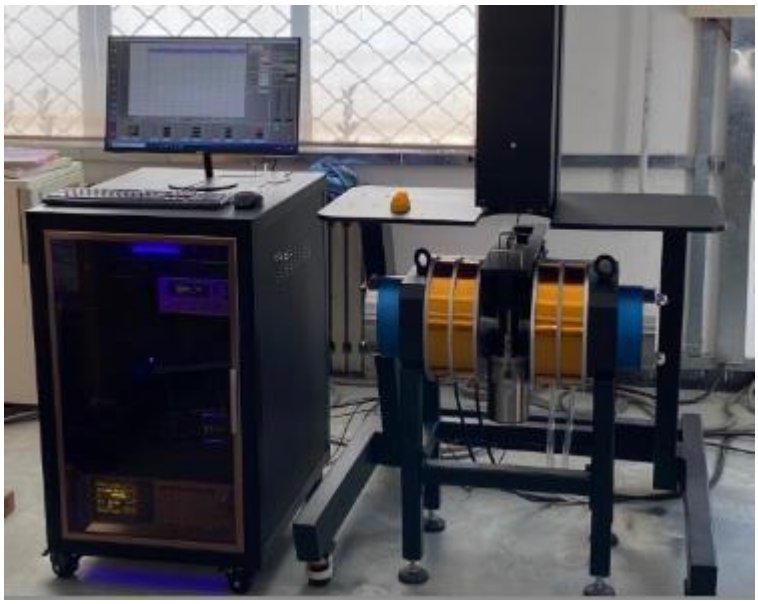


Figure 49: VSM Apparatus for Magnetic measurement

The figure 51 depicted illustrates the magnetic moment (measured in emu/gm) at room temperature plotted against the magnetic field for various composite films. A notable trend emerges from the data: as the volume fraction of FeOOH within the PVDF matrix increases, there is a corresponding enhancement in magnetization. In fact, the composite films exhibit reasonably good ferromagnetic properties until approximately 7.5 vol% of FeOOH, beyond which the magnetization begins to decrease.

This observed phenomenon hints at the intriguing interplay between the FeOOH

nanoparticles and the PVDF matrix. The intrinsic ferromagnetic behavior exhibited by the nanoscale FeOOH particles may stem from the heightened strain experienced by the nanocrystals within the composite structure. This strain-induced magnetization the nanoscale FeOOH particles may stem from the heightened strain experienced by the nanocrystals within the composite structure. This strain-induced magnetization enhancement underscores the complex and nuanced interactions at play within thesenanocomposite materials.

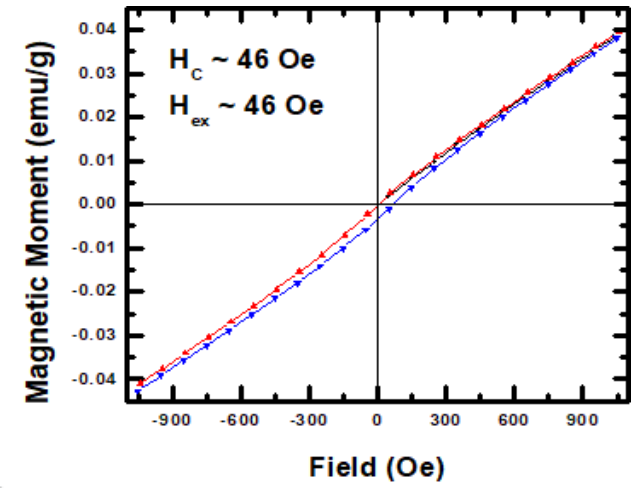


Figure 50: Magnetic Moment Vs Field

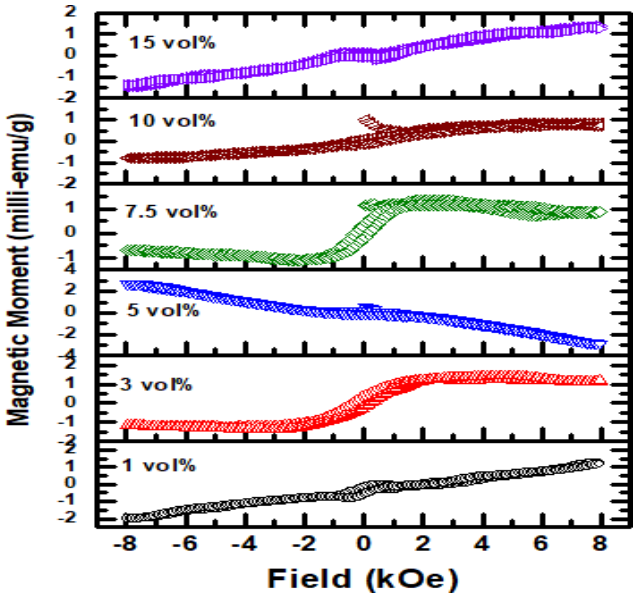


Figure 51: stack plot for all wt%

Understanding the mechanisms underlying this magnetic behavior is crucial for the optimization and application of such composite films in various fields, including magnetic storage, sensors, and biomedical devices. Further investigation into the structural and magnetic properties of these nanocomposites promises to shed light on their potential for advancing technology and materials science.

8. CONCLUSION

The preliminary investigation into the nano composite commenced with a meticulous synthesis process, initiating the formation of α-FeOOH through the well-established hydrothermal method. Following the successful synthesis, the resultant powdered α-FeOOH underwent a crucial phase of integration with a PVDF solution. This integration was meticulously executed across seven separate batches, each meticulously tailored to incorporate varying weight percentages of α-FeOOH. The resultant amalgam, representing a spectrum of compositions, was then meticulously applied onto an ITO substrate utilizing the precise spin coating technique. Through this process, a series of thin films were meticulously fabricated, each bearing the unique composition dictated by the predetermined weight percentages of α-FeOOH.

These thin films, embodying diverse compositional variations, served as the focal point for a comprehensive array of subsequent analyses aimed at unraveling their intricate properties and characteristics. Through a systematic approach, these thin films underwent a battery of examinations, encompassing a spectrum of analytical techniques tailored to probe into their structural, electrical, and magnetic attributes. This multifaceted exploration aimed to elucidate the nuanced interplay between the constituents of the nano composite and unveil the potential implications for various technological application

In summary, our thorough investigation from synthesis to thin film formation has provided valuable insights into the behavior of the nano composite. Specifically, the addition of goethite into the PVDF matrix revealed diverse dielectric behaviors, characterized by a non-monotonic curve. As anticipated, insulating properties sharply increased up to a threshold, except for the 5% mark, where a shift to conducting behavior occurred. Moreover, our investigations into the magnetic properties have yielded compelling insights, particularly showcasing optimal outcomes when the goethite concentration reached 7.5wt% within the PVDF framework, characterized by a discernible hysteresis curve. These revelations serve to underscore the remarkable potential inherent within the PVDF-goethite nanocomposite, poised to find versatile applications across domains such as magneto-dielectric devices and as mediums for charge storage.

Leveraging the synergistic interplay of its distinct electrical and magnetic attributes, this composite material stands as a promising candidate for advancing technological frontiers in various fields.

9. FUTURE STUDIES

Our recent research has unveiled an intriguing dual nature within the PVDF-FeOOH nanocomposite, showcasing both dielectric and magnetic properties. This discovery serves as a catalyst for our future investigations, which will be dedicated entirely to unraveling the intricacies of magnetodielectric behavior across a spectrum of nano-sized particles. By broadening our scope to include various particle sizes, we aim to deepen our understanding of how different dimensions influence the composite's performance, thereby paving the way for more nuanced applications.

Moreover, the nanocomposite we engineered follows a [033] configuration, signifying a homogeneous dispersion of nano fillers throughout the host matrix. This uniform distribution holds significant implications for the material's overall behavior and performance. As we progress, we are keen to extend our research endeavors to explore the [22] configuration, also referred to as the sandwich configuration. Within this arrangement, layers of material are interspersed, presenting a unique opportunity to investigate how the interplay between dielectric and magnetic properties manifests within the intricate structure of the composite.

By delving deeper into these configurations and their associated properties, we anticipate uncovering invaluable insights that will not only enhance our fundamental understanding of nanocomposite behavior but also inform the design and development of future energy storage and electronic devices. Our commitment to this pursuit underscores our dedication to advancing scientific knowledge and fostering innovation in materials science and engineering.

10. REFERENCE

1. Ishida, H., Campbell, S. and Blackwell, J., 2000. General approach to nanocomposite preparation. *Chemistry of Materials*, *12*(5), pp.1260-1267.
2. Al-Mutairi, N.H., Mehdi, A.H. and Kadhim, B.J., 2022. Nanocomposites materials definitions, types and some of their applications: a review. *European Journal of Research Development and Sustainability*, *3*(2), pp.102-108.
3. Liu, Z., Li, G., Qin, Q., Mi, L., Li, G., Zheng, G., Liu, C., Li, Q. and Liu, X., 2021. Electrospun PVDF/PAN membrane for pressure sensor and sodium-ion battery separator. *Advanced Composites and Hybrid Materials*, *4*, pp.1215-1225.
4. Pandey, J.C. and Singh, M., 2021. Dielectric polymer nanocomposites: past advances and future prospects in electrical insulation perspective. *SPE polymers*, *2*(4), pp.236-256.
5. zong, M.Z., Zhang, M.Q. and Ruan, W.H., 2006. Surface modification of nanoscale fillers for improving properties of polymer nanocomposites: a review. *Materials science and technology*, *22*(7), pp.787-796.
6. Thabet, A., Mubarak, Y.A. and Bakry, M.J.J.E.S., 2011. A review of nano-fillers effects on industrial polymers and their characteristics. *J. Eng. Sci*, *39*, pp.377-403.
7. de Oliveira, A.D. and Beatrice, C.A.G., 2018. Polymer nanocomposites with different types of nanofiller. *Nanocomposites-recent evolutions*, pp.103-104.
8. Njuguna, J., Ansari, F., Sachse, S., Rodriguez, V.M., Siqqique, S. and Zhu, H., 2021. Nanomaterials, nanofillers, and nanocomposites: types and properties. In *Health and environmental safety of nanomaterials* (pp. 3-37). Woodhead Publishing.
9. Okpala, C.C., 2013. Nanocomposites–an overview. *International Journal of Engineering Research and Development*, *8*(11), pp.17-23.
10. Al-Mutairi, N.H., Mehdi, A.H. and Kadhim, B.J., 2022. Nanocomposites materials definitions, types and some of their applications: a review. *European Journal of Research Development and Sustainability*, *3*(2), pp.102-108.
11. Tyagi, S., Chaudhary, M., Ambedkar, A.K., Sharma, K., Gautam, Y.K. and Singh, B.P., 2022. Metal oxide nanomaterial-based sensors for monitoring environmental NO 2 and its impact on the plant ecosystem: A review. *Sensors & Diagnostics*, *1*(1), pp.106-129.
12. de Oliveira, A.D. and Beatrice, C.A.G., 2018. Polymer nanocomposites

with different types of nanofiller. *Nanocomposites-recent evolutions*, pp.103-104.
13. Dadkhah, M., Saboori, A. and Fino, P., 2019. An overview of the recent developments in metal matrix nanocomposites reinforced by graphene. *Materials*, *12*(17), p.2823.
14. Saboori, A., Moheimani, S.K., Dadkhah, M., Pavese, M., Badini, C. and Fino, P., 2018. An overview of key challenges in the fabrication of metal matrix nanocomposites reinforced by graphene nanoplatelets. *Metals*, *8*(3), p.172.
15. Hassanzadeh-Aghdam, M.K., Mahmoodi, M.J. and Ansari, R., 2018. A comprehensive predicting model for thermomechanical properties of particulate metal matrix nanocomposites. *Journal of Alloys and Compounds*, *739*, pp.164-177.

16. Cho, J., Boccaccini, A.R. and Shaffer, M.S., 2009. Ceramic matrix composites containing carbon nanotubes. *Journal of Materials Science*, *44*, pp.1934-1951.
17. Azarniya, A., Sovizi, S., Azarniya, A., Boyuk, M.R.R.T., Varol, T., Nithyadharseni, P., Hosseini, H.R.M., Ramakrishna, S. and Reddy, M.V., 2017. Physicomechanical properties of spark plasma sintered carbon nanotube-containing ceramic matrix nanocomposites. *Nanoscale*, *9*(35), pp.12779-12820.
18. Palmero, P., 2015. Structural ceramic nanocomposites: a review of properties and powders' synthesis methods. *Nanomaterials*, *5*(2), pp.656-696.
19. Silvestre, J., Silvestre, N. and De Brito, J., 2015. An overview on the improvement of mechanical properties of ceramics nanocomposites. *Journal of Nanomaterials*, *2015*, pp.3-3.
20. Winey, K.I. and Vaia, R.A., 2007. Polymer nanocomposites. *MRS bulletin*, *32*(4), pp.314-322.
21. Paul, D.R. and Robeson, L.M., 2008. Polymer nanotechnology: nanocomposites. *Polymer*, *49*(15), pp.3187-3204.
22. Fu, S., Sun, Z., Huang, P., Li, Y. and Hu, N., 2019. Some basic aspects of polymer nanocomposites: A critical review. *Nano Materials Science*, *1*(1), pp.2-30.
23. Hiremath, A., Murthy, A.A., Thipperudrappa, S. and KN, B., 2021.

Nanoparticles filled polymer nanocomposites: A technological review. *Cogent engineering*, *8*(1), p.1991229.

24. Ilyas, R.A., Sapuan, S.M., Sanyang, M.L., Ishak, M.R. and Zainudin, E.S., 2018. Nanocrystalline cellulose as reinforcement for polymeric matrix nanocomposites and its potential applications: a review. *Current Analytical Chemistry*, *14*(3), pp.203-225.
25. Mohammadnezhad, G. and Keikavousi Behbahan, A., 2020. Polymer matrix nanocomposites for heavy metal adsorption: a review. *Journal of the Iranian Chemical Society*, *17*(6), pp.1259-1281.
26. Nelson, S.O. and Kraszewski, A.W., 1990. Dielectric properties of materials and measurement techniques. *Drying technology*, *8*(5), pp.1123-1142.
27. Venkatesh, M.S. and Raghavan, G.S.V., 2005. An overview of dielectric properties measuring techniques. *Canadian biosystems engineering*, *47*(7), pp.15-30.
28. Nelson, S.O., 1999. Dielectric properties measurement techniques and applications. *Transactions of the ASAE*, *42*(2), pp.523-529.
29. Ahmad, Z., 2012. Polymer dielectric materials. In *Dielectric material*. IntechOpen.
30. Nelson, S.O. and Kraszewski, A.W., 1990. Dielectric properties of materials and measurement techniques. *Drying technology*, *8*(5), pp.1123-1142.
31. Faivre, D., 2016. *Iron oxides: from nature to applications*. John Wiley & Sons.
32. Schwertmann, U.T.R.M. and Taylor, R.M., 1989. Iron oxides. *Minerals in soil environments*, *1*, pp.379-438.
33. Aghayari, S., 2021. An introduction to PVDF nanofibers properties, and ways to improve them, and reviewing output enhancing methods for PVDF nanofibers nanogenerators.
34. Inderherbergh, J., 1991. Polyvinylidene fluoride (PVDF) appearance, general properties and processing. *Ferroelectrics*, *115*(4), pp.295-302.
35. Dallaev, R., Pisarenko, T., Sobola, D., Orudzhev, F., Ramazanov, S. and Trčka, T., 2022. Brief review of PVDF properties and applications potential. *Polymers*, *14*(22), p.4793.

36. Tashiro, K., 1995. Crystal structure and phase transition of PVDF and related copolymers. *PLASTICS ENGINEERING-NEW YORK-*, *28*, pp.63-63.
37. Xia, W. and Zhang, Z., 2018. PVDF-based dielectric polymers and their applications in electronic materials. *Iet Nanodielectrics*, *1*(1), pp.17-31.
38. Sudapalli, A.M. and Shimpi, N.G., 2023. Hydrothermal synthesis of α-FeOOH (1D) nanorods and their transition to α-Fe 2 O 3 (0D): an efficient photocatalyst in neutralizing hazardous organic dyes. *New Journal of Chemistry*, *47*(30), pp.14323-14334.
39. Godwin, J., Abdus-Salam, N., Haleemat, A.I., Panda, P.K., Panda, J. and Tripathy, B.C., 2022. Facile synthesis of rod-like α-FeOOH nanoparticles adsorbent and its mechanism of sorption of Pb (II) and indigo carmine in batch operation. *Inorganic Chemistry Communications*, *140*, p.109346.
40. Godwin, J., Abdus-Salam, N., Haleemat, A.I., Panda, P.K., Panda, J. and Tripathy, B.C., 2022. Facile synthesis of rod-like α-FeOOH nanoparticles adsorbent and its mechanism of sorption of Pb (II) and indigo carmine in batch operation. *Inorganic Chemistry Communications*, *140*, p.109346.
41. Amani-Ghadim, A.R., Alizadeh, S., Khodam, F. and Rezvani, Z., 2015. Synthesis of rod-like α-FeOOH nanoparticles and its photocatalytic activity in degradation of an azo dye: Empirical kinetic model development. *Journal of Molecular Catalysis A: Chemical*, *408*, pp.60-68.
42. Wang, J., Xie, Y., Liu, J., Zhang, Z., Zhuang, Q. and Kong, J., 2018. Improved energy storage performance of linear dielectric polymer nanodielectrics with polydopamine coated BN nanosheets. *Polymers*, *10*(12), p.1349.
43. Padurariu, L., Brunengo, E., Canu, G., Curecheriu, L.P., Conzatti, L., Buscaglia, M.T., Stagnaro, P., Mitoseriu, L. and Buscaglia, V., 2023. Role of microstructures in the dielectric properties of PVDF-based nanocomposites containing high-permittivity fillers for energy storage. *ACS Applied Materials & Interfaces*, *15*(10), pp.13535-13544.
44. Wang, S., Liu, L., Zeng, Y., Zhou, B., Teng, K., Ma, M., Chen, L. and Xu, Z., 2015. Improving dielectric properties of poly (vinylidene fluoride) composites: effects of surface functionalization of exfoliated graphene. *Journal of Adhesion Science and Technology*, *29*(7), pp.678-

690.
45. Goswami, S., Mishra, S., Sen, S., Ghosh, C.K. and Bhattacharya, D., 2023. Large room-temperature magnetodielectric effect in polyvinylidene fluoride-trifluoroethylene/La0. 7Sr0. 3MnO3 (0-3) nanocomposite thin films. *Journal of Physics and Chemistry of Solids*, *179*, p.111418.
46. Meng, N., Zhu, X., Mao, R., Reece, M.J. and Bilotti, E., 2017. Nanoscale interfacial electroactivity in PVDF/PVDF-TrFE blended films with enhanced dielectric and ferroelectric properties. *Journal of Materials Chemistry C*, *5*(13), pp.3296-3305.
47. Gregorio, R. and Ueno, E.M., 1999. Effect of crystalline phase, orientation and temperature on the dielectric properties of poly (vinylidene fluoride)(PVDF). *Journal of materials science*, *34*, pp.4489-4500.
48. Tyona, M.D., 2013. A theoritical study on spin coating technique. *Advances in materials Research*, *2*(4), p.195.
49. Sahu, N., Parija, B. and Panigrahi, S., 2009. Fundamental understanding and modeling of spin coating process: A review. *Indian Journal of Physics*, *83*(4), pp.493-502.
50. Epp, J., 2016. X-ray diffraction (XRD) techniques for materials characterization. In *Materials characterization using nondestructive evaluation (NDE) methods* (pp. 81-124). Woodhead Publishing.
51. Berthomieu, C. and Hienerwadel, R., 2009. Fourier transform infrared (FTIR) spectroscopy. *Photosynthesis research*, *101*, pp.157-170.
52. Perkampus, H.H., 2013. *UV-VIS Spectroscopy and its Applications*. Springer Science & Business Media.
53. Abd Mutalib, M., Rahman, M.A., Othman, M.H.D., Ismail, A.F. and Jaafar, J., 2017. Scanning electron microscopy (SEM) and energy-dispersive X-ray (EDX) spectroscopy. In *Membrane characterization* (pp. 161-179). Elsevier.